Casimir interaction of rodlike particles in a two-dimensional critical system

E. Eisenriegler[1] and T. W. Burkhardt[2]

[1]*Theoretical Soft Matter and Biophysics, Institute of Complex Systems, Forschungszentrum Jülich, D-52425 Jülich, Germany*

[2]*Department of Physics, Temple University, Philadelphia, Pennsylvania 19122, USA*

(Received 12 February 2016; published 26 September 2016)

We consider the fluctuation-induced interaction of two thin, rodlike particles, or "needles," immersed in a two-dimensional critical fluid of Ising symmetry right at the critical point. Conformally mapping the plane containing the needles onto a simpler geometry in which the stress tensor is known, we analyze the force and torque between needles of arbitrary length, separation, and orientation. For infinite and semi-infinite needles we utilize the mapping of the plane bounded by the needles onto the half plane, and for two needles of finite length we use the mapping onto an annulus. For semi-infinite and infinite needles the force is expressed in terms of elementary functions, and we also obtain analytical results for the force and torque between needles of finite length with separation much greater than their length. Evaluating formulas in our approach numerically for several needle geometries and surface universality classes, we study the full crossover from small to large values of the separation to length ratio. In these two limits the numerical results agree with results for infinitely long needles and with predictions of the small-particle operator expansion, respectively.

DOI: 10.1103/PhysRevE.94.032130

I. INTRODUCTION

Two objects immersed in a near-critical fluid, for example colloidal particles in a binary liquid mixture near the critical point of miscibility, experience a long-range, fluctuation-induced force [1–6]. Changes in the positions of the objects alter the space available to the critically fluctuating fluid, and hence its free energy, giving rise to an effective interaction of the objects. In analogy with the Casimir effect in quantum electrodynamics [7–10], this is known as the critical or thermodynamic Casimir interaction.

The critical Casimir interaction displays a high degree of universality, i.e., is largely independent of microscopic details [3–6]. It depends only on universal properties of the fluid, the universality class of the boundary between the fluid and the immersed particles, and geometrical properties of the particles, such as their size, shape, and relative position.

Fluctuations of the superfluid order parameter also lead to critical Casimir forces, and this has been detected in wetting films of ^{4}He and ^{3}He /^{4}He mixtures [11–15]. Particles immersed in a solution [16–19] of long, flexible polymer chains or particles to which a polymer chain is attached [19,20] experience a similar Casimir interaction due to fluctuations of the polymers [21]. Shape fluctuations of membranes or fluid surfaces lead to a Casimir-type interaction of embedded particles [22–24].

Binary liquid mixtures belong to the Ising universality class. The surfaces of the immersed particles generally attract one of the two components of the mixture preferentially, corresponding to (+ or −) boundary conditions in the Ising model. A surface prepared to suppress the preference corresponds to free-spin boundary conditions [25]. In the terminology of surface critical phenomena, these two surface universality classes [26] are known as "normal" (+ or −) and "ordinary" (O).

In studies of critical Casimir interactions, systems with planar walls and systems with spherical particles have received the most attention [3,13,27–29]. For nonspherical particles the Casimir interaction depends on their orientation as well as their separation; i.e., there is a torque as well as a force. Recently, the universal scaling form of the Casimir interaction of a prolate uniaxial ellipsoid and a planar wall, with pairs ++ or +− of boundary conditions on the two surfaces, was calculated within mean-field theory by Kondrat *et al.* [30].

In this paper we derive exact results for the Casimir interaction of two rodlike particles in a two-dimensional critical system in the Ising universality class. The following considerations provide some motivation:

(i) Recent experiments suggest that biological membranes are tuned close to a critical point of miscibility in two dimensions [31]. The possibility of critical Casimir interactions between inclusions in the membrane has been studied by Machta *et al.* [32,33].

(ii) Systems at the critical point are generally invariant not only under scale transformations, but also under conformal or angle-preserving coordinate transformations [34]. This has far-reaching consequences for the Casimir interaction of two particles, especially in two spatial dimensions [29,35,36].

In general dimension d the region outside two spherical particles with arbitrary radii and separation can be conformally mapped onto the region bounded by two concentric spheres using homogeneous translations, rotations, and dilatations and the inversion. Burkhardt, Eisenriegler, and Ritschel have shown [29] that this mapping determines the asymptotic form of the Casimir interaction for both large and small separation of the spheres in an arbitrary critical medium, not necessarily Ising-like, in arbitrary spatial dimension d.

In $d = 2$ the conformal group is much richer than in general d. Conformal mappings are generated by analytic functions, and the doubly connected region outside two particles of *arbitrary* shape can be conformally mapped onto the annulus bounded by two concentric circles or, equivalently, onto the surface of a cylinder of finite circumference and length. The Casimir interaction of the particles in an infinite, two-dimensional, Ising-like critical medium follows from the free energy of the critical Ising model on the cylindrical surface [29,34–36], which Cardy [37] has derived in analytic form for all aspect ratios and for all pairs of boundary conditions +,

−, and O at the ends of the cylindrical surface. Burkhardt and Eisenriegler [29] and Machta *et al.* [32] followed this route in evaluating the Casimir interaction of two particles with circular shape. Bimonte *et al.* [36] have given a general analysis of asymptotic properties of the Casimir interaction in critical two-dimensional conformal field theories for two particles of arbitrary shape, based on the mapping of the portion of the plane outside the particles onto an annulus.

Being interested in the Casimir torque as well as the force, we consider anisotropic particles. The rodlike particles in our study have negligible width compared with their length, and we model each particle as a segment of a straight line. This shape is extremely simple and highly anisotropic. Following Ref. [35] we refer to the particles as "needles" [38]. The approach we use, which makes use of conformal mappings, is not limited to these needles but is applicable, in principle, to particles in two dimensions of arbitrary shape.

In Sec. II and Appendix A we show how the force and torque between the particles are related to the stress tensor [34], which for our purpose is the quantity most convenient to work with [29,35,36].

In Sec. III we calculate the critical Casimir force between a semi-infinite needle and an infinite needle and between two semi-infinite needles, with arbitrary relative position. These are instructive cases to begin with since the calculations can be carried out analytically, without special functions. The key step is to generate by a conformal mapping $z(w)$ the complex z plane with the two embedded needles from the upper half w plane with the corresponding needles on the real axis. The approach is not limited to needles with homogeneous boundary conditions. In addition to the homogeneous case, we consider needles whose two sides prefer different components of the mixture and also a semi-infinite needle in the presence of a piecewise homogeneous boundary corresponding to "chemical steps" [39–41].

In Sec. IV we discuss the more complicated Schwarz-Christoffel transformation required for two needles of finite length. It generates the complex z plane, with an embedded needle between points z_1 and z_2 and a second needle between points z_3 and z_4, from an annulus, with circular needles on the outer and inner boundaries.

In Sec. V detailed results for the Casimir force and torque between needles of finite length are presented for several configurations of the needles. The results are consistent with predictions of Vasilyev *et al.* [35], who have studied the Casimir interaction of the needles with Monte Carlo simulations and calculated them in certain symmetric cases with conformal invariance methods [42], but without the generality of the approach considered below. The results of Sec. V are also asymptotically consistent with the predictions for infinite or semi-infinite needles derived in Sec. III. Since the torque diverges for needles of infinite length, checking its asymptotic behavior is more subtle and is addressed in Appendix C.

For large separation of the needles in comparison with their lengths [43], the numerical results of Sec. V reproduce the predictions of the "small-particle operator expansion" (SPOE). This expansion, which is reviewed in Appendix B, has proved to be extremely useful in studies of the critical Casimir interaction and is similar in spirit to the operator product expansion [44] in field theory. Large needle separation corresponds to a small ratio of inner to outer radius of the annulus, and the corresponding expansions in Sec. IV and Appendix B allow us to check the agreement with the SPOE analytically.

The final section of the paper, Sec. VI, contains a summary and concluding remarks.

II. FORCE, TORQUE, AND THE STRESS TENSOR

In this section we consider two needles I and II in the $z = r_x + ir_y$ plane and present the formalism for calculating the force (f_x, f_y) and the torque Θ acting on needle I due to needle II. The force and torque follow from the changes δF of the interaction free energy [45] on infinitesimally translating and rotating needle I with needle II kept fixed. As reviewed in Appendix A, these changes can be expressed in terms of the thermal averages $\langle T_{kl}(r_x,r_y)\rangle$ of the Cartesian [46] stress tensor field or its complex [34] counterpart $\langle T(z)\rangle$ for the given needle configuration. In subsequent sections the stress tensor and the corresponding force and torque are calculated for several two-needle geometries of interest. In each case $\langle T(z)\rangle$ is obtained through a conformal mapping $z(w)$ of a simpler geometry in the w plane, for which $\langle T(w)\rangle$ is known, onto the desired geometry in the z plane, using the fundamental transformation property [34]

$$\langle T(z)\rangle = \frac{1}{[z'(w)]^2}\left[\langle T(w)\rangle - \frac{1}{24}S(w)\right]. \tag{2.1}$$

Here $S(w)$ is the Schwarzian derivative

$$S(w) = \frac{z'''(w)z'(w) - (3/2)[z''(w)]^2}{[z'(w)]^2} \equiv \frac{d^2}{dw^2}\ln\frac{dz}{dw} - \frac{1}{2}\left(\frac{d}{dw}\ln\frac{dz}{dw}\right)^2, \tag{2.2}$$

and the primes denote derivatives.

According to Eq. (A11) the force components are given by

$$(f_x, f_y)/(k_BT) = -(\mathrm{Im}, \mathrm{Re})\tau, \tag{2.3}$$

where

$$\tau = \frac{1}{\pi}\int_{\mathcal{C}_1} dz\langle T(z)\rangle = \frac{1}{\pi}\int_{\mathcal{C}} dw z'(w)\langle T(z)\rangle. \tag{2.4}$$

The integration path $\mathcal{C}_\mathrm{I}$ in the z plane encloses needle I in a clockwise fashion, leaving needle II outside, and $\mathcal{C}$ is the corresponding path in the w plane, which maps onto $\mathcal{C}_\mathrm{I}$ under the conformal transformation $z(w)$. With the help of Eq. (2.1), τ can be expressed as

$$\tau = \frac{1}{\pi}\int_{\mathcal{C}} dw\frac{1}{z'(w)}\left[\langle T(w)\rangle - \frac{1}{24}S(w)\right] \equiv \tau^{(T)} + \tau^{(S)}. \tag{2.5}$$

The torque Θ on a needle I with fixed length, extending from z_1 to z_2, and forming an angle $\Phi_\mathrm{I} \equiv \Phi_{12} = \arg(z_1 - z_2)$ with the x axis is given by

$$\Theta = -(\partial/\partial\Phi_\mathrm{I})\delta F, \tag{2.6}$$

where the derivative is taken for an infinitesimal rotation of needle I about its midpoint with the midpoint $z_\mathrm{I} = \frac{1}{2}(z_1 + z_2)$

fixed. According to Eqs. (2.6) and (A12), the torque may be written as

$$\Theta = -k_B T \mathrm{Re}\theta, \tag{2.7}$$

where

$$\theta = \frac{1}{\pi}\int_{\mathcal{C}_\mathrm{I}} dz \langle T(z)\rangle (z - z_\mathrm{I}) \tag{2.8}$$

and the integration path $\mathcal{C}_\mathrm{I}$ is the same as in Eq. (2.4).

To express Θ in terms of $\langle T(w)\rangle$ and $z(w)$, we rewrite the integral in Eq. (2.8) using Eq. (2.1) and the relation

$$z - z_\ell = \int_{w_\ell}^{w} d\tilde{w}(dz/d\tilde{w}) \equiv \zeta_\ell(w); \quad \ell = 1,2, \tag{2.9}$$

where w_ℓ is the point in the w plane which maps onto needle end point z_ℓ. Together with (2.7), this yields

$$\Theta = -k_B T \mathrm{Re}(\theta^{(T)} + \theta^{(S)}), \tag{2.10}$$

where

$$\begin{pmatrix}\theta^{(T)}\\ \theta^{(S)}\end{pmatrix} = \frac{1}{2\pi}\int_{\mathcal{C}} dw \frac{1}{dz/dw}\begin{pmatrix}\langle T(w)\rangle \\ -\frac{1}{24}S(w)\end{pmatrix}[\zeta_1(w) + \zeta_2(w)]. \tag{2.11}$$

Note that the contributions $\tau^{(S)}$ in Eq. (2.5) and $\theta^{(S)}$ in Eq. (2.11) which involve the Schwarzian derivative are purely geometrical and do not depend on the surface universality classes of the needles.

III. INTERACTIONS OF INFINITE AND SEMI-INFINITE NEEDLES

A. Force between a semi-infinite and an infinite needle

In this and subsequent sections we use the notation $z = r_x + i r_y$ and $w = \rho_u + i\rho_v$ for the complex variables z and w and their real and imaginary parts.

The conformal transformation $z(w)$, where

$$z'(w) = \mathcal{A}e^{i\alpha} w^{-\alpha/\pi - 1}(w - 1), \tag{3.1}$$

$$z(w) = \pi \mathcal{A}e^{i\alpha} w^{-\alpha/\pi}\left(\frac{w}{\pi - \alpha} + \frac{1}{\alpha}\right), \tag{3.2}$$

$\mathcal{A}$ is a positive real constant, and $0 < \alpha < \pi$, considered in Sec. 12.1 of Kober [47], maps the upper half w plane, with semi-infinite needles along the positive and negative u axes, onto the upper half z plane with two transformed needles. Needle II, the image of the negative u axis, is infinitely long and corresponds to the entire x axis. Needle I, the image of the positive u axis, is semi-infinite and extends from the point

$$z(1) = \frac{\pi^2}{\alpha(\pi - \alpha)}\mathcal{A}e^{i\alpha} \tag{3.3}$$

to ∞, forming an angle α with the x axis.

The integrand in expressions (2.3)–(2.5) for the Casimir force follows from Eqs. (2.2) and (3.1) and the corresponding stress tensor [48,49],

$$\langle T(w)\rangle = \frac{\tilde{t}}{w^2} = \frac{\left(0,0,\frac{1}{2},\frac{1}{16}\right)}{w^2}, \tag{3.4}$$

for $(OO, ++, +-, O+)$ boundary conditions on the two needles and is given by

$$z'(w)\,\langle T(z)\rangle = -\frac{e^{-i\alpha}}{48\pi^2\mathcal{A}}\frac{w^{\alpha/\pi-1}}{(w-1)^3}[\alpha(2\pi-\alpha)w^2 - 2(2\pi-\alpha)(\pi+\alpha)w + \pi^2 - \alpha^2 - 48\pi^2\tilde{t}(w-1)^2]. \tag{3.5}$$

In Eq. (2.4) integrating clockwise along the edges of needle I in the z plane (path $\mathcal{C}_\mathrm{I}$) corresponds to integrating along the u axis from $w = 0$ to $+\infty$ in the w plane, passing above the pole at $w = 1$ (path $\mathcal{C}$). Combining Eqs. (2.4) and (3.5), evaluating the integral, and making use of Eqs. (2.3) and (3.3), we obtain $f_x = 0$, as expected since needle II is infinite, and [50]

$$\tau = -\frac{f_y}{k_B T} = \frac{1}{96\, r_y(1)}\frac{(2\pi-\alpha)(\pi+\alpha) - 96\pi^2\tilde{t}}{\alpha(\pi-\alpha)}. \tag{3.6}$$

Here $r_y(1) = \mathrm{Im}[z(1)]$ is the distance of the tip of needle I from needle II, and we have used the relation $r_y(1) = \pi^2\mathcal{A}(\sin\alpha)/[\alpha(\pi-\alpha)]$, which follows from Eq. (3.3).

As expected, f_y in Eq. (3.6) is an even function of the deviation $\gamma = \alpha - \frac{1}{2}\pi$ from perpendicular orientation of the needles and diverges in the limit $\gamma \to \pm\frac{1}{2}\pi$, corresponding to parallel needles. From the values of $\tilde{t}$ in Eq.(3.4), it follows that the force between the needles is attractive for OO and $++$ boundaries and repulsive for $+-$ and $O+$ boundaries, with the strongest force in the $+-$ case.

B. Force between two semi-infinite needles

The conformal transformation $w(z)$, where

$$z'(w) = \mathcal{B}e^{i\alpha} w^{-\alpha/\pi - 1}(w - 1)(w + b), \tag{3.7}$$

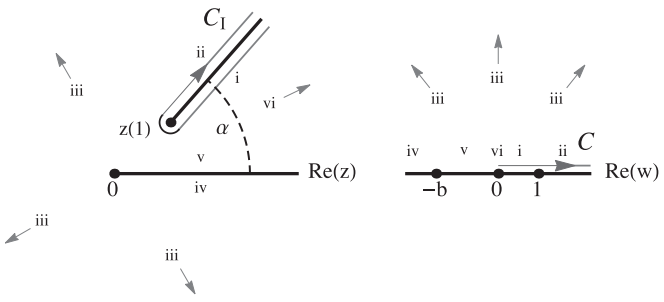

FIG. 1. The configuration of the semi-infinite needles I [with end point $z(1)$] and II (with end point 0) in the full z plane, shown on the left, is generated by the conformal mapping (3.8) from the upper half w plane with needles I and II on the positive and negative real axis, respectively, shown on the right. The two edges of needles I and II in the z plane and their preimages in the upper half w plane are denoted by i, ii and iv, v, respectively. The neighborhoods of $z = \infty$ denoted by iii and vi correspond to the neighborhoods of $w = \infty$ and $w = 0$, respectively, in the upper half w plane. The integration contour $\mathcal{C}_\mathrm{I}$ enclosing needle I and its preimage $\mathcal{C}$ play a role in the calculation of the force and torque, as discussed in Secs. II and III.

$$z(w) = \pi\mathcal{B}\Bigg[e^{i\alpha}w^{-\alpha/\pi+1}\left(\frac{w}{2\pi-\alpha}+\frac{b-1}{\pi-\alpha}+\frac{b}{\alpha w}\right) - b^{-\alpha/\pi+1}\left(\frac{b}{2\pi-\alpha}-\frac{b-1}{\pi-\alpha}+\frac{1}{\alpha}\right)\Bigg], \tag{3.8}$$

where $\mathcal{B}$ and b are positive real constants and $0 < \alpha < \pi$, considered in Sec. 12.3 of Kober [47] and shown schematically in Fig. 1, maps the upper half w plane, with semi-infinite needles along the positive and negative u axes, onto the full z plane with two embedded semi-infinite needles. Needle II, the image of the negative u axis, coincides with the positive x axis. Needle I, the image of the positive u axis, extends from the point

$$z(1) = -\mathcal{B}\pi^2\frac{[\alpha - b(2\pi-\alpha)]e^{i\alpha} + b^{-\alpha/\pi+1}(2\pi-\alpha-b\alpha)}{\alpha(\pi-\alpha)(2\pi-\alpha)} \tag{3.9}$$

to ∞, forming an angle α with needle II.

The integrand in expressions (2.3)–(2.5) for the Casimir force follows from Eqs. (2.2), (3.7), and (3.4) and is given by

$$z'(w)\langle T(z)\rangle = \frac{e^{-i\alpha}}{48\pi^2\mathcal{B}}\frac{w^{\alpha/\pi-1}}{(w-1)^3(w+b)^3}\{(3\pi-\alpha)(\pi-\alpha)w^4 + 2(1-b)\alpha(3\pi-\alpha)w^3 + [-\alpha(2\pi-\alpha) + 2b(5\pi^2+4\pi\alpha-2\alpha^2) - b^2\alpha(2\pi-\alpha)]w^2 - 2b(1-b)(2\pi-\alpha)(\pi+\alpha)w - b^2(\pi^2-\alpha^2) + 48\pi^2\tilde{t}(w-1)^2(w+b)^2\}. \tag{3.10}$$

Integrating along path $\mathcal{C}$ in Eq. (2.4) again amounts to integrating along the u axis from $w = 0$ to $+\infty$ in the w plane, passing above the pole at $w = 1$. Combining Eqs. (2.4) and (3.10), evaluating the integral, and making use of Eq. (2.3), we obtain [50]

$$\tau = -\frac{f_y + if_x}{k_BT} = \frac{1}{96\pi^2\mathcal{B}(1+b)^3\sin\alpha}\{[\alpha(3\pi-\alpha) + 2(3\pi-\alpha)(\pi+\alpha)b + (2\pi-\alpha)(\pi+\alpha)b^2 - 96\pi^2(1+b)^2\tilde{t}] + e^{-i\alpha}b^{\alpha/\pi-1}[(2\pi-\alpha)(\pi+\alpha) + 2(3\pi-\alpha)(\pi+\alpha)b + \alpha(3\pi-\alpha)b^2 - 96\pi^2(1+b)^2\tilde{t}]\}, \tag{3.11}$$

where the parameters $\mathcal{B}$ and b are related to the end point $r_x(1)$,$r_y(1)$ of needle I by Eq. (3.9).

Since needle II corresponds to the positive x axis, one expects to recover the results of the preceding section, in which needle II is infinite, in the limit $r_x(1) \to +\infty$ with $r_y(1)$ and α fixed. According to Eq. (3.9) this limit is achieved on substituting $\mathcal{B} = \mathcal{A}/b$ in the equation and then taking the limit $b \to \infty$ with $\mathcal{A}$ fixed. In this limit the derivative (3.7) reduces to Eq. (3.1), the integrand (3.10) reduces to (3.5), and the Casimir force (3.11) reduces to (3.6).

C. Needles with nonuniform boundary conditions

All of the results of Sec. III B are based on the stress tensor $\langle T(w)\rangle$ of Eq. (3.4) for boundary conditions that change only at $w = 0$ and are uniform along the positive and the negative u axis, which are the preimages of the two edges of needles I and II, respectively (see Fig. 1). Thus, the needles I and II of Sec. III B are allowed to have different boundary conditions, but each needle has the same boundary condition along both of its edges. Beginning instead with the stress tensor $\langle T(w)\rangle = \tilde{t}/(w-1)^2$ for boundary conditions that change only at $w = 1$ (see again Fig. 1) enables us to study the case in which needle I has different universality classes along its two edges while II has the same boundary condition on both edges.

In Appendix D we derive $\langle T(w)\rangle$ for an arbitrary number of changes between surface universality classes + and − at arbitrary points on the u axis. Using this result, we evaluate the interaction between two semi-infinite needles both with different edges, and, on using the transformation $z(w)$ of Sec. III A, the interaction of a semi-infinite needle and an infinite boundary line with "chemical steps" [39].

IV. INTERACTIONS OF NEEDLES OF FINITE LENGTH

In this section the approach for infinite and semi-infinite needles is extended to needles of finite length. The region outside two finite needles, which is doubly connected, is generated from an annulus bounded by two concentric circles, for which the thermal average of the stress tensor is known. The mapping is illustrated schematically in Fig. 2.

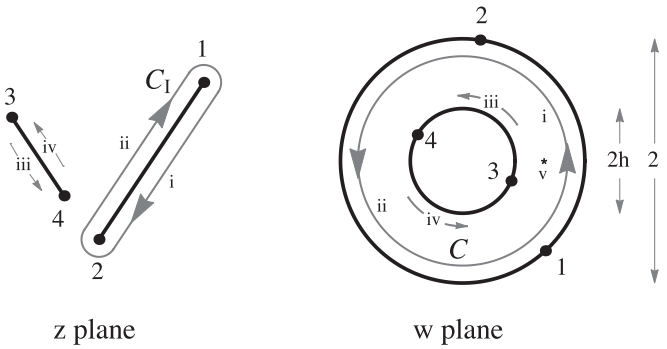

FIG. 2. The configuration of two finite needles in the full z plane, shown on the left, is generated by the conformal mapping with derivative (4.2) from the annulus $h < |w| < 1$ shown on the right. The labels 1, 2 and 3, 4 denote the end points z_1, z_2 and z_3, z_4 of needles I and II in the z plane, respectively, and their preimages w_1, w_2 and w_3, w_4. The edges of needles I and II in the z plane and their preimages in the w plane are denoted by i, ii and iii, iv, respectively. The point $w = c \equiv Ch^{1/2}$ in the annulus labeled by v is mapped onto $z = \infty$ by the transformation. The integration contour $\mathcal{C}_I$ enclosing needle I and its preimage $\mathcal{C}$ as well as the concentric circle $\mathcal{C}_c$ passing through the point $w = c$ play a role in the calculation of the force and torque, as discussed in Secs. II and IV and Appendix B 1 a.

A. Two needles of finite length

1. Conformal mapping

An arbitrary configuration of two non-overlapping needles I and II with finite lengths $D_{\rm I}$ and $D_{\rm II}$ in the z plane can be generated by a conformal transformation $z(w)$ of the Schwarz-Christoffel type, which maps the interior of the annulus $h < |w| < 1$ in the $w \equiv |w|e^{i\varphi}$ plane onto the region outside the two needles in the z plane. As illustrated in Fig. 2, the outer and inner boundary circles of the annulus map onto needles I and II, respectively, and the points $w_1 = e^{i\varphi_1}, w_2 = e^{i\varphi_2}$ and $w_3 = he^{i\varphi_3}, w_4 = he^{i\varphi_4}$ map onto the end points z_1, z_2 and z_3, z_4 of the needles. The corresponding mapping is a special case of the mapping onto the region outside two nonoverlapping polygons derived by Akhiezer in 1928 and given at the end of Sec. 48 of Ref. [51]. In the special case in which the polygons reduce to needles, the mapping $z(w)$ has the derivative

$$z'(w) = \frac{\mu}{w^2}\,\frac{\prod_{\ell=1}^{4}\vartheta_1[(2\pi i)^{-1}\ln(w/w_\ell)]}{\vartheta_1^2[(2\pi i)^{-1}\ln(w/c)]\,\vartheta_1^2[(2\pi i)^{-1}\ln(wc)]}, \tag{4.1}$$

in terms of the elliptic theta functions ϑ_1 with the nome h and constants μ and c defined in Ref. [51].

Substituting $c = Ch^{1/2}$, $\mu = (w_1w_2w_3w_4)^{-1/2}A$ in Eq. (4.1), and using the expression for ϑ_1 in Table IX of [51], we obtain the useful product representation

$$z'(w) = \frac{A}{w^2}\prod_{k=1}^{\infty}\frac{\prod_{\ell=1}^{4}(1-h^{2k-2}w/w_\ell)(1-h^{2k}w_\ell/w)}{(1-h^{2k-5/2}w/C)^2(1-h^{2k+1/2}C/w)^2(1-h^{2k-3/2}wC)^2[1-h^{2k-1/2}/(wC)]^2}. \tag{4.2}$$

We will see that $h \ll 1$ for needles short in comparison with their separation, and in this regime the representation (4.2) is especially convenient [52].

In the mapping with derivative (4.2), shown schematically in Fig. 2, the complex constant A in Eq. (4.2) corresponds to a homogeneous rotation and dilatation, and the positive real constant C, with $h^{1/2} < C < h^{-1/2}$, characterizes the value $Ch^{1/2}$ of w, which is mapped to $z = \infty$. The segments i, ii and iii, iv of the outer and inner boundary circles in Fig. 2, which are separated by w_1, w_2 and w_3, w_4, respectively, map onto the two edges of needles I and II in the z plane. This follows from the changes dz corresponding to displacements $dw = d(e^{i\varphi})$ and $dw = hd(e^{i\varphi})$ along the outer and inner boundaries of the annulus, for which Eq. (4.2) implies

$$dz = \frac{iA}{h}C^2e^{-i(\varphi_3+\varphi_4)}\,\mathcal{G}(\varphi;\varphi_1,\varphi_2)\mathcal{P}(\varphi;\,\varphi_1,\varphi_2;\,\varphi_3,\varphi_4;\,C;\,h)d\varphi \tag{4.3}$$

and

$$dz = \frac{iA}{h}\,\mathcal{G}(\varphi;\varphi_3,\varphi_4)\mathcal{P}(\varphi;\,\varphi_3,\varphi_4;\,\varphi_1,\varphi_2;\,C^{-1};\,h)d\varphi, \tag{4.4}$$

respectively. Here

$$\begin{aligned}\mathcal{G}(\varphi;\varphi_J,\varphi_K) &= e^{-i\varphi}(1-e^{i(\varphi-\varphi_J)})(1-e^{i(\varphi-\varphi_K)})\\ &= -4e^{-i(\varphi_J+\varphi_K)/2}\sin\frac{\varphi-\varphi_J}{2}\sin\frac{\varphi-\varphi_K}{2}\end{aligned} \tag{4.5}$$

and

$$\mathcal{P}(\varphi;\,\varphi_1,\varphi_2;\,\varphi_3,\varphi_4;\,C;\,h) \equiv \prod_{k=1}^{\infty}\frac{\prod_{n=1,2}|1-h^{2k}e^{i(\varphi-\varphi_n)}|^2\prod_{m=3,4}|1-h^{2k-1}e^{i(\varphi-\varphi_m)}|^2}{|1-h^{2k-1/2}C^{-1}e^{i\varphi}|^4|1-h^{2k-3/2}Ce^{i\varphi}|^4}, \tag{4.6}$$

which is always positive.

As φ varies, the argument of dz in Eq. (4.3) stays constant except at $\varphi = \varphi_1$ and $\varphi = \varphi_2$ where, due to the factor $\mathcal{G}(\varphi;\varphi_1,\varphi_2)$, it changes by π. This corresponds to constant slopes along the two edges of needle I with end points z_1 and z_2. Analogous results for needle II follow from Eq. (4.4).

Moreover, moving counterclockwise inside the annulus close to the outer and inner boundary circle corresponds to encircling needle I clockwise and needle II counterclockwise, respectively, in the z plane (see Fig. 2). This is most easily verified near the needle tips z_ℓ, where, due to Eq. (4.2), $dz \equiv z'(w)dw = \text{const} \times (w - w_\ell)dw$, since $w - w_\ell$ turns 180° clockwise and counterclockwise, respectively, on passing point w_ℓ on the outer and inner boundary.

Without loss of generality and for later convenience we assume

$$-\pi < \varphi_\ell \leqslant \pi, \quad \ell = 1,2,3,4, \tag{4.7}$$

for the arguments of the four preimages w_ℓ of the needle ends.

The mapping $z = z(w)$ is required to be single valued, so that the displacement $z(w_a) - z(w_b) = \int_{w_b}^{w_a}(dz/dw)dw$ for any two points w_a and w_b in the annulus is independent of the integration path. For $w_a = w_b$ the integral must vanish, even if the path encloses the inner boundary circle or the singularity at $w = Ch^{1/2}$. To ensure this, we require that the

integrals

$$\int_{\varphi=-\pi}^{\varphi=\pi}\left(\frac{dz}{dw}dw\right)_{w=e^{i\varphi}}=0,\quad \int_{\varphi=-\pi}^{\varphi=\pi}\left(\frac{dz}{dw}dw\right)_{w=he^{i\varphi}}=0, \tag{4.8}$$

around the outer and inner boundary circles vanish. On inserting (4.3)–(4.6) in Eq. (4.8) and discarding φ-independent complex factors, the conditions (4.8) imply the vanishing of two real functions of the six real parameters $\varphi_1,\ldots,\varphi_4,C,h$. This leaves four independent parameters (apart from the complex constant A), consistent with the four degrees of freedom needed to specify (apart from homogeneous translations, rotations, and dilatations) a configuration of two needles, for example, the two lengths and the two angles the needles form with the vector between their midpoints. According to Eqs. (4.3) and (4.4), the second of the conditions (4.8) follows from the first on exchanging the pairs φ_1,φ_2 and φ_3,φ_4 and replacing C with C^{-1}. This leads from one allowed parameter set to another. Explicit expressions for small h are given in Eqs. (4.16) below.

In conformity with above remarks, we use the notation

$$\begin{aligned} z_1-z_2=z_{12}&=|z_{12}|e^{i\Phi_{12}}\equiv D_{\rm I}e^{i\Phi_{\rm I}},\\ z_3-z_4=z_{34}&=|z_{34}|e^{i\Phi_{34}}\equiv D_{\rm II}e^{i\Phi_{\rm II}},\\ (z_1+z_2)/2=z_{\rm I},&\quad (z_3+z_4)/2=z_{\rm II}, \end{aligned} \tag{4.9}$$

and

$$z_{\rm I}-z_{\rm II}=z_{\rm I,II} \tag{4.10}$$

for the needle vectors, the positions of their midpoints, and their separation vector.

The needle vectors z_{12} and z_{34} follow from the first and second integrals in Eq. (4.8) on replacing the lower and upper limits $-\pi$ and π with φ_2 and φ_1 and with φ_4 and φ_3, respectively. This yields

$$\begin{aligned} z_{12}&=e^{-i(\varphi_3+\varphi_4)}(iA/h)C\mathcal{N}(\varphi_1,\varphi_2;\,\varphi_3,\varphi_4;\,C;\,h),\\ z_{34}&=(iA/h)C\mathcal{N}(\varphi_3,\varphi_4;\,\varphi_1,\varphi_2;\,C^{-1};\,h), \end{aligned} \tag{4.11}$$

where, on using Eqs. (4.5) and (4.6),

$$\begin{aligned} &\mathcal{N}(\varphi_1,\varphi_2;\,\varphi_3,\varphi_4;\,C;\,h)\\ &\quad=e^{-i(\varphi_1+\varphi_2)/2}\mathrm{sgn}(\varphi_1-\varphi_2)P(\varphi_1,\varphi_2;\,\varphi_3,\varphi_4;\,C;\,h). \end{aligned} \tag{4.12}$$

Here

$$\begin{aligned} &P(\varphi_1,\varphi_2;\,\varphi_3,\varphi_4;\,C;\,h)\\ &\quad=4C\left|\int_{\varphi_2}^{\varphi_1}d\varphi\,\sin\frac{\varphi-\varphi_1}{2}\right.\\ &\qquad\left.\times\,\sin\frac{\varphi-\varphi_2}{2}\mathcal{P}(\varphi;\,\varphi_1,\varphi_2;\,\varphi_3,\varphi_4;\,C;\,h)\right|, \end{aligned} \tag{4.13}$$

where $\mathcal{P}$ is given in Eq. (4.6).

For the angle enclosed by the two needles, Eqs. (4.11)–(4.13) imply the simple relation

$$e^{i(\Phi_{12}-\Phi_{34})}=e^{-i(\varphi_1+\varphi_2+\varphi_3+\varphi_4)/2}\,\mathrm{sgn}(\varphi_1-\varphi_2)\,\mathrm{sgn}(\varphi_3-\varphi_4). \tag{4.14}$$

Note that in the sector (4.7) the complex numbers $e^{-i(\varphi_1+\varphi_2)/2}$ and $e^{-i(\varphi_3+\varphi_4)/2}$ and the signs of $\varphi_1-\varphi_2$ and $\varphi_3-\varphi_4$ are uniquely determined by w_1,w_2 and by w_3,w_4, respectively.

For the ratio of needle lengths, Eqs. (4.11)–(4.13) yield

$$\begin{aligned} D_{\rm I}/D_{\rm II}&\equiv|z_{12}|/|z_{34}|\\ &=P(\varphi_1,\varphi_2;\,\varphi_3,\varphi_4;\,C;\,h)/P(\varphi_3,\varphi_4;\,\varphi_1,\varphi_2;\,C^{-1};\,h), \end{aligned} \tag{4.15}$$

so that exchanging the pairs φ_1,φ_2 and φ_3,φ_4 and replacing C with C^{-1} changes $D_{\rm I}/D_{\rm II}$ to its inverse. For the special parameter sets $C=1$ with either $\varphi_3=\varphi_1$, $\varphi_4=\varphi_2$ or $\varphi_3=-\varphi_1$, $\varphi_4=-\varphi_2$, the two needles have equal lengths $|z_{12}|=|z_{34}|$. For the second set this follows from Eq. (4.6), which implies $\mathcal{P}(\varphi;\,\varphi_1,\varphi_2;\,-\varphi_1,-\varphi_2;\,C;\,h)=\mathcal{P}(-\varphi;\,-\varphi_1,-\varphi_2;\,\varphi_1,\varphi_2;\,C;\,h)$, yielding $P(\varphi_1,\varphi_2;\,-\varphi_1,-\varphi_2;\,1;\,h)=P(-\varphi_1,-\varphi_2;\,\varphi_1,\varphi_2;\,1;\,h)$.

We mention another, rather obvious, property of the transformation (4.2): Changing the parameters from $(\varphi_1,\varphi_2;\varphi_3,\varphi_4;C;h)$ to $(-\varphi_1,-\varphi_2;-\varphi_3,-\varphi_4;C;h)$, i.e., changing all four w_ℓ to $w_\ell^\star$, leads from one single-valued mapping to another, in which the needle configuration is changed from $(z_{12},z_{34};z_{\rm I,II})$ to $(z_{12}^\star,z_{34}^\star;z_{\rm I,II}^\star)$, assuming A is real. Here and below an asterisk denotes complex conjugation.

Except for the enclosed angle it is, in general, not obvious how to choose the parameters in the transformation (4.2) to generate a given configuration of the two needles. Here we list some simple classes (A)–(E) of needle configurations which require only a parameter search in a reduced subspace. We choose the vector between the needle centers to be parallel to the real axis, so that $z_{\rm I,II}=|z_{\rm I,II}|$, with needle I to the right of needle II, and refer to the ratios $|z_{12}|/|z_{\rm I,II}|$ and $|z_{34}|/|z_{\rm I,II}|$ as the "reduced needle lengths."

(A) *Symmetric-perpendicular configurations of two needles of arbitrary reduced lengths with the symmetry of the letter T, corresponding to Fig. 3(A).* To be specific, we consider the needle vectors $z_{12}=i|z_{12}|$ and $z_{34}=-|z_{34}|$. These configurations can be generated from parameters in the subspace $(\varphi_1,\varphi_2,\varphi_3,\varphi_4)=(-|\varphi_1|,|\varphi_1|,0,\pi)$, where $w_2=w_1^\star$, $w_3=h$, $w_4=-h$. The reason is that on choosing A real, the integrals over (4.2) from $w=w_2$ to $w=w_3$ and from $w=w_1$ to $w=w_3$ (and likewise those from $w=w_2$ to $w=w_4$ and from $w=w_1$ to $w=w_4$) are complex conjugates, implying the properties $z_2-z_3=(z_1-z_3)^\star$ and $z_2-z_4=(z_1-z_4)^\star$. Since the expression multiplying $d\varphi$ in Eq. (4.4) is an odd function of φ, the integral in Eq. (4.8) around the inner circle vanishes for all values of φ_1, C, and h. The requirement that the integral over the outer circle vanish implies a relation $\varphi_1=\psi(C,h)$, leaving C and h free to generate given values for the two reduced needle lengths. Note, finally, that the general enclosed angle relation (4.14) is satisfied, since both of its sides equal $-i$ in the above subspace of parameters in the annulus and for the needle configuration in which $e^{i\Phi_{12}}=i$, $e^{i\Phi_{34}}=-1$.

(B) *Symmetric-parallel configurations of two needles with arbitrary reduced lengths perpendicular to the vector between their centers, corresponding to Fig. 3(B).* To be specific, we choose $z_{12}=i|z_{12}|$ and $z_{34}=i|z_{34}|$, so that the needles are parallel to the imaginary axis. These configurations are

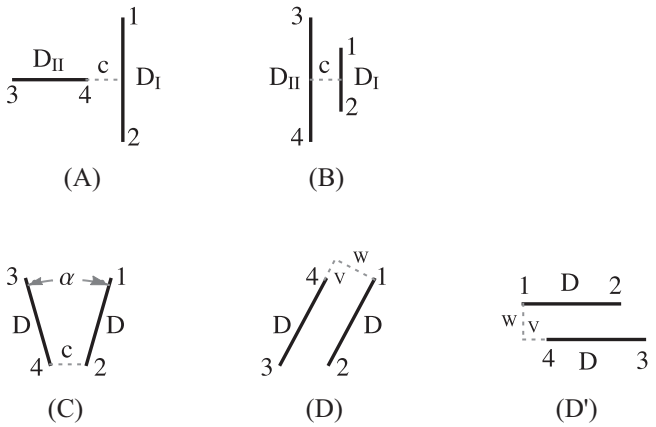

FIG. 3. Simple needle configurations described in Sec. IV A 1, for which the six mapping parameters C, h, φ_1,..., φ_4 of the conformal mapping are restricted to subspaces of lower dimension. The labels 1, 2 and 3, 4 denote the end points z_1, z_2 and z_3, z_4 of needles I and II, respectively. Configurations (A)–(D) are oriented as in Sec. IV A 1, with the line from the midpoint $z_{\rm II}$ of needle II to the midpoint $z_{\rm I}$ of needle I parallel to the x or horizontal axis. Configuration (D′) is the same as (D), apart from a rotation to orient the needles along the x axis. Our results for the force and torque in configurations (A), (B), (C), and (D′), as functions of the needle lengths $D_{\rm I}$, $D_{\rm II}$, D, the minimum separation c, the angle α between the needles, and the distances W and V, are shown in Figs. 4–8.

generated by $(\varphi_1,\varphi_2,\varphi_3,\varphi_4) = (-|\varphi_1|,|\varphi_1|,-|\varphi_3|,|\varphi_3|)$, i.e., by $w_2 = w_1^\star$, $w_4 = w_3^\star$, since, as in case (A), for real values of the parameter A there is reflection symmetry about the real axis, and the integrals over (4.2) from $w = w_2$ to $w = w_3$ and from $w = w_1$ to $w = w_4$ (and likewise those from $w = w_2$ to $w = w_4$ and from $w = w_1$ to $w = w_3$) are complex conjugates, implying the properties $z_2 - z_3 = (z_1 - z_4)^\star$ and $z_2 - z_4 = (z_1 - z_3)^\star$. The vanishing of the two integrals (4.8) implies relations $\varphi_1 = \chi(C,h)$ and $\varphi_3 = \omega(C,h)$, and the two parameters C and h can be adjusted to generate the two reduced needle lengths. The enclosed angle relation (4.14) is satisfied, with both sides equal to 1.

(C) *Configurations of two needles which are mirror symmetric about the imaginary axis, corresponding to Fig. 3(C).* Here $z_{12} = |z_{12}|e^{i\Phi_{12}}$, $z_{34} = |z_{12}|e^{i(\pi-\Phi_{12})} = -z_{12}^\star$. The needles have the same arbitrary reduced length, and with no loss of generality the angle $\alpha \equiv \pi - 2\Phi_{12}$ between them can be restricted to values between 0 and π.

(D) *Nonsymmetric parallel needles of equal length, corresponding to Fig. 3(D).* Here $z_{12} = |z_{12}|e^{i\Phi_{12}} = -z_{34}$ (see [53] for an alternate representation), where the angle Φ_{12} is arbitrary [54].

The needle configurations (C) and (D) are generated by $C = 1$ in both cases and by $\varphi_3 = \varphi_1$, $\varphi_4 = \varphi_2$ in case (C) and $\varphi_3 = -\varphi_1$, $\varphi_4 = -\varphi_2$ in case (D). In both subspaces the lengths $|z_{12}|$, $|z_{34}|$ of the two needles are equal for arbitrary values of the three parameters φ_1, φ_2, and h, and the two conditions in Eq. (4.8) reduce to a single condition [see the remarks below Eqs. (4.15) and (4.8), respectively]. This leaves two free parameters, which can be adjusted to generate the given common reduced length of the needles and the angle Φ_{12} needle I forms with the distance vector $z_{\rm I,II}$ between the needle midpoints. In case (C) the enclosed angle relation (4.14) predicts $e^{2i\Phi_{12}} = -e^{-i(\varphi_1+\varphi_2)}$, and in case (D) it is satisfied since both sides equal -1.

Typical configurations from classes (A)–(D) are shown in Fig. 3. Classes (B), (C), and (D) encompass two particularly simple needle configurations for which the conformal mapping can be found in the literature.

(i) Collinear needles of equal length with $\Phi_{12} = 0$ and $\Phi_{34} = \pi$ are generated by $(w_1, w_2, w_3, w_4) = (1, -1, h, -h)$ and $C = 1$, which is a special case of both (C) and (D). In this case the two conditions (4.8) are satisfied, since both integrands (4.3) and (4.4) are odd functions of φ. The reduced needle length is determined by the parameter h. The corresponding conformal transformation $z(w)$ is discussed in Refs. [47,51].

(ii) Symmetric-parallel needles of equal length with $\Phi_{12} = \Phi_{34} = \pi/2$, i.e., a configuration with the symmetry of the letter H: This needle geometry is generated by $(\varphi_1, \varphi_2, \varphi_3, \varphi_4) = (-|\varphi_1|, |\varphi_1|, -|\varphi_1|, |\varphi_1|)$ and $C = 1$ and is a special case of (B), (C), and (D) [53]. The two parameters $|\varphi_1|$ and h are chosen to satisfy the two *identical* conditions (4.8) and to generate a given reduced needle length. The conformal transformation leading to this needle configuration is considered in some detail in Refs. [47,51].

(E) *Widely separated needles.* Needles with lengths $|z_{12}|$, $|z_{34}|$ much smaller than their separation $|z_{\rm I,II}|$ are generated by Eq. (4.2) on choosing C of order 1 and $h \ll 1$. While detailed results for the mapping in cases (A)–(D) for needles of arbitrary length can only be obtained numerically (see Sec. V), for widely separated needles analytic results may be derived by expanding in terms of the small parameter $h^{1/2}$. Using the two conditions (4.8) to express φ_2 and φ_4 in terms of the four free parameters φ_1, φ_3, C, and h leads to

$$\varphi_2 = \varphi_1 - \pi\,\mathrm{sgn}(\varphi_1 - \varphi_2) + G(\varphi_1;\,\varphi_3;\,C;\,h), \quad \varphi_4 = \varphi_3 - \pi\,\mathrm{sgn}(\varphi_3 - \varphi_4) + G(\varphi_3;\,\varphi_1;\,C^{-1};\,h), \tag{4.16}$$

where

$$G(\varphi_1;\,\varphi_3;\,C;\,h) = 4h^{1/2}C\sin\varphi_1 + 4hC^2\sin(2\varphi_1) - 4h^{3/2}\left\{\tfrac{1}{3}C^3(7 - 16\cos^2\varphi_1)\sin\varphi_1 + C^{-1}[2\sin\varphi_3\cos(\varphi_1 - \varphi_3) - \sin\varphi_1]\right\}, \tag{4.17}$$

apart from terms of order h^2. Equations (4.16) reflect the symmetry mentioned below Eq. (4.8) and are consistent with our assumption (4.7). The dependence of the needle configuration on the four free parameters is given by

$$\frac{z_{12}}{z_{\rm I,II}} = R(\varphi_1, \varphi_3, C, h), \quad \frac{z_{34}}{z_{\rm I,II}} = -R(\varphi_3, \varphi_1, C^{-1}, h)^\star, \tag{4.18}$$

where

$$R(\varphi_1,\varphi_3,C,h)=4Ch^{1/2}e^{-i\varphi_1}\{1-2ih^{1/2}C\sin\varphi_1-h[C^{-2}(1+2e^{2i\varphi_3})+C^2]+\mathcal{O}(h^{3/2})\}. \tag{4.19}$$

The symmetry embodied in Eqs. (4.18), which we have checked within the h expansion, is expected to hold for arbitrary h. Starting from a set $(\varphi_1,\varphi_2;\varphi_3,\varphi_4;C,h)$ of six parameters obeying the two conditions (4.8) and replacing it with $(\varphi_3,\varphi_4;\varphi_1,\varphi_2;C^{-1},h)$ corresponds to reflecting the two needle configuration about the symmetry axis of the needle midpoints, i.e., about the imaginary axis of the z plane if we choose $z_{\rm I}=|z_{\rm I}|$ and $z_{\rm II}=-|z_{\rm I}|$ by adjusting A appropriately. This is consistent with the above discussion of the reflection-invariant needle configuration (C), for which $C=1$.

For the ratio of needle vectors, Eqs. (4.18) and (4.19) imply

$$\frac{z_{12}}{z_{34}}=C^2[1+2h(C^2\cos^2\varphi_1-C^{-2}\cos^2\varphi_3)]\exp\left(-i\left\{\varphi_1+\varphi_3+\pi+\tfrac{1}{2}[G(\varphi_1;\varphi_3;C;h)+G(\varphi_3;\varphi_1;C^{-1};h)]\right\}\right)+\mathcal{O}(h^{3/2}), \tag{4.20}$$

where the phase factor and modulus are consistent with the enclosed angle relation (4.14) and the ratio of needle lengths (4.15), respectively. We also note the relation

$$z_{\rm I,II}=A\,h^{-3/2}Ce^{-2i\varphi_3}\{1+2h^{1/2}C^{-1}(-e^{i\varphi_3}+e^{-i\varphi_3})+h[C^{-2}(2e^{2i\varphi_3}-3+4e^{-2i\varphi_3})+C^2(1+2e^{-2i\varphi_1})]+\mathcal{O}(h^{3/2})\}, \tag{4.21}$$

which determines the value of A needed to generate a given $z_{\rm I,II}=|z_{\rm I,II}|$.

2. *Force and torque*

The force and torque on needle I due to needle II can be evaluated using Eqs. (2.2)–(2.5) and (2.7)–(2.11), respectively. The stress tensor average in the annulus [55,56] was determined by Cardy [37] and can be written as

$$\langle T(w)\rangle\equiv\langle T(w)\rangle_{\rm annulus}=\frac{1}{2w^2}t(h), \tag{4.22}$$

where

$$t(h)\equiv h\frac{d}{dh}\ln\left(\{1+[(\mathcal{S}_{11}+\mathcal{S}_{21})/2,\mathcal{S}_{11},\mathcal{S}_{21},\mathcal{S}_{22}]\}\prod_{n=1}^{\infty}(1-h^{2n})^{-1}\right) \tag{4.23}$$

for the combinations OO, $++$, $+-$, $O+$ of universality classes of the two needles [49]. Here

$$\mathcal{S}_{pq}\equiv\mathcal{S}_{pq}(h)=\sum_{r=2}^{\infty}h^{(r^2-1)/24}\sin\frac{\pi pr}{3}\sin\frac{\pi qr}{4}\Big/\left(\sin\frac{\pi p}{3}\sin\frac{\pi q}{4}\right), \tag{4.24}$$

where the series converges for $h<1$. For the integration path $\mathcal{C}$ in Eqs. (2.5) and (2.11), which goes around the inner boundary circle counterclockwise, it is most convenient to use the circle $\mathcal{C}_c$ given by $w=Ch^{1/2}e^{i\varphi}$, which passes through the preimage $w=Ch^{1/2}$ of $z=\infty$.

Unlike the force and torque contributions $\tau^{(T)}$ and $\theta^{(T)}$ in Eqs. (2.5) and (2.11), which depend, via Eqs. (4.22)–(4.24), on the surface universality classes of the two needles, the contributions $\tau^{(S)}$ and $\theta^{(S)}$, which involve $z'(w)$ and the Schwarzian derivative (2.2), are solely determined by the geometric configuration of the needles and in this sense "hyperuniversal." This was already mentioned at the end of Sec. II, and it applies to the semi-infinite and infinite needles of Sec. III. The occurrence of a hyperuniversal term in the free energy of interaction of a noncircular particle with other particles in a near-critical two-dimensional system is well known from the SPOE. As discussed in Refs. [17,57] and Appendix B 2, the hyperuniversal interaction arises from the stress tensor in the operator expansion corresponding to the particle, in our case a needle. The hyperuniversal term in the expansion depends on the orientation of the needle, is proportional to the square of its length (which is the smallest power involving its orientation dependence), and reproduces the results corresponding to the $h\to 0$ contributions of $\tau^{(S)}$ and $\theta^{(S)}$, as we show in Eqs. (4.29)–(4.31).

In general, the force vector is neither parallel nor antiparallel to the vector $z_{\rm I,II}$ between the needle midpoints, as seen, for example, in Eq. (4.29). However, for the symmetric-perpendicular and -parallel configurations in (A) and (B) and for the mirror-symmetric configurations (C), the force clearly points along $z_{\rm I,II}$ or $-z_{\rm I,II}$. Detailed numerical results for force and torque in cases (A)–(D) are reported in Sec. V. Here we give a few analytic results for the case (E) of two short needles or, equivalently, two widely separated needles.

According to Eqs. (4.18) and (4.19), this regime corresponds to small h, and in leading order

$$\tau^{(T)}=\frac{2i}{z_{\rm I,II}}t(h\ll 1),\quad \tau^{(S)}=\frac{2i}{z_{\rm I,II}}h^2e^{2i(-\varphi_1+\varphi_3)}, \tag{4.25}$$

for the two contributions to the force on needle I in Eq. (2.3). For more details, see Eqs. (B1)–(B6) in Appendix B. On using (4.23) and (4.24), we obtain

$$t(h \ll 1) = [h, -h] \tag{4.26}$$

for needle pairs of type $[OO, O+]$, while for pairs of type $[++, +-]$

$$t(h \ll 1) = \frac{1}{8}[\sqrt{2}h^{1/8}/(1+\sqrt{2}h^{1/8}),\ -\sqrt{2}h^{1/8}/(1-\sqrt{2}h^{1/8})], \tag{4.27}$$

for h values which are small compared to 1 without requiring $h^{1/8}$ to be small. The force (f_x, f_y) on needle I in Eq. (2.3) is thus dominated by the contribution from $\tau^{(T)}$. In the remainder of this section we again assume that $z_{\mathrm{I,II}} \equiv |z_{\mathrm{I,II}}|$, so that the distance vector $z_{\mathrm{I,II}}$ between needle centers is parallel to the x axis. Using $h \to |z_{12}||z_{34}|/(16|z_{\mathrm{I,II}}^2|)$ due to (4.18) and (4.19), one finds

$$f_x/k_BT = -\frac{1}{|z_{\mathrm{I,II}}|} \times \left[\pm\frac{1}{8}\frac{D_\mathrm{I}D_\mathrm{II}}{|z_{\mathrm{I,II}}|^2},\ \pm\frac{1}{4}\frac{(D_\mathrm{I}D_\mathrm{II})^{1/8}}{|z_{\mathrm{I,II}}|^{1/4}} \Big/ \left(1 \pm \frac{(D_\mathrm{I}D_\mathrm{II})^{1/8}}{|z_{\mathrm{I,II}}|^{1/4}}\right)\right] \tag{4.28}$$

and $f_y/(k_BT) = 0$ for the force components in leading order. Here the upper and lower signs describe the needle universality classes $[OO, ++]$ and $[O+, +-]$, respectively, and $D_\mathrm{I} \equiv |z_{12}|$ and $D_\mathrm{II} \equiv |z_{34}|$ are the needle lengths introduced in Eq. (4.9). For needles with equal (unequal) universality classes the force is antiparallel (parallel) to the distance vector $z_{\mathrm{I,II}}$, i.e., attractive (repulsive), as expected. As in a multipole expansion, the shape anisotropy does not appear in the leading "monopole" contribution (4.28), in which the force is independent of the needle orientations Φ_{12} and Φ_{34}, but it appears in higher order in the needle lengths. Unlike the corresponding higher-order contributions from $\tau^{(T)}$, which also depend on the needle universality classes, the contributions from $\tau^{(S)}$ are hyperuniversal, as mentioned above. Equations (4.18) and (4.19) imply $e^{-i\varphi_1} \to e^{i\Phi_{12}}$ and $e^{i\varphi_3} \to -e^{i\Phi_{34}}$, and the lowest-order hyperuniversal term, given by the second expression in Eq. (4.25), leads to

$$\left(f_x^{(S)}, f_y^{(S)}\right)/(k_BT) = -\frac{D_\mathrm{I}^2 D_\mathrm{II}^2}{2^7|z_{\mathrm{I,II}}|^5}\{\cos[2(\Phi_{12}+\Phi_{34})],\ -\sin[2(\Phi_{12}+\Phi_{34})]\}. \tag{4.29}$$

As expected, the force is unchanged on rotating a needle through 180°.

We now turn from Eq. (4.29) to the hyperuniversal contribution $-\mathrm{Re}\,\theta^{(S)}$ to the reduced torque $\Theta/(k_BT)$, introduced in Eqs. (2.7)–(2.11). Calculating $\theta^{(S)}$ by means of the mapping (4.2), one obtains

$$\theta^{(S)} \to -ih^2 e^{2i(-\varphi_1+\varphi_3)}, \quad \mathrm{Re}\theta^{(S)} \to \frac{D_\mathrm{I}^2 D_\mathrm{II}^2}{2^8|z_{\mathrm{I,II}}|^4}\sin[2(\Phi_{12}+\Phi_{34})] \tag{4.30}$$

in leading order. For more details, see the paragraph containing Eqs. (B7) and (B8) in Appendix B.

A detailed discussion of the force and torque for two short needles, based on the SPOE, is given in Appendix B 2 a. With this entirely different approach we confirm the leading behavior (4.28) for the force and obtain

$$\delta F^{(\mathrm{hu})}/(k_BT) = -\frac{D_\mathrm{I}^2 D_\mathrm{II}^2}{2^{10}}\left(e^{2i(\Phi_{12}+\Phi_{34})}\frac{1}{z_{\mathrm{I,II}}^4} + \mathrm{c.c.}\right) \tag{4.31}$$

for the hyperuniversal (hu) contribution to the free energy of interaction [45] of the needles, which agrees with the results for the force components in Eq. (4.29) and the torque in Eq. (4.30).

B. Interaction of a finite and a semi-infinite needle

Consider the case in which needle 12 has a finite length $D_\mathrm{I} \equiv |z_{12}|$ but needle 34 is semi-infinite, with $z_3 = z_\mathrm{e}$ and $z_4 = \infty$. This needle geometry is generated by Eq. (4.2) in the limit $C = h^{1/2}$ and $w_4 = h$ in which the preimages w_4 and $Ch^{1/2}$ of $z = z_4$ and $z = \infty$, respectively, coincide, so that

$$z'(w) = \frac{A}{h^2}\prod_{k=1}^{\infty}\left[\frac{(1-h^{2k-3}e^{-i\varphi_\mathrm{e}}w)(1-h^{2k+1}e^{i\varphi_\mathrm{e}}/w)}{(1-h^{2k-3}w)^3(1-h^{2k+1}/w)^3}\prod_{n=1,2}(1-h^{2k-2}e^{-i\varphi_n}w)(1-h^{2k}e^{i\varphi_n}/w)\right]. \tag{4.32}$$

This implies

$$dz = (d\varphi)iA\,e^{-i\varphi_\mathrm{e}}\,\mathcal{G}(\varphi;\varphi_1,\varphi_2)\prod_{k=1}^{\infty}\frac{|1-h^{2k-1}e^{i(\varphi-\varphi_\mathrm{e})}|^2\prod_{n=1,2}|1-h^{2k}e^{i(\varphi-\varphi_n)}|^2}{|1-h^{2k-1}e^{i\varphi}|^6} \tag{4.33}$$

and

$$dz = -(d\varphi)\frac{iA}{h}\,e^{-i\varphi_\mathrm{e}/2}\,\frac{\sin[(\varphi-\varphi_\mathrm{e})/2]}{4\sin^3(\varphi/2)}\prod_{k=1}^{\infty}\frac{|1-h^{2k}e^{i(\varphi-\varphi_\mathrm{e})}|^2\prod_{n=1,2}|1-h^{2k-1}e^{i(\varphi-\varphi_n)}|^2}{|1-h^{2k}e^{i\varphi}|^6}, \tag{4.34}$$

for displacements $dw = d(e^{i\varphi})$ and $dw = hd(e^{i\varphi})$ around the outer and inner boundaries of the annulus, respectively. Here $\mathcal{G}$ is defined in Eq. (4.5), and $w_3 \equiv w_e = he^{i\varphi_e}$ is the preimage of z_e. The behavior (4.34) near $\varphi = 0$ implies that the semi-infinite needle extends from $z = z_e$ to $z = s|\infty|$ along the tangential unit vector $s = -i(A/|A|)e^{-i\varphi_e/2}\,\mathrm{sgn}\varphi_e$ with $\varphi_e \equiv \varphi_3$ obeying (4.7). For convenience we choose the semi-infinite needle to coincide with the positive real axis, i.e., $z_e = 0$ and $s = 1$, so that

$$A = i|A|e^{i\varphi_e/2}\mathrm{sgn}\varphi_e. \tag{4.35}$$

From Eq. (4.14) we obtain

$$e^{i\Phi_{12}} = -e^{-i(\varphi_1+\varphi_2+\varphi_e)/2}\,\mathrm{sgn}(\varphi_1-\varphi_2)\,\mathrm{sgn}\varphi_e, \tag{4.36}$$

since $\Phi_{34} = \pi$, $\varphi_4 = 0$, and $\varphi_3 = \varphi_e$.

Apart from homogeneous dilatations, the needle configuration is determined by three parameters: the length ratio $|z_{12}|/|z_I|$ and the two angles $\arg z_I$ and Φ_{12} which z_I and z_{12} form with the semi-infinite needle. Here $z_I \equiv r_{I,x} + ir_{I,y}$ is the vector from $z_e = 0$ to the midpoint of needle 12. Correspondingly, there are, apart from $|A|$, three independent mapping parameters. Since the derivative dz/dw is analytic in the interior of the annulus, imposing the requirement

$$I_{\mathrm{outer}} \equiv \int_{\mathcal{C}_{\mathrm{outer}}} dw(dz/dw) = 0 \tag{4.37}$$

on the four parameters $h, \varphi_1, \varphi_2, \varphi_e$ ensures that the mapping $z = z(w)$ is single valued.

Now consider the case of a finite needle which is much shorter than its distance from the closest point of the semi-infinite needle, so that $|z_{12}|^2 \ll |z_I|(|z_I| - r_{I,x})$. Explicit results for the force and torque in this regime can be obtained by expanding in terms of h and are expected to agree with the SPOE. In the remainder of this section this is checked in leading order.

For small h the constraint (4.37) reads

$$\varphi_2 = \varphi_1 - \pi\,\mathrm{sgn}(\varphi_1-\varphi_2) + 2h[3\sin\varphi_1 - \sin(\varphi_1-\varphi_e)] + \mathcal{O}(h^2), \tag{4.38}$$

yielding in terms of independent parameters the needle configuration

$$z_I \to \frac{|A|}{4h|\sin\varphi_e/2|}e^{-i\varphi_e}, \tag{4.39}$$

$$z_{12} \to -4|A|ie^{-i\varphi_1}e^{-i\varphi_e/2}\mathrm{sgn}\varphi_e, \tag{4.40}$$

to leading order in h. Since $ie^{-i\varphi_1}$ equals $e^{-i(\varphi_1+\varphi_2)/2}\mathrm{sgn}(\varphi_1-\varphi_2)$ in leading order [see Eq. (4.16)], Eq. (4.40) is consistent with (4.36). Equations (4.39) and (4.40) allow us to express $|A|, h, \varphi_1, \varphi_e$ in terms of needle parameters, and we note that

$$|A| \to |z_{12}|/4 \tag{4.41}$$

and

$$h \to \frac{1}{8}\frac{|z_{12}|}{\sqrt{2|z_I|(|z_I| - r_{I,x})}} \tag{4.42}$$

for use below.

The force (f_x, f_y) on the 12 needle follows from Eqs. (2.3) and (2.5) on substituting the derivative (4.32), integrating along a circle infinitesimally larger than the inner boundary circle of the annulus, avoiding the singularity at $w = w_e = he^{i\varphi_e}$.

The leading contribution comes from $\tau^{(T)}$ and is given by

$$\tau^{(T)}/t(h) \to \frac{1}{4|z_I|}\frac{e^{i\varphi_e/2}(e^{i\varphi_e}-3)}{\sin(\varphi_e/2)}, \tag{4.43}$$

yielding

$$[(f_x - if_y)/(k_BT)]/t(h) \equiv i\tau/t(h) \to -\frac{3z_I - |z_I|}{2z_I(z_I - |z_I|)}, \tag{4.44}$$

since $z_I/|z_I| \to e^{-i\varphi_e}$; see Eq. (4.39). The leading contribution to the force follows from Eq. (4.44) on replacing $t(h)$ with $t(h \ll 1)$ in Eqs. (4.26) and (4.27) and on replacing h with the right-hand side of Eq. (4.42). As in Eq. (4.28), the leading contribution is independent of the orientation Φ_{12} of the small needle. The leading dependence on orientation comes from $\tau^{(S)}$ in Eq. (2.5) in higher order in h. In Appendix B 2 b we use the SPOE to calculate the leading isotropic and angle-dependent contributions to the force and the leading contribution to the torque on the 12 needle. The SPOE prediction is in complete agreement with the h-expansion result for the force given in Eq. (4.44).

C. Interaction of a finite and an infinite needle

On setting $w_3 = w_4 = Ch^{1/2} = h$ in Eq. (4.2), both z_3 and z_4 become infinite, so that the 34 needle takes the form of an infinite needle or boundary line. For $A = -i|A|$, the infinite needle coincides with the boundary $\mathrm{Im}z = 0$ of the upper half plane. The derivative of the transformation is given by

$$z'(w) = -i|A|\frac{1}{h^2}\prod_{k=1}^{\infty} \times \frac{\prod_{n=1,2}(1 - h^{2k-2}e^{-i\varphi_n}w)(1 - h^{2k}e^{i\varphi_n}/w)}{(1-h^{2k-3}w)^2(1-h^{2k+1}/w)^2}, \tag{4.45}$$

so that

$$dz = (d\varphi)|A|\mathcal{G}(\varphi;\varphi_1,\varphi_2) \times \prod_{k=1}^{\infty}\frac{\prod_{n=1,2}|1-h^{2k}e^{i(\varphi-\varphi_n)}|^2}{|1-h^{2k-1}e^{i\varphi}|^4} \tag{4.46}$$

and

$$dz = -(d\varphi)\frac{|A|}{h}\frac{1}{4\sin^2(\varphi/2)} \times \prod_{k=1}^{\infty}\frac{\prod_{n=1,2}|1-h^{2k-1}e^{i(\varphi-\varphi_n)}|^2}{|1-h^{2k}e^{i\varphi}|^4} \tag{4.47}$$

for displacements $dw = d(e^{i\varphi})$ and $dw = hd(e^{i\varphi})$ along the outer and inner boundary circles, respectively. Thus, a counterclockwise path around the inner circle corresponds to a path along the real axis from $+\infty$ to $-\infty$, and a counterclockwise path around the outer circle to a clockwise path around the 12 needle along its edges. The function $\mathcal{G}$ is defined by Eq. (4.5).

As in the case (4.32) of a finite needle interacting with a semi-infinite needle, the constraint $I_{\text{outer}} = 0$ ensures that the mapping Eqs. (4.45) is single valued, so that only two of the three parameters h, φ_1, φ_2 are independent. They can be adjusted to fix the angle Φ_{12} between needle and boundary and the ratio of the length $|z_{12}|$ of the needle and its distance to the boundary. According to the argument leading to Eq. (4.14), the unit vector characterizing the direction of z_{12} is given by

$$e^{i\Phi_{12}} \equiv \frac{z_{12}}{|z_{12}|} = e^{-i(\varphi_1+\varphi_2)/2}\text{sgn}(\varphi_1 - \varphi_2). \tag{4.48}$$

1. Distant needle

A needle far from the boundary in comparison with its length corresponds to $h \ll 1$. The products in Eqs. (4.45)–(4.47) can be expanded in powers of h, and Eq. (4.37) yields

$$\begin{aligned} &\varphi_2 = \varphi_1 - \pi\,\text{sgn}(\varphi_1 - \varphi_2) + g(\varphi_1; h), \\ &g(\varphi_1; h) \equiv 4h\sin\varphi_1 + 4h^2\sin(2\varphi_1) + \mathcal{O}(h^3), \end{aligned} \tag{4.49}$$

which is consistent with the constraint (4.38) in Sec. IV B on setting $\varphi_e = 0$ there. For the vector z_{12} between the ends of the needle and for the distance $r_{I,y} \equiv \text{Im}z_I \equiv \text{Im}(z_1 + z_2)/2$ of the needle center from the boundary, one obtains

$$\begin{aligned} z_{12} &\to 4|A|(1 + 2h^2\cos^2\varphi_1)e^{-i\{\varphi_1+[-\pi+g(\varphi_1;h)]/2\}} + \mathcal{O}(h^3), \\ r_{I,y} &\to \frac{|A|}{2h}\{1 + 2h^2[1 + 2\cos(2\varphi_1)] + \mathcal{O}(h^3)\}. \end{aligned} \tag{4.50}$$

The direction of the needle, given by the phase factor of z_{12} in Eq. (4.50), is consistent with the general expression on the right-hand side of Eq. (4.48).

2. Force and torque

The force and the torque which the boundary exerts on needle 12 are again given by Eqs. (2.3)–(2.5) and (2.7)–(2.11) together with (4.22)–(4.24), except that now dz/dw and $S(w)$ follow from (4.45). It is most convenient to use the integration path $\mathcal{C}$ in Eqs. (2.5) and (2.11) along the inner boundary circle of the annulus. Since there is no force f_x parallel to the boundary, the imaginary part of τ must vanish.

For a distant needle the force is determined by $\tau^{(T)}$ for $h \ll 1$. In this regime Eqs. (2.5), (4.22), and (4.47) imply $\tau^{(T)}/t(h) \to 2h/|A|$, and using Eqs. (4.50), one obtains

$$\frac{f_y}{k_B T} \to -\frac{1}{r_{I,y}} t(h \ll 1), \quad h \to \frac{|z_{12}|}{8r_{I,y}}, \tag{4.51}$$

where $t(h \ll 1)$ is taken from Eqs. (4.26), and (4.27). As expected, this result is in agreement with (4.44) in Sec. IV B for $r_{I,x} \to +\infty$. An orientation dependence of the needle only appears in higher order and is determined explicitly for the needle geometry considered here with the SPOE in Appendix B 2 c. As for $\tau^{(S)}$, we have checked that its leading h power is higher than h^3, so that $\tau^{(S)}$ does not contain a term proportional to $|z_{12}|^2/r_{I,y}^3$. This is consistent with the vanishing of the stress-tensor average in the half plane and the absence in the SPOE of a hyperuniversal contribution $\propto|z_{12}|^2$ to the free energy, force, and torque.

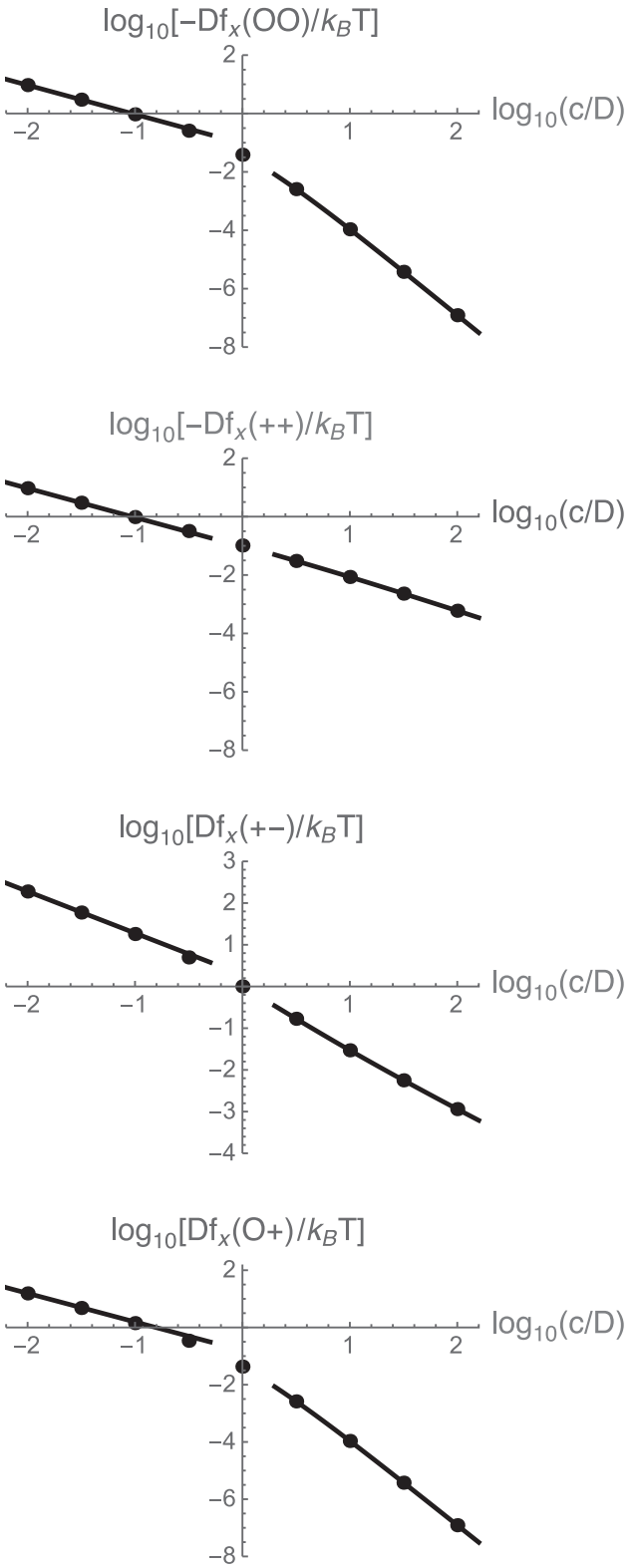

FIG. 4. Component f_x of the force exerted on needle I by needle II for needles of equal length $D_I = D_{II} = D$ in the symmetric-perpendicular configuration (A) shown in Fig. 3. Here $c = z_I - z_4$ is the distance from the right tip of needle II to the midpoint of needle I. The points indicate the numerical predictions of our exact approach, and the two curves show the asymptotic forms derived in the text for large and small c/D. The force component f_y and the torque vanish due to symmetry. For more details, see Sec. V.

The leading contribution to the torque Θ is determined by $\theta^{(T)}$ and is given by

$$\frac{\Theta}{k_BT} \to -\mathrm{Re}\theta^{(T)} \to 6h^2\sin(2\varphi_1)\,t(h \ll 1);$$
$$\sin(2\varphi_1) \to \sin(2\Phi_{12}), \quad h \to \frac{|z_{12}|}{8r_{\mathrm{I},y}}, \tag{4.52}$$

where the h expansion of $\mathrm{Re}\,\theta^{(T)}/t(h)$ is derived in Appendix B 1 b and Eqs. (4.48)–(4.50) have been used. Equations (4.51) and (4.52) are consistent with the SPOE results in Appendix B 2 c.

V. RESULTS FOR ARBITRARY NEEDLE LENGTHS

We now consider some simple needle geometries in which the needle length is neither very large nor very small compared to the distance between the needles. Calculating the force and torque requires the full machinery described in Sec. IV for arbitrary values of the mapping parameter h in the interval $0 < h < 1$. Unlike the completely analytic approaches for semi-infinite needles in Sec. III and for short needles (small h expansion) in Sec. IV, we now resort to numerical evaluation, which, however, yields results over the entire range from small to large needle lengths [58]. Actually, we restrict our attention to needle configurations for which the six mapping parameters are restricted to subspaces of lower dimension. These include

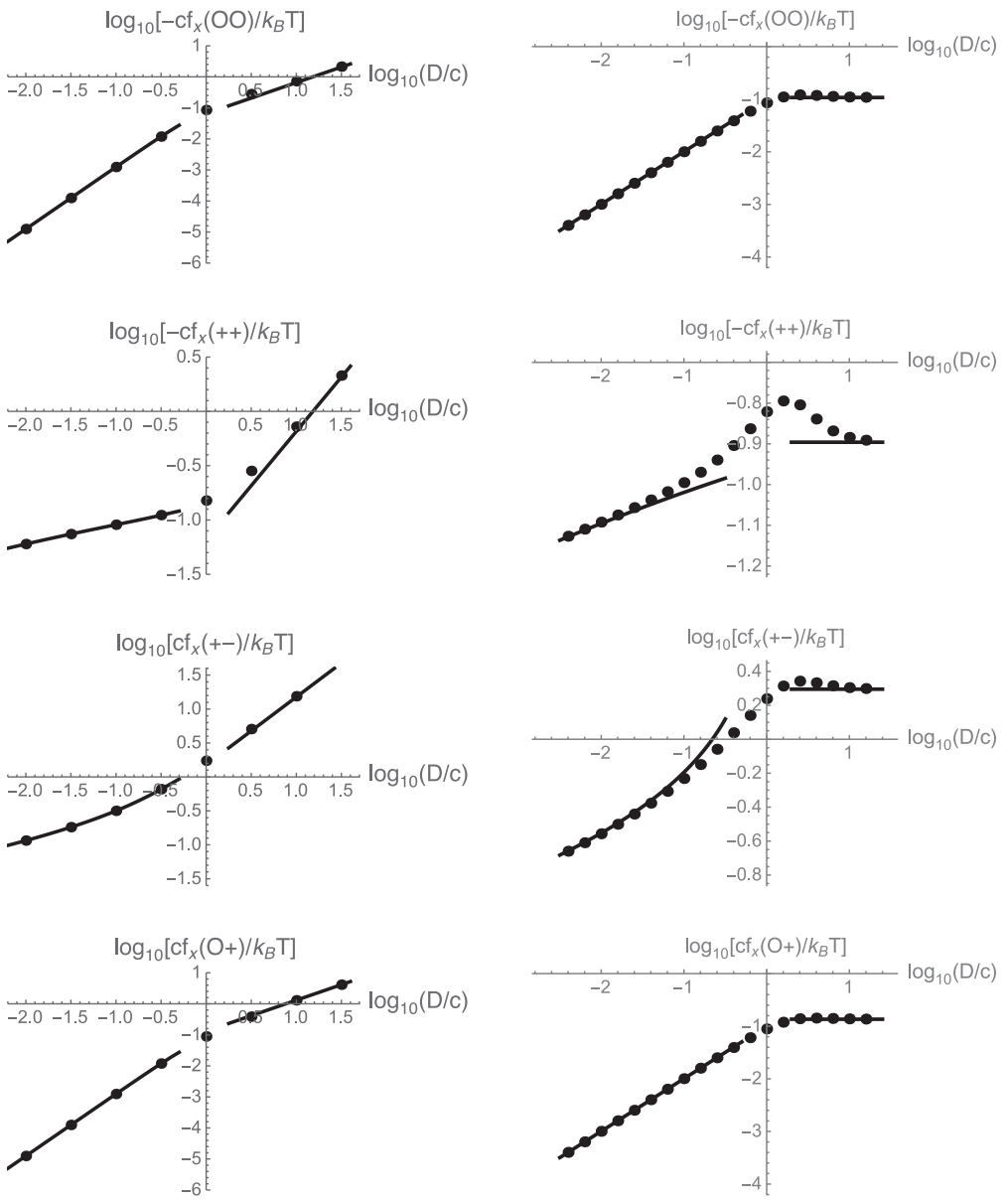

FIG. 5. Component f_x of the force exerted on needle I by needle II for needles with separation $c = z_{\mathrm{I}} - z_{\mathrm{II}}$ in the symmetric-parallel configuration (B) in Fig. 3. The results in the left and right columns are for needles of the same length $D_{\mathrm{I}} = D_{\mathrm{II}} = D$ and for needles with different lengths, $D_{\mathrm{I}} = D$ and $D_{\mathrm{II}} = c$, respectively. The points indicate the numerical predictions of our exact approach, and the curves show the asymptotic forms derived in the text for large and small D/c. The force component f_y and the torque vanish due to symmetry. For more details, see Sec. V.

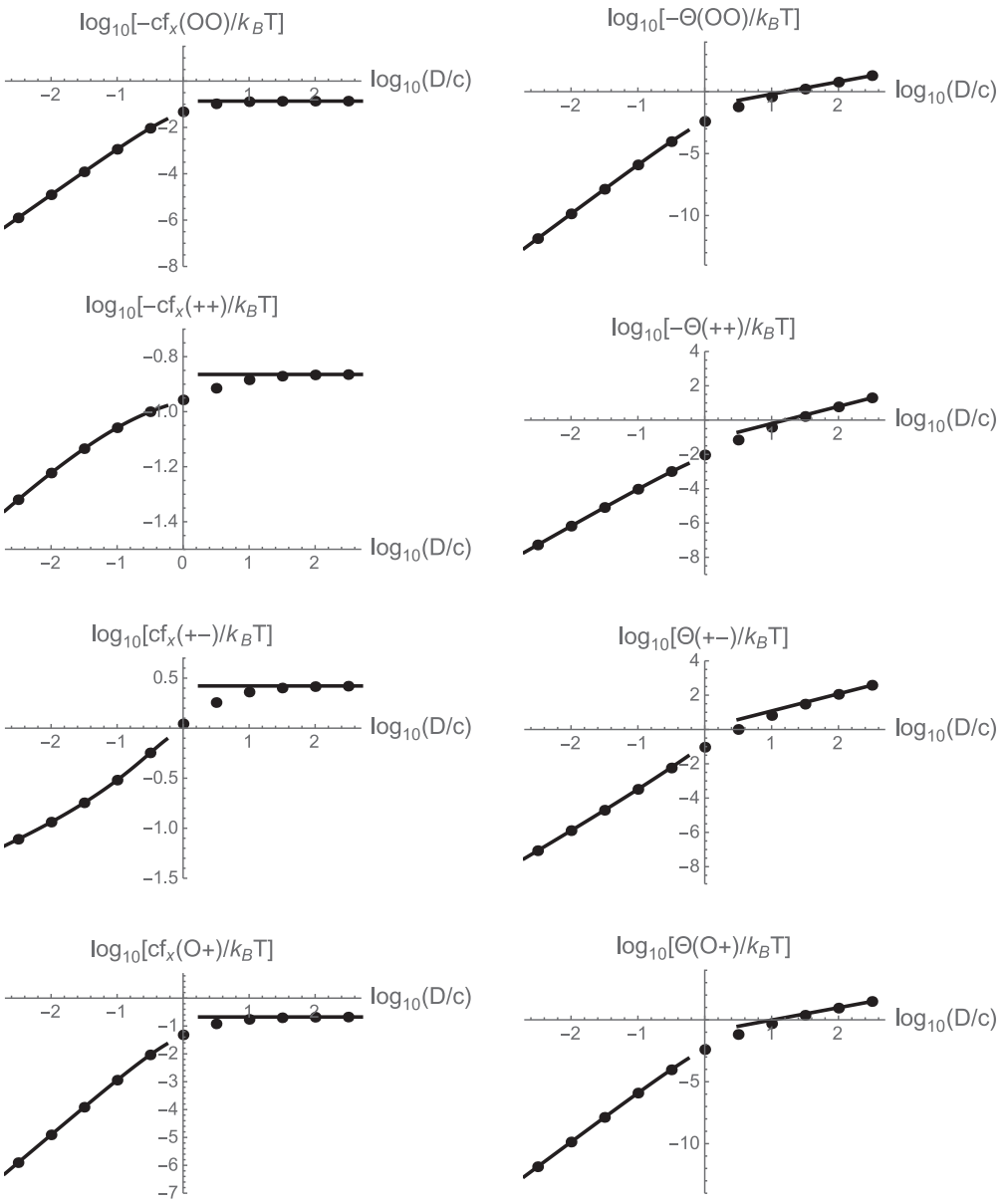

FIG. 6. Force f_x and torque Θ exerted on needle I by needle II for needles of equal length D in the mirror-symmetric configuration (C) shown in Fig. 3. Here $c = z_2 - z_4$ is the distance between the closest points of the needles, and the angle α between them is $\pi/5$. The points indicate the numerical predictions of our exact approach, and the two curves show the asymptotic forms derived in the text for large and small D/c. The force component f_y vanishes due to symmetry. For more details, see Sec. V.

configurations (A)–(D) introduced between Eqs. (4.15) and (4.16) and the configurations of a finite needle in the half plane, discussed in Sec. IV C:

(A) For the symmetric-perpendicular configuration (A) defined in Sec. IV A 1 and shown in Fig. 3, the force component f_y and the torque on needle I vanish, due to symmetry. The component f_x is attractive ($f_x < 0$) for needle university classes OO, $++$ and repulsive ($f_x > 0$) for classes $+-$, $O+$. We consider the case of equal needle lengths $D_{\rm I} = D_{\rm II} = D$, in which $Df_x/(k_BT)$, apart from the universality classes, only depends on $\tilde{c} = c/D$, where $c = z_1 - z_4$ is the minimum distance between the needles. In Fig. 4 the numerical results of our exact approach for $Df_x/(k_BT)$ in the region $10^{-2} < \tilde{c} < 10^2$ are indicated by full points. For large and small $\tilde{c}$ there is excellent agreement with the asymptotic behavior (B32) and (B33) for short needles and with the results of Sec. III for semi-infinite needles, respectively. In the latter limit, $\tilde{c} \to 0$, and the force f_x becomes independent of D and is given by f_y in Eq. (3.6) with $\alpha = \pi/2$ and $r_y(1) = c$.

(B) In the symmetric-parallel configuration (B) defined in Sec. IV A 1 and shown in Fig. 3, the force component f_y and the torque on needle I also vanish by symmetry. We have evaluated f_x numerically in two special cases, B1 and B2. In case B1, which is denoted by (ii) in Sec. IV A 1 and is a special case of classes (B), (C), and (D) [53], both needles have the same length $D_{\rm I} = D_{\rm II} = D$. In case B2 we denote the length $D_{\rm I}$ of needle I by D and choose the length $D_{\rm II}$ of needle II equal to the needle separation $c = z_{\rm I} - z_{\rm II}$. The dependence of cf_x on D/c in both cases, B1 and B2, is shown in Fig. 5. Again our numerical results (points) merge nicely with the asymptotic

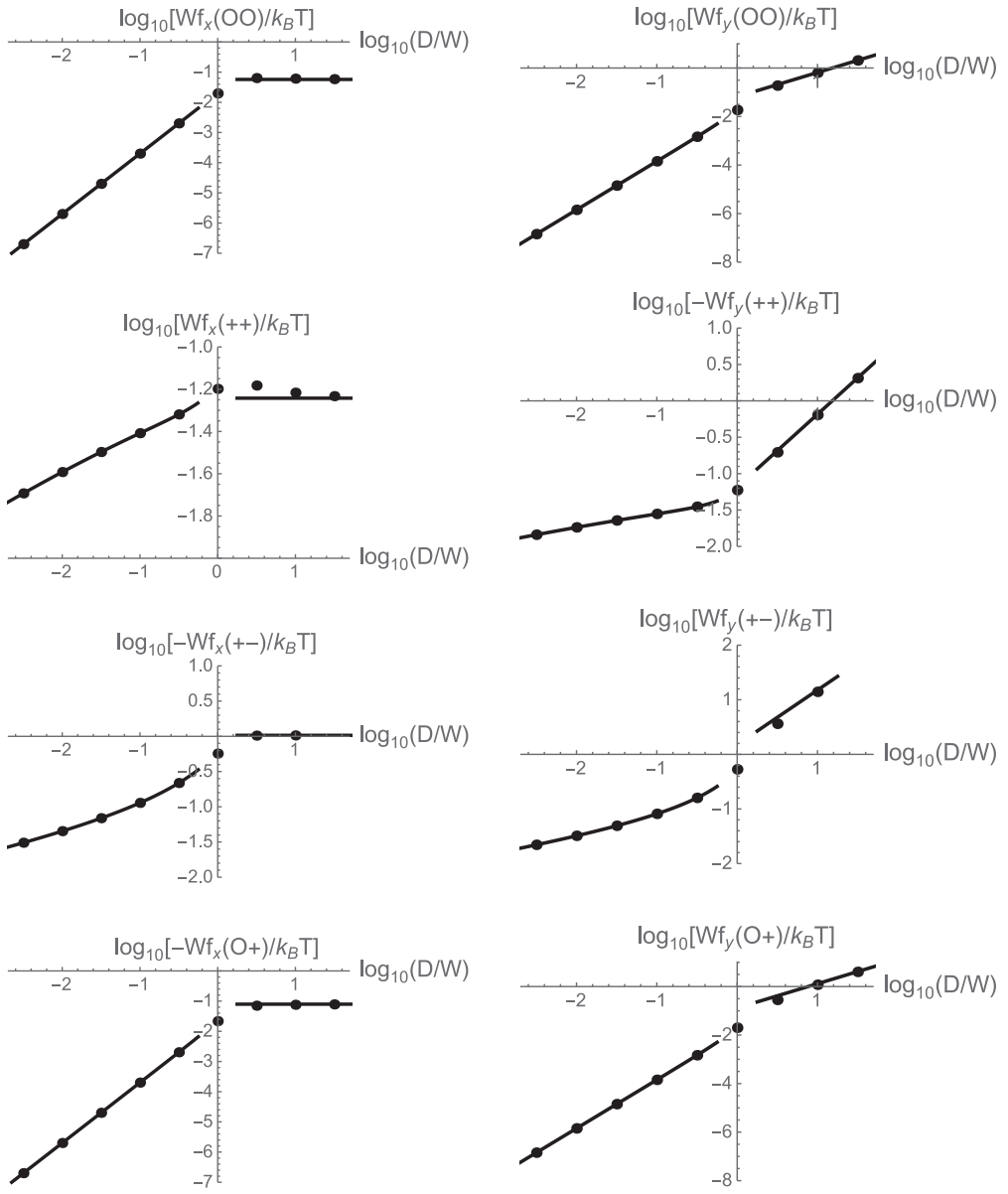

FIG. 7. Components f_x, f_y of the force exerted on needle I by needle II for needles of equal length D in the nonsymmetric parallel configuration (D′) shown in Fig. 3. Here $W = r_{1,y} - r_{4,y} \equiv \mathrm{Im}(z_1 - z_4)$ is the vertical separation of the needles, and $V = r_{4,x} - r_{1,x} \equiv \mathrm{Re}(z_4 - z_1)$ is the relative horizontal displacement. Results are shown for the fixed ratio $V/W = 1.4$. The points indicate numerical predictions of our exact approach, and the two curves show the asymptotic forms derived in the text for large and small D/W. For more details, see Sec. V.

expressions (curves) for small and large D/c. For small D/c these follow from Eqs. (B35) and (B36) with $\alpha = 0$ in case B1 and from Eqs. (B59)–(B61) in case B2. For large D/c case B1 reduces to an infinitely long strip, and $cf_x/(k_BT) \to \Delta D/c$, where $\Delta = \pi(\tilde{t} - 1/48)$, with $\tilde{t}$ given in Eq. (3.4), is the corresponding Casimir amplitude [56]. For large D/c case B2 reduces to a needle II parallel to the boundary of a half plane, a geometry considered in the last two paragraphs of this section, and $cf_x/(k_BT)$ is the same as $Df_y/(k_BT)$ for $\tilde{B} = 1$ and $\Phi = 0$ in Fig. 10. Note that in case B2 the dependence of f_x is nonmonotonic and displays a maximum. We attribute the decrease of $c|f_x|$ for large increasing D/c to the fact that for finite D both sides of needle I contribute to the interaction, while for $D = \infty$ it is only the side which faces needle II. For the case in which the length of needle II is much smaller than the needle separation c, one can derive the complete nonmonotonic dependence on D/c, including the maximum, analytically using Eqs. (B58)–(B61).

(C) For the mirror-symmetric configuration (C) defined in Sec. IV A 1 and shown in Fig. 3, the force component f_y vanishes for all angles $\pi - 2\Phi_{12} \equiv \alpha$ between the needles. The component f_x and the torque Θ are nonzero, with the exception of the torque at $\alpha = 0$ and π. Figure 6 shows f_x and Θ for needles forming an angle $\alpha = \pi/5 = 36^\circ$ and with lengths ranging from short to long. The quantities $cf_x/(k_BT)$ and $\Theta/(k_BT)$ are plotted as functions of $D/c \equiv 1/\tilde{c}$, where the minimum separation $c = z_{24} = z_2 - z_4$ of the needles is the distance between the two lower needle ends. For small D/c

the numerical data (solid points) merge nicely with the results of the small needle expansion given in Eqs. (B35) and (B36). For large D/c the data for the (D-independent) force are in excellent agreement with the corresponding force for mirror-symmetric semi-infinite needles following from Eqs. (3.9) and (3.11) with $b = 1$. The torque appears to vary linearly with D for large D, in agreement with the analytic argument at the end of Appendix C.

(D) Next we consider the force and torque on needles of equal length in the nonsymmetric parallel configuration defined in Sec. IV A 1. We use the orientation (D′) illustrated in Fig. 3(D′), where the needles are parallel to the x axis [54], with $z_{34} = -z_{12} = D$. The configuration is uniquely specified by the value of D, the vertical separation of the needles $W = r_{1,y} - r_{4,y}$, and the relative horizontal displacement $V = r_{4,x} - r_{1,x}$. For the fixed ratio $V/W = 1.4$, Figs. 7 and 8 show our numerical results (points) for $Wf_x/(k_BT)$, $Wf_y/(k_BT)$, and $\Theta/(k_BT)$ as functions of D/W. For small D/W we show the small needle prediction following from Eqs. (B41)–(B46). For large D/W the perpendicular force component f_y is dominated by the usual Casimir force for a long strip [34], so that $Wf_y/(k_BT) \to (D/W)\Delta$ with Δ from [56]. This and the behavior of the (D-independent) parallel force component f_x and of the torque Θ for large D/W, derived in Eqs. (C4), (C5), and (C3), respectively, are also indicated by solid lines in the figures.

Finally, we consider the force and torque on a single needle in the upper half plane for various ratios $\tilde{B} \equiv r_{1,y}/D$ of the distance of the needle center from the boundary to the needle length and for various angles $\Phi_{12} \equiv \Phi$ between the needle and the boundary. The torque vanishes by symmetry for $\Phi = 0$ and $\Phi = \pm\pi/2$. The results for $\tilde{B} = 10$ and $0 < \Phi < \pi/2$, shown in Fig. 9, are in perfect agreement with the predictions (B56) and (B57) of the operator expansion for a distant needle. In this case $f_y - f_y|_{\Phi=\pi/4}$ and Θ are odd and even functions, respectively, of $\Phi - \pi/4$. Figure 10 shows corresponding results for the intermediate distance ratio $\tilde{B} = 1$, where the minimum distance between the needle and the boundary, which corresponds to the perpendicular orientation $\Phi = \pi/2$, is half the length of the needle. As expected, there are significant deviations from our operator expansion of low order, in particular for the force near $\Phi = \pi/2$. As implied by Eqs. (B55) and (B56) and illustrated in Fig. 10, the convergence of the SPOE with increasing reduced distance $\tilde{B}$ is slowest for the mixed boundary condition (+−). This is not surprising, since for this combination of boundary conditions the perturbation of one needle due to the other is the most severe, with, in Ising language, the spins forced to reverse direction.

For $\tilde{B} < 1/2$ the needle touches the boundary before attaining the perpendicular orientation, and the force and torque diverge. Figure 11 shows the case $\tilde{B} = \sqrt{3}/4 = 0.433$ for $0 < \Phi < \pi/3$, with diverging results as Φ approaches the angle $\pi/3$ and the distance $r_{2,y} = \frac{1}{2}D(\sin\frac{\pi}{3} - \sin\Phi)$ of the needle tip z_2 from the boundary shrinks to zero. Since the divergence is a local effect, for $r_{2,y} \ll D$ one expects f_y to be independent of D and the same as the force (3.6) on a semi-infinite needle with the same end point $r_{2,y} \equiv r_y(1)$ and angle $\Phi \equiv \alpha$ in the notation of Sec. III A. From Eq. (3.6) we obtain $Df_y/k_BT \approx -\frac{1}{12}(5 - 216\,\tilde{t})(\frac{\pi}{3} - \Phi)^{-1}$ for the leading divergent term, which is plotted in Fig. 11. The exact numerical data (points) in the figure are in excellent agreement with this prediction, and for all four sets of boundary conditions it gives an astonishingly good fit over the entire range $0 < \Phi < \pi/3$. Heuristic arguments (see last two paragraphs of Appendix C) suggest that the torque also diverges as $(\frac{\pi}{3} - \Phi)^{-1}$, and the exact numerical data in Fig. 11 appear to support this.

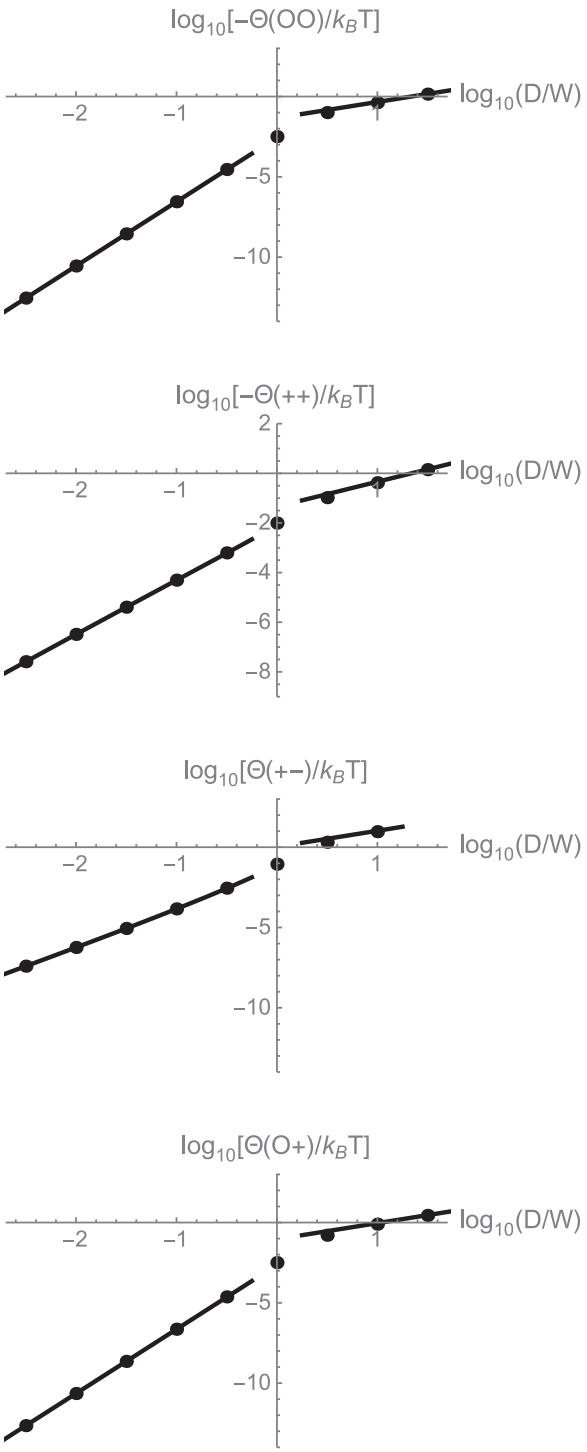

FIG. 8. Torque Θ on needle I for the same nonsymmetric parallel configuration considered in Fig. 7.

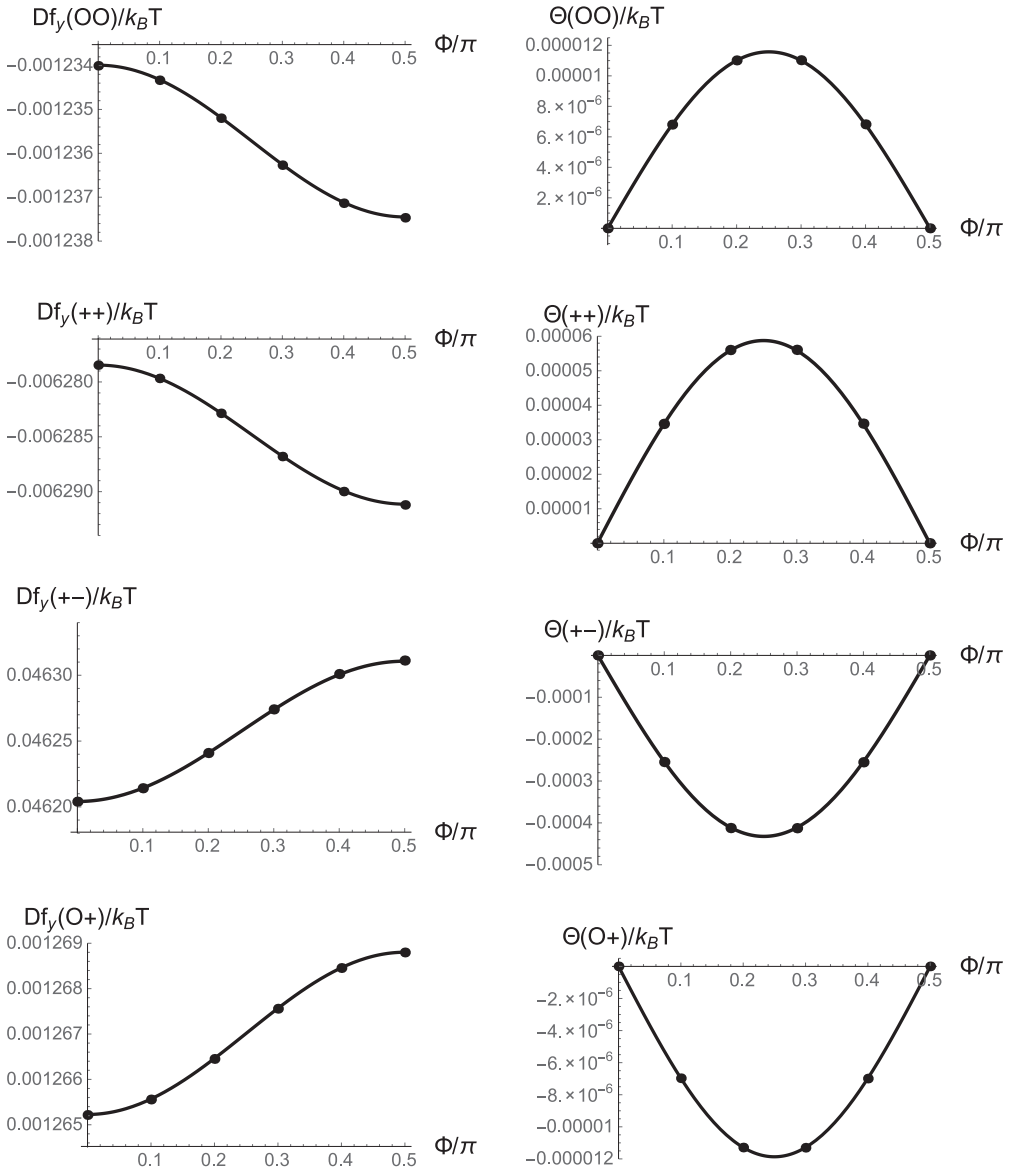

FIG. 9. Dependence of the force f_y and torque Θ on a needle of length D in the upper half plane on the angle Φ between the needle and the boundary. The ratio $\tilde{B} = r_{1,y}/D$, where $r_{1,y}$ is the distance of the needle midpoint from the boundary, has the value $\tilde{B} = 10$. The points indicate numerical predictions from the exact approach, and the curves show the analytic results (B56) and (B57) of the operator expansion for a distant needle, i.e., for large $\tilde{B}$. The force component f_x vanishes. For more details see Sec. V.

VI. SUMMARY AND CONCLUDING REMARKS

The Casimir interaction of particles immersed in a binary liquid mixture near a critical point of miscibility has a long range and universal character, and nonspherical particles experience both a force and a torque. We consider the interaction of two needle-shaped particles right at the critical point of a two-dimensional fluid in the Ising universality class. While particular needle configurations have been considered before [35], the approach of this paper allows us to calculate the interaction for two needles of arbitrary lengths, separations, and orientations for various combinations of surface universality classes [26].

As in earlier work [17,29,35,36,57], we utilize the conformal invariance of two-dimensional critical systems and generate the needle geometry of interest from a simpler standard geometry by means of a conformal mapping. As outlined in Sec. II and Appendix A, we work with the stress tensor, which has well-understood conformal transformation properties, is known in the simple standard geometry, and determines the force and torque in the needle geometry of interest.

In Secs. III A and III B we consider arbitrary configurations of an infinite and a semi-infinite needle and of two semi-infinite needles and obtain the results for the force given in Eqs. (3.3), (3.6), (3.9), and (3.11), respectively. The simple form of the force follows from the simplicity of the stress tensor in the standard geometry and of the mapping generating the needles. The region outside the needles is simply connected, and the standard geometry is the upper half plane with the two needles on the x axis. In Sec. III C and Appendix D we show how to extend the approach to needles with different boundary

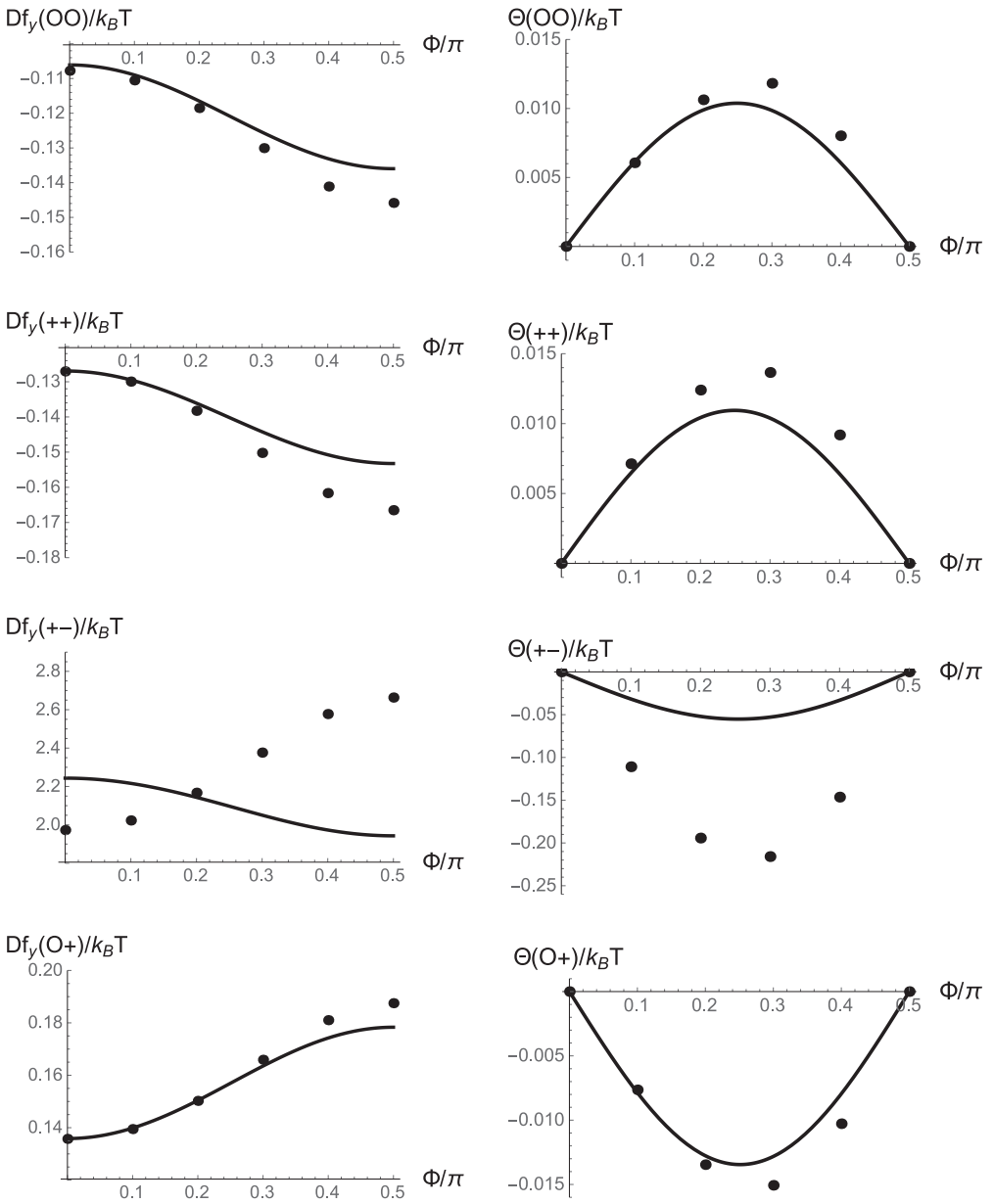

FIG. 10. Same as Fig. 9, except that the ratio $\tilde{B}$ has the value $\tilde{B} = 1$ instead of 10. Since the distant needle condition $\tilde{B} \gg 1$ is not satisfied, the numerical predictions from the exact approach (points) deviate significantly from the predictions (curves) of the operator expansion for a distant needle. For more details, see Sec. V.

conditions on the two sides, for example, a needle along the x axis with its upper edge in the class $-$ and its lower edge in the class $+$. Explicit results are given for the force between (i) two semi-infinite collinear needles [see Eqs. (D7)–(D9)] and (ii) a semi-infinite needle perpendicular to the boundary of the half plane. In the latter case we also consider a boundary with "chemical steps" [40], which separate the x axis into segments with $+$ and $-$ boundary conditions, and our results for the normal and lateral forces acting on the needle in the case of one and two chemical steps are given in Eqs. (D10)–(D18) [59]. In this context we have obtained new results (D2)–(D4) for the stress tensor in the half plane with an inhomogeneous boundary [60].

For needles of finite length the space bounded by the needles is doubly connected, and the standard geometry is an annulus with circular needles on its boundaries. The stress tensor in the annulus is known from Cardy's work [37,55] and is summarized in Eqs. (4.22)–(4.24). The mapping onto the two-needle geometry is a special case of Akhiezer's formula [51] for mapping the annulus onto the region outside two nonoverlapping polygons, and its derivative is given by Eq. (4.2) in Sec. IV A. Two conditions (4.8) are imposed to ensure that the mapping is single valued. Searching for values of the six parameters $h, C, \varphi_1, \ldots, \varphi_4$ in Eq. (4.2) that satisfy these two conditions and generate a given needle configuration is a formidable task. The simple relation (4.14), which expresses the angle enclosed by the two needles in terms of the sum $\varphi_1 + \cdots + \varphi_4$ reduces the space of parameters in which one must search, and we have found some simple configurations (A)–(D) of the needles, discussed in Sec. IV A 1

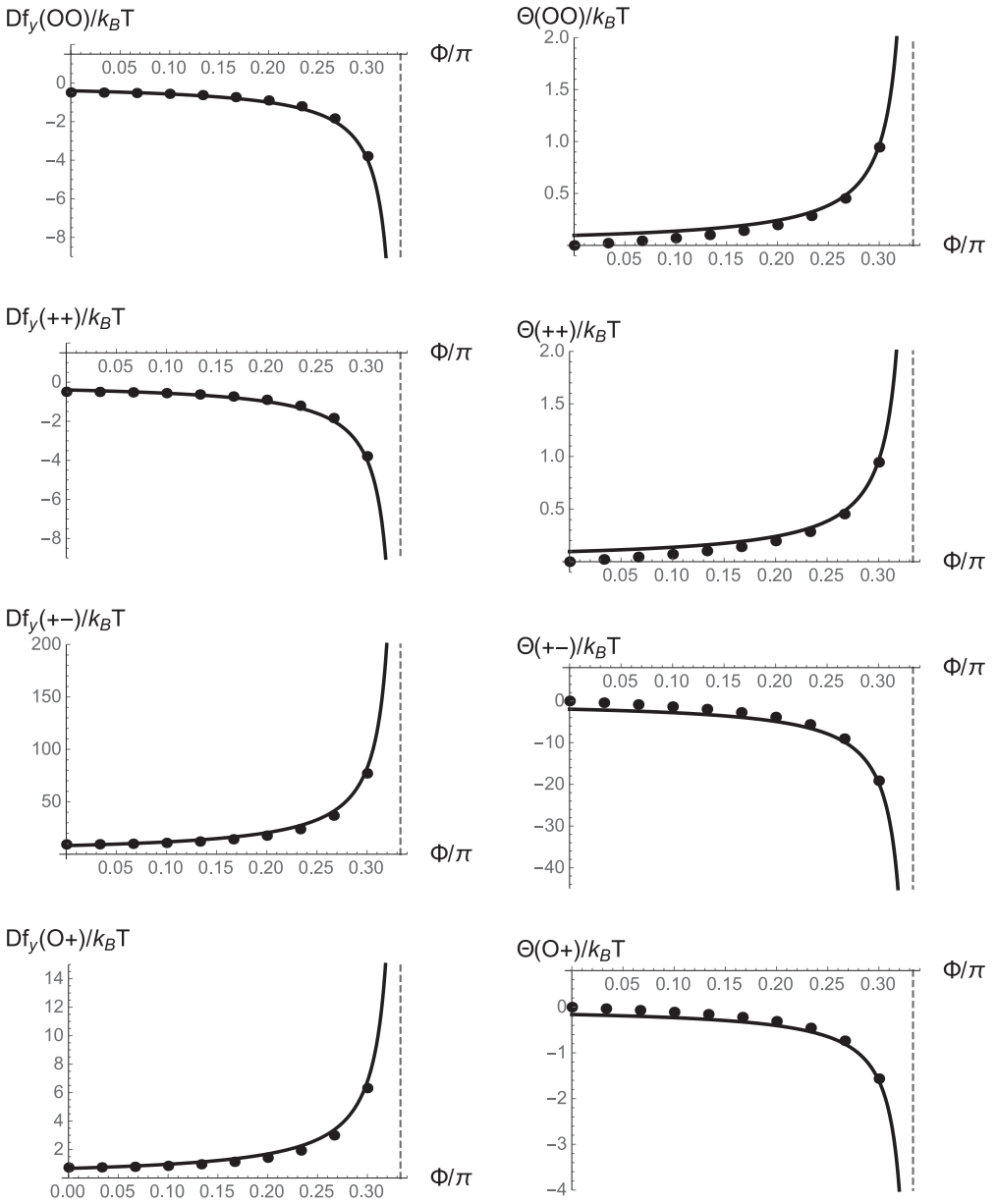

FIG. 11. Same as Fig. 9 except that $\tilde{B} = \sqrt{3}/4 = 0.433$. Both f_y and Θ diverge as Φ approaches $\pi/3$, the angle at which the needle tip touches the boundary. For Φ close to $\pi/3$, the numerical predictions (points) for f_y agree with the asymptotic expression (curves) given in the last paragraph of Sec. V. Like f_y, Θ also appears to diverge as $(\frac{\pi}{3} - \Phi)^{-1}$. The numerical results for Θ are compared with fits of the form $\Theta_{\rm fit}(\Phi) = A(\frac{\pi}{3} - \Phi)^{-1}$, with A chosen to reproduce the rightmost point in each graph.

and shown in Fig. 3, in which the space can be further reduced. In Secs. IV B and IV C we analyze the special case in which one of the needles has a finite length and the other is semi-infinite or infinite.

We have put the finite-needle approach to work in two ways:

(a) First of all, we have analyzed the case of needles with separation much greater than their lengths analytically. In this regime the inner radius $h \ll 1$ of the annulus is much smaller than the outer radius of 1, and both the small h expansion and the small-particle operator expansion (SPOE) yield information on the force and torque. Beginning in paragraph (E) of Sec. IV A 1 and continuing in Secs. IV A 2, IV B, and IV C and Appendix B, we show the consistency of these two approaches. For example, the hyperuniversal contribution to force and torque, which is independent of the surface universality class and arises via (2.3)–(2.11) from the Schwarzian derivative of the mapping, is provided within the SPOE (B15) by the stress-tensor operator (B18).

(b) Second, by using the same conformal mapping approach and evaluating formulas numerically, we have studied the force and torque over the full range from small to large values of the ratio of needle length to needle separation. Results for several types of needle configurations (see Fig. 3) and several combinations of universality classes are shown in Figs. 4–11 and discussed in Sec. V. In all cases the force is attractive for OO and $++$ boundaries and repulsive for $+-$ and $O+$. For needles which are very short or very long in comparison with their separation, the numerical results

in Figs. 4–11, shown by points, are in excellent agreement with the curves, indicating the exact asymptotic behavior. The asymptotic behavior for short needles follows from the SPOE. For long needles it follows from the results for needles of infinite length in Sec. III and for strongly overlapping and long mirror-symmetric needles in Appendix C. In configuration (D′), for example, the force component f_x and the torque Θ are predicted [see Eqs. (C4), (C5), and (C3)] to be independent of D and to vary linearly with D, respectively, in the large D limit, as shown in Figs. 7 and 8. For the mirror-symmetric configuration (C) the torque Θ is also predicted to vary linearly with D for large D (see end of Appendix C), as shown in Fig. 6. All of the asymptotic predictions in Figs. 4–11 are free of adjustable parameters, except for the torque Θ in Fig. 6 for large D and in Fig. 11 for $\Phi/\pi \to 1/3$ (see the discussion in Sec. V). Finally, we recall that for certain configurations of needles of intermediate length, there is an interesting nonmonotonic dependence of the force on needle length, see, e.g., the right side of Fig. 5 and the discussion at the end of paragraph (B) in Sec. V.

We close by comparing the advantages and disadvantages of the conformal mapping approach of Secs. IV and V and of the approach based on the SPOE. For evaluating the force and torque for arbitrary size to separation ratios, as in Sec. V, the former is clearly superior. However, it is limited to two-dimensional critical systems with conformal symmetry, to particle surfaces with uniform boundary conditions, and to the interaction of two particles [61] immersed in the critical medium. The SPOE is applicable only if the particle size is small compared to the interparticle separation and to the correlation length of the medium in which the particles are immersed. However, the SPOE is not limited to two dimensions, is valid in near-critical as well as critical systems, and also applies if there are more than two immersed particles [62] and if the particles have nonuniform boundary conditions [63]. In addition to spherical and nonspherical particles embedded in near-critical fluids [29,57], the SPOE method has been applied to particles bound to fluctuating surfaces in Ref. [24], where it is called "effective field theory."

APPENDIX A: TRANSLATION AND ROTATION OF ONE OF TWO PARTICLES

A general infinitesimal coordinate transformation,

$$\hat{\mathbf{r}} = \mathbf{r} + \mathbf{a}(\mathbf{r}), \tag{A1}$$

changes the geometry of a critical system, including the sizes, shapes, separations, and orientations of embedded particles, from G to $\hat{G}$. The corresponding change in the universal scaling part [64] of the free energy is given by

$$F_{\hat{G}} - F_G = -k_B T_c \int d\mathbf{r} \sum_{k,\ell} [\partial a_k(\mathbf{r})/\partial r_\ell] \langle T_{k\ell}(\mathbf{r})\rangle_G \tag{A2}$$

to first order in $\mathbf{a}$, where $T_{k\ell}$ is the stress tensor [34,46].

For two particles in the (r_x, r_y) plane, the force and torque on particle I due to particle II follow directly from the change in free energy as particle I is translated by an infinitesimal vector (dR_x, dR_y) or rotated by an infinitesimal angle $d\Phi$ about a point $(r_{0,x}, r_{0,y})$, while keeping particle II fixed. Assuming that particles I and II are located above and below the line $r_y = \tilde{r}_y$, respectively, we fix particle II by choosing

$$(a_x(\mathbf{r}), a_y(\mathbf{r})) = (A_x(\mathbf{r}), A_y(\mathbf{r})) \times \Theta(r_y - \tilde{r}_y), \tag{A3}$$

where Θ is the standard unit step function. To translate and rotate I, we choose

$$(A_x, A_y) = (dR_x, dR_y), \tag{A4}$$

$$(A_x(\mathbf{r}), A_y(\mathbf{r})) = (-r_y + r_{0,y}, r_x - r_{0,x}) d\Phi, \tag{A5}$$

respectively. On substituting

$$\partial a_k/\partial r_\ell = [\partial A_k/\partial r_\ell] \times \Theta(r_y - \tilde{r}_y) + A_k \delta_{\ell,y} \delta(r_y - \tilde{r}_y) \tag{A6}$$

in Eq. (A2), the first term on the right-hand side does not contribute, since $\partial A_k/\partial r_\ell$ vanishes for the shift and is antisymmetric in $k\ell$ for the rotation, while $T_{k\ell}$ is symmetric. Thus,

$$F_{\hat{G}} - F_G = -k_B T_c \int_{-\infty}^{\infty} dr_x J,$$
$$J = \sum_{k=x,y} A_k(r_x, \tilde{r}_y) \langle T_{ky}(r_x, \tilde{r}_y)\rangle_G. \tag{A7}$$

Of course, $F_{\hat{G}} - F_G$ should not depend on the precise choice of $\tilde{r}_y$, and this property follows from the vanishing of $\partial(\int_{-\infty}^{\infty} dr_x J)/\partial \tilde{r}_y$ due to the continuity equation $\sum_\ell \partial \langle T_{k\ell}(\mathbf{r})\rangle_G/\partial r_\ell = 0$ at any point $\mathbf{r}$ outside the particles. Using the relations

$$\langle T_{yy}(r_x, \tilde{r}_y)\rangle_G = -\langle T_{xx}(r_x, \tilde{r}_y)\rangle_G = \mathrm{Re}\, \vartheta(z),$$
$$\langle T_{xy}(r_x, \tilde{r}_y)\rangle_G = \langle T_{yx}(r_x, \tilde{r}_y)\rangle_G = \mathrm{Im}\, \vartheta(z), \tag{A8}$$
$$\vartheta(z) \equiv \langle T(z)\rangle_G/\pi, \quad z = r_x + i\tilde{r}_y,$$

between the Cartesian components and complex form of the stress tensor (see [34,46]), one finds

$$J = dR_x \mathrm{Im}\, \vartheta(z) + dR_y \mathrm{Re}\, \vartheta(z), \tag{A9}$$

$$J = d\Phi \mathrm{Re}[(z - z_0)\vartheta(z)], \quad z_0 = r_{0x} + i r_{0y}, \tag{A10}$$

for the translation and rotation, respectively. Together with Eq. (A7) and $dr_x = dz$, this implies

$$F_{\hat{G}} - F_G = k_B T \left[dR_x \mathrm{Im} \int_{\mathcal{C}_\mathrm{I}} dz \vartheta(z) + dR_y \mathrm{Re} \int_{\mathcal{C}_\mathrm{I}} dz \vartheta(z) \right], \tag{A11}$$

$$F_{\hat{G}} - F_G = k_B T d\Phi \mathrm{Re} \int_{\mathcal{C}_\mathrm{I}} dz (z - z_0)\vartheta(z), \tag{A12}$$

where the closed integration contour $\mathcal{C}_\mathrm{I}$ goes clockwise around particle I, with particle II outside the contour. In arriving at this result, we first deformed the integration path in Eq. (A7) to a counterclockwise loop around needle I, as allowed by the analyticity [34] and large z properties of $\vartheta(z)$ and of $(z - z_0)\vartheta(z)$. We then replaced this integral by minus the integral around the clockwise contour $\mathcal{C}_\mathrm{I}$.

Equations (A11) and (A12) are more general than our derivation and also apply to configurations in which the two particles do not lie above and below a line parallel to the

r_x axis. The same is true of the corresponding expressions (2.4) and (2.8) for the force and the torque. Two needles can always be separated by a straight line, and after an appropriate global rotation of the system, Eq. (A3) can be applied. On rotating counterclockwise by an arbitrary finite angle ω, $\langle T(z)\rangle \to e^{-2i\omega}\langle T(z)\rangle$, $dz \to e^{i\omega}dz$, $z - z_{\rm I} \to e^{i\omega}(z - z_{\rm I})$, and Eqs. (2.4) and (2.8) correctly predict the rotation $f_x + if_y \to e^{i\omega}(f_x + if_y)$ of the force and that the torque is unchanged. Expressions (A11) and (A12) hold for two particles of arbitrary shape, even if they are positioned so that no separating straight line exists. This follows from a modified infinitesimal transformation (A3) in which the region onto which the step function Θ projects is not a half plane.

For the special case of two widely separated needles we have checked the consistency of Eqs. (A11) and (A12) with the small-particle operator expansion reviewed in Appendix B 2.

APPENDIX B: EXPANSIONS FOR SHORT NEEDLES

The Casimir interaction of a needle which is short compared to the distance to other particles and to the boundary can be studied analytically in a power series expansion. In Appendix B 1 we consider the small h expansion, where h is the ratio of the inner to outer radius of the annulus, and provide more details on the derivation of the distant needle results for force and torque presented in Sec. IV. In Appendix B 2 we study the interaction of the needles with the SPOE. Since the two methods must lead to identical results, one can make useful checks.

1. Expanding for small h

a. Two small needles

To arrive at the form of $\tau^{(S)}$ for widely separated needles given in Eq. (4.25), we expand the Schwarzian derivative on the circle $\mathcal{C} = \mathcal{C}_c$, defined below Eq. (4.24) and considered in Fig. 2, in terms of h, obtaining

$$S(w = h^{1/2}Ce^{i\varphi}) \times C^2e^{2i\varphi}/6 =: \sigma(\varphi) = \sigma_0(\varphi) + h^{1/2}\sigma_1(\varphi) + h\sigma_2(\varphi) + \mathcal{O}(h^{3/2}), \tag{B1}$$

where

$$\begin{aligned}
\sigma_0 &= -C^2e^{2i\varphi}e^{-2i\varphi_1} - C^{-2}e^{-2i\varphi}e^{2i\varphi_3},\\
\sigma_1 &= 2\{C^3e^{2i\varphi}(e^{-i\varphi_1} - e^{-3i\varphi_1}) + C^{-3}e^{-2i\varphi}(e^{i\varphi_3} - e^{3i\varphi_3})\},\\
\sigma_2 &= C^4e^{2i\varphi}[-1 + e^{-2i\varphi_1}(6 - 4e^{i\varphi}) + e^{-4i\varphi_1}(-5 + 4e^{i\varphi} - 2e^{2i\varphi})] + 2e^{-2i\varphi_1}e^{2i\varphi_3}\\
&\quad + C^{-4}e^{-2i\varphi}[-1 + e^{2i\varphi_3}(6 - 4e^{-i\varphi}) + e^{4i\varphi_3}(-5 + 4e^{-i\varphi} - 2e^{-2i\varphi})].
\end{aligned} \tag{B2}$$

The invariance of the right-hand sides on exchanging $(C,\varphi,\varphi_1,\varphi_3) \leftrightarrow (C^{-1},-\varphi,-\varphi_3,-\varphi_1)$ presumably persists in higher order. On the circle $\mathcal{C}_c$ the prefactor of the square bracket in the integral (2.5) reads

$$\frac{1}{z'(w)} = -\frac{1}{A}h^2(1 - e^{i\varphi})^2e^{2i\varphi_3}[1 + h^{1/2}\delta_1(\varphi) + h\delta_2(\varphi) + \mathcal{O}(h^{3/2})], \tag{B3}$$

where

$$\delta_1 = 2C^{-1}(e^{i\varphi_3} - e^{-i\varphi_3}), \quad \delta_2 = -4C^{-2} + C^{-2}e^{2i\varphi_3}(4 - 2e^{-i\varphi} + e^{-2i\varphi}) + C^2e^{-2i\varphi_1}(-2e^{i\varphi} + e^{2i\varphi}), \tag{B4}$$

and implies

$$\tau^{(S)} \equiv \int_{\mathcal{C}_c} dw \frac{1}{dz/dw}(-)\frac{1}{24}S(w)/\pi = \frac{ih^{5/2}}{4\pi AC}e^{2i\varphi_3}\mathrm{I}, \tag{B5}$$

where

$$\begin{aligned}
\mathrm{I} &= \int_0^{2\pi} d\varphi(e^{-i\varphi} - 2 + e^{i\varphi})(1 + h^{1/2}\delta_1 + h\delta_2 + \cdots)(\sigma_0 + h^{1/2}\sigma_1 + h\sigma_2 + \cdots)\\
&= h\int_0^{2\pi} d\varphi(e^{-i\varphi} - 2 + e^{i\varphi})(\sigma_2 + \delta_2\sigma_0) + \mathcal{O}(h^{3/2}) = 8\pi he^{-2i\varphi_1}e^{2i\varphi_3}.
\end{aligned} \tag{B6}$$

Together with Eq. (4.21), this leads to the result for $\tau^{(S)}$ in Eq. (4.25).

Next we derive (4.30) of $\theta^{(S)}$ for two widely separated needles. Since in Eq. (2.11) we again integrate w counterclockwise around the circle $\mathcal{C} = \mathcal{C}_c$, the two required quantities $\zeta_n(w)$ are conveniently obtained by splitting the $\tilde{w}$ integration paths in Eq. (2.9) into three parts (see Fig. 2): $[\alpha]$ from w_1 or w_2 along the outer boundary circle to the point -1; $[\beta]$ from -1 along the negative real axis to $-Ch^{1/2}$; $[\gamma]$ from $-Ch^{1/2}$ along the circle $\mathcal{C}_c$ to the point $w \equiv Ch^{1/2}\exp(i\varphi)$. This yields

$$\zeta_n(w) = \zeta_n^{[\alpha]} + \zeta^{[\beta]} + \zeta^{[\gamma]}(w), \quad n = 1,2, \tag{B7}$$

where

$$\zeta_n^{[\alpha]}/A = \mathcal{O}(1/h), \quad \zeta^{[\beta]}/A = -h^{-3/2}(C/2)e^{-2i\varphi_3} + \mathcal{O}(1/h),$$
$$\zeta^{[\gamma]}(w)/A = -h^{-3/2}Ce^{-2i\varphi_3}\Big\{[1-h^{1/2}2C^{-1}(e^{i\varphi_3}-e^{-i\varphi_3})]\Big(\frac{1}{1-\Omega}-\frac{1}{2}\Big) + h\Big[4C^{-2}(-1+e^{-2i\varphi_3})\Big(\frac{1}{1-\Omega}-\frac{1}{2}\Big)$$
$$+ C^{-2}e^{2i\varphi_3}\Big(\frac{1}{1-\Omega}+\frac{1}{\Omega}+\frac{1}{2}\Big) + C^2e^{-2i\varphi_1}\Big(\frac{1}{1-\Omega}-\Omega-\frac{3}{2}\Big)\Big] + \mathcal{O}(h^{3/2})\Big\}, \tag{B8}$$

and $\Omega \equiv e^{i\varphi}$. By construction, only the first term $\zeta_n^{[\alpha]}$ in Eq. (B7) depends on n, and only the third term $\zeta^{[\gamma]}(w)$ depends on w. The h expansion for $\theta^{(S)}$ is obtained by substituting $1/z'(w)$, $S(w)$, and ζ_n from Eqs. (B1)–(B4), (B7), and (B8) in Eq. (2.11). One (readily) finds that $\zeta_n^{[\alpha]}$ and (with more work) that $\zeta^{[\gamma]}(w)$ only contribute to $\theta^{(S)}$ in orders higher than h^2, while $\zeta^{[\beta]}$ makes the leading contribution $\theta^{(S)} \to \zeta^{[\beta]}\tau^{(S)}$ given in Eq. (4.30), which is of order h^2. Here Eqs. (B5) and (B6) have been used in the last step.

b. A small needle in the half plane

Here we derive, within the h expansion, the contribution $-\mathrm{Re}\,\theta^{(T)}$ to the torque acting on a small needle in the half plane shown in Eq. (4.52). For the integration path $\mathcal{C}$ in Eq (2.11), we use the inner boundary circle $w = he^{i\varphi}$ and split the integrations for $\zeta_n(w)$, as in Eq. (B7), where for $[\alpha]$ the integration is as before, while for $[\beta]$ and $[\gamma]$ it goes from -1 to $-h$ and from $-h$ to $w = he^{i\varphi}$, respectively. For $[\gamma]$ we integrate over the segment of the inner circle, which does not contain the singular point $w = h$ of $z'(w)$. Instead of φ it is convenient to use the deviation $\chi = \varphi - \pi$ from $\varphi = \pi$ as the integration variable on the inner circle, and with the help of Eq. (4.47), one obtains

$$\zeta^{[\gamma]}(w = he^{i\varphi})/|A| \equiv -\frac{1}{h}\int_0^\chi d\chi' \frac{1}{4\cos^2(\chi'/2)}\tilde{\mathcal{P}}(\chi')$$
$$\to -\frac{1}{2h}\tan(\chi/2) + h\{2(1-\cos\chi)\sin(2\varphi_1) + [2\sin\chi - \tan(\chi/2)]\cos(2\varphi_1)\}. \tag{B9}$$

Here $\tilde{\mathcal{P}}$ is the product in Eq. (4.47), and we have used its behavior for small h,

$$\tilde{\mathcal{P}}(\chi) \equiv \prod_{k=1}^{\infty}\frac{\prod_{n=1,2}|1+h^{2k-1}e^{i(\chi-\varphi_n)}|^2}{|1+h^{2k}e^{i\chi}|^4} \to 1 - 2h^2\{[2\sin\chi + \sin(2\chi)]\sin(2\varphi_1) + [2\cos\chi + \cos(2\chi)]\cos(2\varphi_1)\}. \tag{B10}$$

To first order in h,

$$\big(\zeta_1^{[\alpha]} + \zeta_2^{[\alpha]}\big)/(2|A|) = -i(1+e^{-2i\varphi_1}) - 4he^{-2i\varphi_1}\sin\varphi_1, \tag{B11}$$

$$\Big(\frac{\zeta_1^{[\alpha]}+\zeta_2^{[\alpha]}}{2} + \zeta^{[\beta]}\Big)\Big/|A| = -\frac{i}{2h} + ih\Big(-1 + \frac{1}{2}e^{2i\varphi_1} - \frac{5}{2}e^{-2i\varphi_1}\Big), \tag{B12}$$

so that

$$\mathrm{Re}\Big(\frac{\zeta_1^{[\alpha]}+\zeta_2^{[\alpha]}}{2} + \zeta^{[\beta]}\Big)\Big/|A| = -3h\sin(2\varphi_1), \tag{B13}$$

and Eq. (4.52) then follows from

$$\frac{2\pi}{t(h)}\mathrm{Re}\theta^{(T)} \equiv h\int_{-\pi}^{\pi} d\chi\, 4\cos^2(\chi/2)\frac{1}{\tilde{\mathcal{P}}(\chi)}\Big\{\mathrm{Re}\Big(\frac{\zeta_1^{[\alpha]}+\zeta_2^{[\alpha]}}{2} + \zeta^{[\beta]}\Big) + \zeta^{[\gamma]}(he^{i\varphi})\Big\}\Big/|A|. \tag{B14}$$

Inserting Eq. (B9) in Eq. (B14), one finds that $\zeta^{[\gamma]}$ does not contribute to the leading-order result shown on the right-hand side of Eq. (4.52).

2. Operator expansion for a distant needle

Like a product of two operators in the "operator-product expansion" [44], a small particle can be represented by a sum of operators with appropriate prefactors [29,57]; see also [17]. Consider a distant needle J, i.e., a needle of short [43] length D_J and surface universality class H_J, with center at $\mathbf{r}_\mathrm{J}$, and directed along the unit vector $\mathbf{n}_\mathrm{J}$. Inserting it into the $d = 2$ Ising model at the critical point changes the Boltzmann weight of the corresponding field theory by a factor

$$e^{-\delta\mathcal{H}_\mathrm{J}} \propto 1 + s_\mathrm{J}, \tag{B15}$$

where s_J is the operator series [35]

$$s_J = \sum_{\mathcal{O}=\phi,\epsilon} \mathcal{A}_{\mathcal{O}}^{(H_J)} \left(\frac{D_J}{2}\right)^{x_{\mathcal{O}}} \left\{1 + \left(\frac{D_J}{2}\right)^2 \left[\frac{1}{16 x_{\mathcal{O}}} \Delta_{\mathbf{r}_J} + \frac{3}{8(1+x_{\mathcal{O}})} \left(\mathcal{D}_J - \frac{1}{2}\Delta_{\mathbf{r}_J}\right)\right]\right\} \mathcal{O}(\mathbf{r}_J) - \frac{\pi}{2}\left(\frac{D_J}{2}\right)^2 \tilde{T}(J) + \cdots . \tag{B16}$$

Here $\Delta_{\mathbf{r}}$ is the Laplacian operator, and the expressions

$$\mathcal{D}_J = \sum_{k,\ell=x,y} n_{J,k}\, n_{J,\ell}\, \partial_{r_{J,k}}\, \partial_{r_{J,\ell}} \tag{B17}$$

and

$$\tilde{T}(J) = \sum_{k,\ell=x,y} n_{J,k}\, n_{J,\ell}\, T_{k\ell}(\mathbf{r}_J) \tag{B18}$$

are the second derivative and the component of the stress tensor [46], respectively, in the needle direction. In Eq. (B16) all the operators $\mathcal{O}$ are subtracted so that their bulk mean values vanish at the critical point, and $\langle s_J\rangle_{\text{bulk}} = 0$. The operators $\mathcal{O} = \phi$ and $\mathcal{O} = \epsilon$ correspond to the order parameter and energy densities, respectively, and are normalized according to

$$\langle \mathcal{O}(\mathbf{r})\mathcal{O}(\mathbf{r}')\rangle_{\text{bulk}} = |\mathbf{r} - \mathbf{r}'|^{-2x_{\mathcal{O}}}, \tag{B19}$$

with $x_\phi = 1/8$ and $x_\epsilon = 1$. The universal quantities $\mathcal{A}_{\mathcal{O}}^{(H_J)}$ in Eq. (B16) are the amplitudes of the corresponding density profiles $\langle \mathcal{O}(r_x, r_y)\rangle_{\text{uhp}} = \mathcal{A}_{\mathcal{O}}^{(H_J)} r_y^{-x_{\mathcal{O}}}$ in the upper half plane (uhp) with the boundary at $r_y = 0$ belonging to the surface class H_J. They are given by [34]

$$\mathcal{A}_\phi^{(O)} = 0, \quad \mathcal{A}_\phi^{(+)} = -\mathcal{A}_\phi^{(-)} = 2^{1/8}, \quad \mathcal{A}_\epsilon^{(O)} = -\mathcal{A}_\epsilon^{(+)} = -\mathcal{A}_\epsilon^{(-)} = 1/2. \tag{B20}$$

The amplitudes $\mathcal{A}_{\mathcal{O}}^{(H)}$ should not be confused with the prefactor $\mathcal{A}$ of the conformal transformation in Sec. III A. Denoting the angle between the unit vector $\mathbf{n}_J = (n_{J,x}, n_{J,y})$ and the x axis by Φ_J and using complex notation,

$$r_x + i r_y = z, \quad r_x - i r_y = \bar{z}, \quad n_x + i n_y = e^{i\Phi}, \tag{B21}$$

one obtains the useful relation

$$\tilde{T}(J) = \cos(2\Phi_J) T_{xx}(\mathbf{r}_J) + \sin(2\Phi_J) T_{xy}(\mathbf{r}_J) = -\frac{1}{2\pi}[e^{2i\Phi_J} T(z_J) + e^{-2i\Phi_J} \bar{T}(\bar{z}_J)]. \tag{B22}$$

Here $T(z)$ and $\bar{T}(\bar{z})$ are components of the complex stress tensor [34], and Ref. [46] was used in the last step. Note that the prefactor of the $\tilde{T}(J)$ term in Eq. (B16) is independent of the surface universality class H_J of the needle, i.e., "hyperuniversal" [65]. The ellipsis in Eq. (B16) represents contributions from higher descendants of 1, ϕ, ϵ, each of which is compatible with all symmetries of the needle and which, due to their scaling dimensions, are multiplied by powers of D_J, greater by at least 2 than the powers shown.

a. Two small needles

For two small needles I and II the free energy of interaction δF is determined by [45]

$$e^{-\delta F/(k_B T)} = 1 + \langle s_I s_{II}\rangle_{\text{bulk}}, \tag{B23}$$

where, on using (B16)–(B20),

$$\langle s_I s_{II}\rangle_{\text{bulk}} = \pm\mathcal{E} + \mathcal{H} + \cdots \tag{B24}$$

for needle classes OO (upper sign) and $O+$ (lower sign), while

$$\langle s_I s_{II}\rangle_{\text{bulk}} = \pm\mathcal{F} + \mathcal{E} + \mathcal{H} + \cdots \tag{B25}$$

for classes $++$ (upper sign) and $+-$ (lower sign). Here

$$\mathcal{E} = \frac{D_I D_{II}}{16}\left[1 + \left(\frac{D_I}{8}\right)^2 \left(-\frac{1}{2}\Delta_{r_I} + 3\mathcal{D}_I\right) + \left(\frac{D_{II}}{8}\right)^2 \left(-\frac{1}{2}\Delta_{r_{II}} + 3\mathcal{D}_{II}\right)\right] \frac{1}{|\mathbf{r}_I - \mathbf{r}_{II}|^2} = \frac{D_I D_{II}}{16|\mathbf{r}_I - \mathbf{r}_{II}|^2}[1 + 2^{-3}(\beta_I + \beta_{II})], \tag{B26}$$

$$\mathcal{F} = (D_I D_{II})^{1/8}\left[1 + \frac{D_I^2}{12}\left(\Delta_{r_I} + \mathcal{D}_I\right) + \frac{D_{II}^2}{12}\left(\Delta_{r_{II}} + \mathcal{D}_{II}\right)\right] \frac{1}{|\mathbf{r}_I - \mathbf{r}_{II}|^{1/4}} = \left(\frac{D_I D_{II}}{|\mathbf{r}_I - \mathbf{r}_{II}|^2}\right)^{1/8} [1 + 2^{-6}(\beta_I + \beta_{II})], \tag{B27}$$

and the hyperuniversal contribution (see Refs. [34,46]) is

$$\mathcal{H} = \left(\frac{\pi}{2}\right)^2 \left(\frac{D_I D_{II}}{4}\right)^2 \langle \tilde{T}(I)\tilde{T}(II)\rangle_{\text{bulk}} = 2^{-10}(D_I D_{II})^2 \left[\frac{e^{2i(\Phi_I + \Phi_{II})}}{(z_I - z_{II})^4} + \text{c.c.}\right]. \tag{B28}$$

The quantity $\beta_{\rm J}$ is defined by

$$\beta_{\rm J} = \frac{D_{\rm J}^2}{|\mathbf{r}_{\rm I} - \mathbf{r}_{\rm II}|^2}(-1 + 3\{[\mathbf{n}_{\rm J}(\mathbf{r}_{\rm I} - \mathbf{r}_{\rm II})]/|\mathbf{r}_{\rm I} - \mathbf{r}_{\rm II}|\}^2), \tag{B29}$$

where the curly bracket depends on the angle between the direction of needle J and the vector between the two needle centers. As expected, all the terms in the free energy remain unchanged if either needle is rotated about its center by 180°.

The force (f_x, f_y) on needle I follows from

$$(f_x, f_y) = -\left(\frac{\partial}{\partial r_{{\rm I},x}}, \frac{\partial}{\partial r_{{\rm I},y}}\right)\delta F, \tag{B30}$$

and the torque Θ from Eq. (2.7) with $\Phi_{12} \equiv \Phi_{\rm I}$.

For illustration, consider the symmetric-perpendicular (letter T) needle configuration with needle centers on the x axis and $r_{{\rm I},x} - r_{{\rm II},x} > 0$, as described in paragraph (A) of Sec. IV A 1, and assume that the two needles have equal lengths $D_{\rm I} = D_{\rm II} \equiv D$. Denoting by $B = |\mathbf{r}_{\rm I} - \mathbf{r}_{\rm II}|/D \equiv (r_{{\rm I},x} - r_{{\rm II},x})/D \equiv |z_{\rm I,II}|/D$ the center-to-center distance of the needles in units of D, one finds

$$\mathcal{E} = 2^{-4}B^{-2} + 2^{-7}B^{-4}, \quad \mathcal{F} = B^{-1/4} + 2^{-6}B^{-9/4}, \quad \mathcal{H} = -2^{-9}B^{-4}. \tag{B31}$$

The component f_y of the force on needle I vanishes, and

$$Df_x/(k_BT) = (d/dB)\ln[1 + (+1,-1) \times 2^{-4}B^{-2} + (3,-5) \times 2^{-9}B^{-4}] \tag{B32}$$

for needle classes OO (left entry), $O+$ (right entry), and, via [66],

$$Df_x/(k_BT) = (d/dB)\ln[1 \pm (B^{-1/4} + 2^{-6}B^{-9/4}) + 2^{-4}B^{-2} + \mathcal{O}(B^{-4})] \tag{B33}$$

for classes $++$ (upper sign) and $+-$ (lower sign).

As another example, consider needle configurations mirror symmetric about the imaginary axis, which correspond to class (C) in Sec. IV A 1. By symmetry $f_y = 0$. In terms of the angle $\alpha = \Phi_{34} - \Phi_{12} \equiv \Phi_{\rm II} - \Phi_{\rm I}$ enclosed by the two needles, Eqs. (B26)–(B29) lead to

$$\begin{aligned}\mathcal{E} &= 2^{-4}B^{-2} + 2^{-6}\{-1 + 3[\sin(\alpha/2)]^2\}B^{-4},\\ \mathcal{F} &= B^{-1/4} + 2^{-5}\{-1 + 3[\sin(\alpha/2)]^2\}B^{-9/4}, \quad \mathcal{H} = +2^{-9}B^{-4},\end{aligned} \tag{B34}$$

and

$$Df_x/(k_BT) = (\partial/\partial B)\ln[1 + (1,-1) \times 2^{-4}B^{-2} + \{(-7,9) + (24,-24)[\sin(\alpha/2)]^2\} \times 2^{-9}B^{-4}] \tag{B35}$$

for $(OO, O+)$ and [66]

$$Df_x/(k_BT) = (\partial/\partial B)\ln[1 \pm (B^{-1/4} + 2^{-5}\{-1 + 3[\sin(\alpha/2)]^2\}B^{-9/4}) + 2^{-4}B^{-2} + \mathcal{O}(B^{-4})] \tag{B36}$$

for $++$ (upper sign) and $+-$ (lower sign). The special cases (i) and (ii) of collinear and symmetric-parallel needles correspond to $\alpha = \pi$ and $\alpha = 0$, respectively. For $0 < \alpha < \pi$ needle II exerts a nonvanishing torque Θ on needle I, where $\Theta/(k_BT) = -(\partial/\partial\Phi_{\rm I})\delta F/(k_BT)$ is given by the right-hand sides of Eqs. (B35) and (B36) with $\partial/\partial B$ replaced with $-\partial/\partial\alpha$. For $(OO, O+)$ one finds from Eq. (B35) that $\Theta/(k_BT) = (-1,1)2^{-7}3B^{-4}\sin\alpha + \mathcal{O}(B^{-6})$. The sign of Θ indicates that the interaction is dominated by the two closer needle halves.

We also consider case (D) in Sec. IV A 1, in which the two needles of equal length D form angles $\Phi_{12} \equiv \Phi_{\rm I} \equiv \Phi$ and $\Phi_{34} = \Phi + \pi$ with the vector $z_{\rm I} - z_{\rm II} > 0$ between their centers on the x axis. For this geometry Eqs. (B23)–(B30) yield

$$Df_x/(k_BT) = (\partial/\partial B)\ln(1 + S), \quad S = \pm[2^{-4}B^{-2} + \{-1 + 3(\cos\Phi)^2\}2^{-6}B^{-4}] + \cos(4\Phi)2^{-9}B^{-4}, \tag{B37}$$

and

$$Df_y/(k_BT) = [\pm 6\sin(2\Phi) + \sin(4\Phi)]2^{-7}B^{-5}/(1 + S) \tag{B38}$$

for needle classes OO (upper sign) and $O+$ (lower sign). For needle classes $++$ (upper sign) and $+-$ (lower sign) the force components are

$$\begin{aligned}Df_x/(k_BT) &= (\partial/\partial B)\ln(1 + S'),\\ S' &= \pm[B^{-1/4} + \{-1 + 3(\cos\Phi)^2\}2^{-5}B^{-9/4}] + 2^{-4}B^{-2} + \{-1 + 3(\cos\Phi)^2\}2^{-6}B^{-4} + \cos(4\Phi)2^{-9}B^{-4},\end{aligned} \tag{B39}$$

and

$$Df_y/(k_BT) = \{\pm 3[\sin(2\Phi)]2^{-5}B^{-13/4} + [6\sin(2\Phi) + \sin(4\Phi)]2^{-7}B^{-5}\}/(1 + S'). \tag{B40}$$

In Sec. V we found it convenient to rotate this same configuration by an angle $\pi - \Phi$, so that needles I and II are antiparallel and parallel to the real axis and $z_{\rm I} - z_{\rm II} = |\mathbf{r}_{\rm I} - \mathbf{r}_{\rm II}|e^{i(\pi-\Phi)}$, implying $[r_{{\rm I},x} - r_{{\rm II},x}, r_{{\rm I},y} - r_{{\rm II},y}] = |\mathbf{r}_{\rm I} - \mathbf{r}_{\rm II}| \times \{\sin[\Phi - (\pi/2)],\ \cos[\Phi - (\pi/2)]\}$. For this orientation,

$$Df_x/(k_BT) = (\pm\{(2B)^{-3} + (2B)^{-5}[-5 + 9(\cos\Phi)^2]\}\cos\Phi + 2^{-7}B^{-5}\cos(5\Phi))/(1+S), \tag{B41}$$

$$Df_y/(k_BT) = (\pm\{-(2B)^{-3} + (2B)^{-5}[2 - 9(\cos\Phi)^2]\}\sin\Phi - 2^{-7}B^{-5}\sin(5\Phi))/(1+S), \tag{B42}$$

for needle universality classes OO (upper sign) and $O+$ (lower sign), while for $++$ (upper sign) and $+-$ (lower sign)

$$Df_x/(k_BT) = (\pm\{B^{-5/4} - 2^{-5}3B^{-13/4}[11 - 17(\cos\Phi)^2]\}(\cos\Phi)/4 + \{(2B)^{-3} + (2B)^{-5}[-5 + 9(\cos\Phi)^2]\}\cos\Phi + 2^{-7}B^{-5}\cos(5\Phi))/(1+S'), \tag{B43}$$

$$Df_y/(k_BT) = (\pm\{-B^{-5/4} + 2^{-5}3B^{-13/4}[3 - 17(\cos\Phi)^2]\}(\sin\Phi)/4 + \{-(2B)^{-3} + (2B)^{-5}[2 - 9(\cos\Phi)^2]\}\sin\Phi - 2^{-7}B^{-5}\sin(5\Phi))/(1+S'). \tag{B44}$$

As required by symmetry, f_x and f_y in Eqs. (B37)–(B40) are even and odd in Φ, respectively, and in Eqs. (B41)–(B44) they are odd and even in $\Phi - (\pi/2)$. For the torque Θ in case (D) our operator expansion yields

$$\Theta/(k_BT) = -[\pm 6\sin(2\Phi) + \sin(4\Phi)]2^{-8}B^{-4}/(1+S) \tag{B45}$$

for needle classes OO (upper sign) and $O+$ (lower sign) and

$$\Theta/(k_BT) = -\{\pm 3[\sin(2\Phi)]2^{-6}B^{-9/4} + [6\sin(2\Phi) + \sin(4\Phi)]2^{-8}B^{-4}\}/(1+S') \tag{B46}$$

for needle classes $++$ (upper sign) and $+-$ (lower sign).

For two small needles with arbitrary lengths $D_{\rm I}$, $D_{\rm II}$ and with their centers on the x axis, the SPOE reproduces the leading force contribution (4.28) to f_x and yields

$$f_y/k_BT = \pm\frac{3}{64}\frac{(D_{\rm I}D_{\rm II})^{1/8}}{|z_{\rm I,II}|^{13/4}}\left[D_{\rm I}^2\sin(2\Phi_{\rm I}) + D_{\rm II}^2\sin(2\Phi_{\rm II})\right]/(1\pm\sigma),$$

$$\Theta/k_BT = \mp\frac{3}{64}\frac{(D_{\rm I}D_{\rm II})^{1/8}D_{\rm I}^2}{|z_{\rm I,II}|^{9/4}}\sin(2\Phi_{\rm I})/(1\pm\sigma), \tag{B47}$$

where $\sigma \equiv (D_{\rm I}D_{\rm II})^{1/8}/|z_{\rm I,II}|^{1/4}$, for the leading contributions to f_y and Θ in the case of needle universality classes $++$ (upper case) and $+-$ (lower case). The SPOE also reproduces the leading hyperuniversal contributions (4.29) and (4.30) to the force and torque derived from the h expansion. For the latter quantities this is apparent from Eqs. (4.31) and (B28) since $\delta F^{\rm (hu)}/(k_BT) = -\mathcal{H}$.

b. A small and a semi-infinite needle

The interaction free energy δF [45] of a small needle I and a semi-infinite needle (semi), i.e., the free energy required to transfer I from the bulk plane to the plane with the semi-infinite needle, is determined by

$$e^{-\delta F/(k_BT)} = 1 + \langle s_{\rm I}\rangle_{\rm semi}. \tag{B48}$$

Here $s_{\rm I}$ is the operator series in Eq. (B16), and $\langle\,\rangle_{\rm semi}$ denotes a thermal average in the $z = r_x + ir_y$ plane with a semi-infinite needle of class $H_{\rm semi}$ coinciding with the positive real axis, as in Sec. IV B. Since the semi-infinite needle can be generated from the boundary of the upper half w plane by the conformal transformation $z = w^2$, the averages of the various operators on the right-hand side of Eq. (B48) follow from their counterparts in the half plane. From Eqs. (B22) and (2.1) and the vanishing of $\langle T(w)\rangle_{\rm half\ plane}$, we obtain

$$\langle\mathcal{O}(r_{{\rm I},x}, r_{{\rm I},y})\rangle_{\rm semi} = \mathcal{A}_{\mathcal{O}}^{(H_{\rm semi})}[2|z_{\rm I}|\sin((\arg z_{\rm I})/2)]^{-x_{\mathcal{O}}} = \mathcal{A}_{\mathcal{O}}^{(H_{\rm semi})}[2|z_{\rm I}|(|z_{\rm I}| - r_{{\rm I},x})]^{-x_{\mathcal{O}}/2} \tag{B49}$$

and

$$\langle\tilde{T}({\rm I})\rangle_{\rm semi} = -\cos\left[2(\Phi_{\rm I} - \arg z_{\rm I})\right]/(64\pi|z_{\rm I}|^2), \tag{B50}$$

where $0 < \arg z_{\rm I} < 2\pi$ and the position vector $z_{\rm I} = r_{{\rm I},x} + ir_{{\rm I},y}$ is defined below Eq. (4.36). The expression

$$\frac{f_x - if_y}{k_BT} = \frac{1}{1 + \langle s_{\rm I}\rangle_{\rm semi}}\left(\frac{\partial}{\partial r_{{\rm I},x}} - i\frac{\partial}{\partial r_{{\rm I},y}}\right)\langle s_{\rm I}\rangle_{\rm semi} \tag{B51}$$

for the force, which follows from Eqs. (B48) and (B16), reproduces, in leading order, the result from the h expansion given below Eq. (4.44). The reason is that in

$$\left(\frac{\partial}{\partial r_{{\rm I},x}} - i\frac{\partial}{\partial r_{{\rm I},y}}\right)\langle\mathcal{O}\rangle_{\rm semi} = -x_{\mathcal{O}}\frac{3z_{\rm I} - |z_{\rm I}|}{2z_{\rm I}(z_{\rm I} - |z_{\rm I}|)}\langle\mathcal{O}\rangle_{\rm semi}, \tag{B52}$$

with $\langle\mathcal{O}\rangle_{\rm semi}$ from Eq. (B49), the same fraction appears on the right-hand side as in Eq. (4.44), and on expressing $\langle\mathcal{O}\rangle_{\rm semi}$ via (4.42) in terms of $h/|z_{12}| \equiv h/D_{\rm I}$, one may use that

$$\sum_{\mathcal{O}=\phi,\epsilon} \mathcal{A}_{\mathcal{O}}^{(H_{\rm I})}\, \mathcal{A}_{\mathcal{O}}^{(H_{\rm semi})}\, x_{\mathcal{O}}\, (4h)^{x_{\mathcal{O}}} \;\to\; t(h\to 0) \;\equiv\; \{h, -h, (\sqrt{2}/8)h^{1/8}, -(\sqrt{2}/8)h^{1/8}\} \tag{B53}$$

for $\{O\,O, O+, ++, +-\}$. Moreover, in the cases $++$ and $+-$, the denominator on the right - side of (B51) is consistent with the denominators in Eq. (4.27).

The orientation-dependent contribution to $e^{-\delta F/(k_B T)}$ of lowest order in the needle length,

$$2^{-9}(D_{\rm I}/|z_{\rm I}|)^2\, \cos[2(\Phi_{\rm I} - \arg z_{\rm I})], \tag{B54}$$

comes from inserting the stress tensor average (B50) in Eq. (B48), using Eq. (B16), and is independent of the needle classes $H_{\rm I}$ and $H_{\rm semi}$. For universality classes $O\,O$ and $O+$, the contribution (B54) clearly dominates the orientation dependence $\propto D_{\rm I}^{x_\epsilon+2} = D_{\rm I}^3$ coming from the $\mathcal{D}_{\rm I}\mathcal{O}$-term in Eq. (B16), provided that the components $r_{{\rm I},x}$ and $r_{{\rm I},y}$ of $z_{\rm I}$ are of the same order. However, on approaching the limit $r_{{\rm I},x} \to +\infty$ with $r_{{\rm I},y}$ finite, the contribution from the $\mathcal{D}_{\rm I}\mathcal{O}$ term approaches the finite orientation dependence of a needle in the half plane [see Eq. (B55) below], while the contribution (B54) vanishes. For classes $++$ and $+-$ the $\mathcal{D}_{\rm I}\mathcal{O}$ term contributes an orientation dependence preceded by a power law $D_{\rm I}^{(1/8)+2}$ with an exponent which is only slightly larger than the exponent of the power $D_{\rm I}^2$ in Eq. (B54). Note that Eq. (B54) favors needle orientations parallel and antiparallel to the vector $z_{\rm I}$ from the midpoint of the finite needle to the finite end of the semi-infinite needle.

c. A small needle in the half plane and in the symmetric-parallel configuration

For a small needle I in the uhp the free energy δF of interaction [45] with the boundary of surface class $H_{\rm S}$ at $r_y = 0$ is determined by Eq. (B48), with $\langle\,\rangle_{\rm semi}$ replaced with the average $\langle\,\rangle_{\rm uhp}$ in the half plane. The expressions for $\langle\mathcal{O}\rangle_{\rm uhp}$ given above Eq. (B20) and the vanishing of the stress tensor average imply

$$e^{-\delta F/(k_B T)} = 1 + \sum_{\mathcal{O}=\phi,\epsilon} \mathcal{A}_{\mathcal{O}}^{(H_{\rm I})}\mathcal{A}_{\mathcal{O}}^{(H_{\rm S})}\left(\frac{D_{\rm I}}{2r_{{\rm I},y}}\right)^{x_{\mathcal{O}}}\left\{1 + \left(\frac{D_{\rm I}}{2r_{{\rm I},y}}\right)^2 \frac{1}{16}[x_{\mathcal{O}} + 1 - 3x_{\mathcal{O}}\cos(2\Phi_{\rm I})]\right\}. \tag{B55}$$

Both the force and the torque follow from Eq. (B55).

The force $f = -\partial\delta F/\partial r_{{\rm I},y}$ with $D_{\rm I}$ and $\Phi_{\rm I}$ fixed is given by

$$D_{\rm I} f/(k_B T) = (\partial/\partial\tilde{B})\ln\left(1 \pm \tfrac{1}{4}(2\tilde{B})^{-1}\left\{1 + (2\tilde{B})^{-2}\tfrac{1}{16}[2 - 3\cos(2\Phi_{\rm I})]\right\}\right) \tag{B56}$$

for classes $O\,O$ (upper sign) and $O+$ (lower sign), and by

$$D_{\rm I} f/(k_B T) = (\partial/\partial\tilde{B})\ln\left(1 \pm 2^{1/4}(2\tilde{B})^{-1/8}\left\{1 + (2\tilde{B})^{-2}\frac{3}{2^7}[3 - \cos(2\Phi_{\rm I})]\right\} + \frac{1}{4}(2\tilde{B})^{-1}\left\{1 + (2\tilde{B})^{-2}\frac{1}{16}[2 - 3\cos(2\Phi_{\rm I})]\right\}\right) \tag{B57}$$

for $++$ (upper sign) and $+-$ (lower sign). Here $\tilde{B} = r_{{\rm I},y}/D_{\rm I}$.

The expressions for the torque per $k_B T$, $-\partial(\delta F/k_B T)/\partial\Phi_{\rm I}$, follow for the various cases of universality classes $H_{\rm I}\,H_{\rm S}$ from the corresponding right-hand sides of Eqs. (B56) and (B57) on replacing $(\partial/\partial\tilde{B})$ with $(\partial/\partial\Phi_{\rm I})$.

Next we consider a small needle in the symmetric-parallel configuration (B) of Fig. 3, assuming $D_{\rm I}/c \ll 1$ and $D_{\rm II}/c$ arbitrary, where $c = z_{\rm I} - z_{\rm II}$ is the distance between the needles. The limits $D_{\rm II}/c \to \infty$ and $D_{\rm II}/c \ll 1$ correspond to a small needle in the half plane and configuration (B) with two small needles of different lengths, respectively. The free energy δF is determined by Eq. (B48) with $\langle\,\rangle_{\rm semi}$ replaced with the average $\langle\,\rangle_{\rm II}$ in the plane containing needle II. For a needle II with boundary class $H_{\rm II}$, centered about the origin and extending along the y axis, the profiles of the order parameter and energy density are given by (see, e.g., Appendix A 1 in the first paper of Ref. [17])

$$\langle\mathcal{O}(r_x,0)\rangle_{\rm II}^{(H_{\rm II})} = \mathcal{A}_{\mathcal{O}}^{(H_{\rm II})}(D_{\rm II}/2)^{-x_{\mathcal{O}}}[\Xi(2|r_x|/D_{\rm II})]^{x_{\mathcal{O}}}, \tag{B58}$$

$$\Xi(\xi) \equiv \xi^{-1}(\xi^2+1)^{-1/2}, \tag{B59}$$

for $\mathcal{O} = \phi$ and $\mathcal{O} = \epsilon$, respectively.

Making use of this result and retaining only the the leading monopole contribution in the SPOE, one obtains

$$D_{\rm II} f_x/(k_B T) = 2(\partial/\partial\xi)\ln\left\{1 \pm \tfrac{1}{4}(D_{\rm I}/D_{\rm II})\Xi(\xi)\right\}\big|_{\xi=2c/D_{\rm II}} \tag{B60}$$

for classes $O\,O$ (upper sign), $O+$ (lower sign) and

$$D_{\rm II} f_x/(k_B T) = 2(\partial/\partial\xi)\ln\{1 \pm 2^{1/4}(D_{\rm I}/D_{\rm II})^{1/8}[\Xi(\xi)]^{1/8}\}|_{\xi=2c/D_{\rm II}} \tag{B61}$$

for $++$ (upper sign), $+-$ (lower sign).

APPENDIX C: NONSYMMETRIC PARALLEL NEEDLES WITH STRONG OVERLAP AND LONG MIRROR-SYMMETRIC NEEDLES

Consider configuration (D′) of Fig. 3, corresponding to two needles of equal length oriented parallel to the x axis [54], in the limit of strong overlap. In this limit the distances $|z_1 - z_4| = |z_2 - z_3|$ between the left ends z_1 and z_4 and the right ends z_2 and z_3 of needles I and II, respectively, are much smaller than their lengths $|z_2 - z_1| = |z_3 - z_4| = D$, so that the two needles form boundaries of a long strip of width $W = |r_{1,y} - r_{4,y}| = |r_{2,y} - r_{3,y}|$.

First, we evaluate the torque on needle I using Eqs. (2.7) and (2.8). On integrating closely around needle I, which is located above needle II, the only contributions to θ in Eq. (2.8) come from regions with a width of order $|z_1 - z_4| = |z_2 - z_3|$ near the ends of the needles, i.e., near the ends of the strip. The reason is that (i) $\langle T(z)\rangle$ vanishes outside the strip over most of its length, i.e., over most of the upper edge of needle I, and (ii) inside the strip $\langle T(z)\rangle$ is independent of z and equal to its value $\pi\Delta/W^2$ in an infinite strip, with Δ from [56]. Thus, by virtue of the odd factor $z - z_{\rm I} = r_x - r_{1,x}$ in Eq. (2.8), the interval of integration centered about $r_{1,x} = (r_{1,x} + r_{2,x})/2$ and comprising nearly all of the lower edge of needle I gives a vanishing contribution. For large D/W the two end regions are uncorrelated, and each is equivalent to the end region of a system of two semi-infinite needles. Replacing $z - z_{\rm I}$ in the left and right end contributions by $-D/2$ and $D/2$, respectively, we obtain

$$\pi\theta \to -(D/2)\lim_{d\to+\infty} \times\left[\int_{\mathcal{C}_{\rm I+}(d)} dz\langle T(z)\rangle_{\rm si+} - \int_{\mathcal{C}_{\rm I-}(d)} dz\langle T(z)\rangle_{\rm si-}\right]. \quad \text{(C1)}$$

Here si+ denotes a system of two semi-infinite needles I_+ and II_+ extending from z_1 and z_4 to $z_1 + |\infty|$ and $z_4 + |\infty|$, respectively, while si− is the system of two needles I_- and II_- extending from z_2 and z_3 to $z_2 - |\infty|$ and $z_3 - |\infty|$. The integration path $\mathcal{C}_{\rm I+}(d)$ goes clockwise around the tip z_1 of needle I_+, starting at $z = z_1 + d - i0$ and ending at $z = z_1 + d + i0$. Similarly, $\mathcal{C}_{\rm I-}(d)$ goes clockwise around the tip z_2 of needle I_-, starting at $z = z_2 - d + i0$ and ending at $z = z_2 - d - i0$.

On rotating by 180°, the si− system is mapped onto the si+ system, with needle I_- mapped onto needle II_+, i.e., z_2 onto z_4, and needle II_- mapped onto I_+, i.e., z_3 onto z_1. Since exchanging the universality classes in a two-needle system does not change the stress tensor average [49], it is the same for the si+ and rotated si− systems. Moreover, the rotation changes $dz \to -dz$, while no prefactor arises in front of T, and Eq. (C1) yields

$$\pi\theta \to -(D/2)\lim_{d\to+\infty}\int_{\mathcal{C}_{\rm I+}(d)+\mathcal{C}_{\rm II+}(d)} dz\langle T(z)\rangle_{\rm si+}. \quad \text{(C2)}$$

Here the path $\mathcal{C}_{\rm II+}(d)$ encircles the tip z_4 of needle II_+ clockwise, starting at $z_4 + d - i0$ and ending at $z_4 + d + i0$. The integration path in Eq. (C2) becomes connected, leading to a vanishing result, if one adds both a vertical segment from $z_4 + d + i0$ to $z_1 + d + r_{4,x} - r_{1,x} - i0$ and a horizontal segment from $z_1 + d + r_{4,x} - r_{1,x} - i0$ to $z_1 + d - i0$ to the integration path. Since for both segments $\langle T(z)\rangle_{\rm si+}$ equals its value inside the infinite strip, and since the vertical segment leads to a purely imaginary result, the torque $\Theta = -k_BT\,\mathrm{Re}\,\theta$ on needle I is given by $-1/\pi$ times the contribution of the horizontal segment, with the result

$$\frac{\Theta}{k_BT} = -\frac{D}{2}\frac{(r_{1,x} - r_{4,x})\Delta}{W^2}, \quad \text{(C3)}$$

where Δ depends on the universality classes of the two needles, as specified in Ref. [56].

We now calculate the component f_x of the force on needle I due to needle II. For this, it is convenient to place the origin at the center of reflection of the needle configuration by setting $z_3 = -z_1$, $z_4 = -z_2$ and to integrate along a path $\mathcal{C}_{\rm I}$ in Eq. (2.4) midway between the needles along the real axis from $z = +\infty$ to $z = -\infty$, closing the path with a semicircle of infinite radius which does not contribute to the integral. Since $\langle T(z = r_x)\rangle = \langle T(z = -r_x)\rangle$, and since $\mathrm{Im}\langle T(z = r_x)\rangle$ vanishes except near the ends of the needle, the desired integral over $\mathrm{Im}\langle T(z = r_x)\rangle$ equals twice the corresponding integral with I and II replaced with their semi-infinite counterparts I_+ and II_+. In this way we obtain

$$\frac{f_x}{k_BT} = \frac{\pi}{W}\left(\frac{1}{48}\frac{1 + 3b - 3b^2 - b^3}{1 + 3b + 3b^2 + b^3} - \frac{1 - b}{1 + b}\tilde{t}\right), \quad \text{(C4)}$$

where $\tilde{t}$ is given in Eq. (3.4). Here b is positive and related by

$$(r_{1,x} - r_{4,x})/W = \frac{1}{2\pi}(2\ln b + b - 1/b) \quad \text{(C5)}$$

to the ratio $(r_{1,x} - r_{4,x})/W$ of the parallel and perpendicular components of the vector between the two left needle ends. As expected, $f_x/(k_BT)$ is an odd function of $r_{1,x} - r_{4,x}$ and tends to Δ/W, $-\Delta/W$, and 0 in the cases $b \to +\infty$, 0, and 1 in which the ratio on the left-hand side of (C5) tends to $+\infty$, $-\infty$, and 0, respectively.

To derive Eqs. (C4) and (C5), we first generate the geometry of parallel semi-infinite needles I_+ and II_+ from the upper half w plane by means of the conformal transformation [67]

$$z(w) = \frac{W}{\pi}\left[\frac{w^2}{2b} + w\left(1 - \frac{1}{b}\right) + \frac{1}{4}\left(\frac{1}{b} + b\right) - 1 - \ln\frac{w}{\sqrt{b}} + \frac{i\pi}{2}\right]. \quad \text{(C6)}$$

Together with (C5) this transformation conveniently places the tips of I_+ and II_+ symmetrically about the origin, at $z = z(1) \equiv z_1 = r_{1,x} + iW/2$ and $z = z(-b) \equiv z_4 = -z_1$, respectively. The integration path mentioned just above Eq. (C4), which is midway between the semi-infinite needles I_+ and II_+, corresponds, according to Eqs. (2.4) and (2.5), to the imaginary axis of the upper half w plane. Similarly, the integral over $\mathrm{Im}\langle T(z = r_x)\rangle$ corresponds to the integral of a real rational function of $|w|$ from 0 to $+\infty$ and leads to a force f_x on needle I_+ due to II_+ which is exactly half of f_x in Eq. (C4) [68].

Finally, we consider the mirror-symmetric needle configuration [class (C) of Sec. IV A 1] and argue that in this case the torque Θ also increases linearly with the needle length D for $D \to \infty$. First we place needles I and II so that $z_2 = 1$, $z_1 = D + 1$ and $z_4 = e^{i\alpha}z_2$, $z_3 = e^{i\alpha}z_1$. We also introduce

an auxiliary "wedge" configuration of two corresponding semi-infinite needles which extend from $z = 0$ to $|\infty|$ and to $e^{i\alpha}|\infty|$, dividing the z plane into two wedges of opening angles α and $2\pi - \alpha$. To evaluate θ in Eq. (2.8), we choose $\mathcal{C}_{\rm I}$ so that it encircles needle I closely and subtract and add $\langle T(z)\rangle_{\rm wedge}$ to $\langle T(z)\rangle$. This leads to $\theta = \delta\theta + \tilde{\theta}$, where

$$\delta\theta = \int_{\mathcal{C}_{\rm I}} dz[\langle T(z)\rangle - \langle T(z)\rangle_{\rm wedge}]\left\{r_x - \left(\frac{D}{2}+1\right)\right\},$$
$$\tilde{\theta} = \int_1^{D+1} dr_x \langle T(r_x + i0) - T(r_x - i0)\rangle_{\rm wedge} \times \left\{r_x - \left(\frac{D}{2}+1\right)\right\}. \tag{C7}$$

Since $\langle T(z)\rangle_{\rm wedge} \propto z^{-2}$ [34], its average in the integral for $\tilde{\theta}$ is proportional to r_x^{-2}, and calculating the integral reveals the leading behavior $\tilde{\theta} \propto D$ for $D \gg 1$. Since the square bracket becomes arbitrarily small, for $z = r_x + i0$ and $z = r_x - i0$, in the "central" region $1 \ll r_x \ll D$, the quantity $\delta\theta$ represents the contribution to the torque from the ends of the needles, and $\delta\theta$ can be written as a sum of two expressions. One of these, $\delta_<\theta$, corresponds to semi-infinite needles extending from 1 to $|\infty|$ and from $e^{i\alpha}$ to $e^{i\alpha}|\infty|$. The other contribution, $\delta_>\theta$, corresponds to needles extending from 0 to D and from 0 to $e^{i\alpha}D$. In the case of $\delta_<\theta$, the difference $\langle T(z)\rangle - \langle T(z)\rangle_{\rm wedge}$ for $r_x \gg 1$ is proportional to $r_x^{-2-(2\pi/\alpha)}$, if $z = r_x + i0$, and to $r_x^{-2-[2\pi/(2\pi-\alpha)]}$, if $z = r_x - i0$. This follows from Eqs. (3.7)–(3.10) for the mirror-symmetric case considered here with $b = 1$. Thus, only r_x values of order 1 contribute, and $\delta_<\theta$ is proportional to D for $D \to \infty$. As for $\delta_>\theta$, its needle geometry can be mapped either by the dilatation $z/D \to z$ to needles of length 1 or by the inversion $D/z \to z$ to the needle geometry of $\delta_<$. Either way, one realizes that $\delta_>\theta$ is of order 1. The plausible assumption that the D dependence from $\tilde{\theta}$ and $\delta_<\theta$ does not cancel leads to the predictions $\theta \propto D$ and $\Theta \propto D$ for $D \to \infty$, in agreement with the numerical results for case (C) in Sec. V.

For a needle I with ends at $e^{i\Phi}$ and $(D+1)e^{i\Phi}$ in the upper half plane, similar arguments also imply $\Theta \propto D$ for $D \to \infty$. This is consistent with the numerical results for the torque in Fig. 11 for Φ close to $\pi/3$.

APPENDIX D: NEEDLES WITH MIXED BOUNDARY CONDITIONS

1. Half plane with inhomogeneous boundary conditions

We begin with a discussion of $\langle T(w)\rangle_{u_1,u_2,\ldots,u_N}$ in the upper half w plane with boundary conditions on the real axis that alternate between $+$ and $-$ at the N points $u_1, u_2, \ldots, u_N$. If, for example, the boundary condition for $-\infty < u < u_1$ is $+$, then it is $-$ for $u_1 < u < u_2$, $+$ for $u_2 < u < u_3$, etc. The stress tensor for such mixed boundary conditions is of interest in its own right and is also the starting point for studying the Casimir interaction of needles with mixed boundary conditions.

For $N = 0$, $\langle T(w)\rangle$ vanishes, and for $N = 1, 2$ [48]

$$\langle T(w)\rangle_{u_1} = \frac{\tilde{t}}{(w-u_1)^2},$$
$$\langle T(w)\rangle_{u_1,u_2} = \tilde{t}\left(\frac{1}{w-u_1} - \frac{1}{w-u_2}\right)^2, \tag{D1}$$
$$\tilde{t} = \tilde{t}_{+-} \equiv 1/2.$$

For $N = 3$

$$\langle T(w)\rangle_{u_1,u_2,u_3} = \frac{1}{(u_{12})^{-1} - (u_{13})^{-1} + (u_{23})^{-1}}\{[12] - [13] + [23] + (12,3) - (13,2) + (23,1)\},$$
$$[ab] \equiv \frac{\langle T(w)\rangle_{u_a,u_b}}{u_{ab}}, \quad (ab,c) \equiv \frac{1}{u_{ab}}\langle T(w)\rangle_{u_c}, \tag{D2}$$

and for $N = 4$

$$\langle T(w)\rangle_{u_1,u_2,u_3,u_4} = \frac{1}{(u_{12}u_{34})^{-1} - (u_{13}u_{24})^{-1} + (u_{23}u_{14})^{-1}}([12]/u_{34} - [13]/u_{24} + [14]/u_{23} + [23]/u_{14} - [24]/u_{13} + [34]/u_{12}), \tag{D3}$$

respectively, where $u_{ab} = u_a - u_b$. For N an arbitrary even integer $\geqslant 4$

$$\langle T(w)\rangle_{u_1,u_2,\ldots,u_N} = \left(\mathrm{Pf}^{(N)}\frac{1}{u_{ij}}\right)^{-1} \times \frac{\partial}{\partial\lambda}\mathrm{Pf}^{(N)}\left(\frac{1}{u_{ij}} + \lambda[ij]\right)\Big|_{\lambda=0}$$
$$= \left(\mathrm{Pf}^{(N)}\frac{1}{u_{ij}}\right)^{-1} \times \sum_{1\leqslant a<b\leqslant N}(-1)^{a+b+1}[ab]\,\mathrm{Pf}_{ab}^{(N\to N-2)}\frac{1}{u_{ij}}. \tag{D4}$$

Here $\mathrm{Pf}^{(N)}A_{ij}$ is the Pfaffian [69] of the $N \times N$ antisymmetric matrix with elements $A_{ij} = -A_{ji}$, the sum in Eq. (D4) contains $\frac{1}{2}N(N-1)$ terms, and $\mathrm{Pf}_{ab}^{(N\to N-2)}A_{ij}$ is the Pfaffian of the $(N-2)\times(N-2)$ matrix obtained from the $N \times N$ matrix by removing the ath and bth rows and columns. In the limit $u_N \to \infty$ Eq. (D4) yields the stress tensor for an arbitrary odd number $N-1$ of switches. Equation (D3) follows from Eq. (D4) for $N = 4$ and Eq. (D2) from Eq. (D3) in the limit $u_4 \to \infty$. Since the operator T is even in the order parameter field ϕ, $\langle T(w)\rangle_{u_1,u_2,\ldots,u_N}$ is unchanged on exchanging $+$ and $-$ in the boundary conditions.

Equation (D4) follows from the result

$$\langle\phi(w_1,\bar w_1)\,\phi(w_2,\bar w_2)\rangle_{u_1,u_2,\ldots,u_N} = \left(\mathrm{Pf}^{(N)}\frac{1}{u_{ij}}\right)^{-1}\langle\phi(w_1,\bar w_1)\,\phi(w_2,\bar w_2)\rangle\,\mathrm{Pf}^{(N)}\left[\frac{1}{u_{ij}}\frac{\langle\phi(w_1,\bar w_1)\,\phi(w_2,\bar w_2)\rangle_{u_i,u_j}}{\langle\phi(w_1,\bar w_1)\,\phi(w_2,\bar w_2)\rangle}\right] \tag{D5}$$

of Burkhardt and Guim [70] for the two-point correlations of the order parameter in the presence of mixed boundary conditions. In this expression the angular brackets without subscripts denote thermal averages for a homogeneous + or − boundary condition. In the limit that w_1 is much closer to w_2 than to the boundary, Eq. (D5) must be consistent with the OPE,

$$\phi(w_1,\bar w_1)\,\phi(w_2,\bar w_2) \to |w_{12}|^{-1/4}\big\{1-\tfrac{1}{2}|w_{12}|\epsilon(w,\bar w)+\tfrac{1}{4}\big[w_{12}^2T(w)+\bar w_{12}^2\bar T(\bar w)\big]+\mathcal{O}(|w_{12}|^3)\big\},$$
$$w_{12}\equiv w_1-w_2,\quad w\equiv(w_1+w_2)/2, \tag{D6}$$

see, e.g., Eq. (2.39) and Sec. III C in Ref. [57]. Substituting the expansion (D6) in all the averages in Eq. (D5) and comparing the coefficients of $|w_{12}|^{-1/4}w_{12}^2$ on the right- and left-hand sides leads to Eq. (D4).

2. Interaction of semi-infinite needles with mixed boundary conditions

Under the mapping (3.8) of the upper half w plane onto the z plane with two embedded semi-infinite needles, the intervals $-\infty<u<-b$, $-b<u<0$ and $0<u<1$, $1<u<+\infty$, which we denote by (i), (ii) and (iii), (iv), respectively (not the same notation as in Fig. 1), map onto the edges of the semi-infinite needles II and I, respectively. In the notation of the preceding section, we consider the following distributions of surface universality classes + and − along the u axis:

(1) $N=0$,
(2) $N=2, u_1=-b, u_2=1$,
(3) $N=3, u_1=-b, u_2=0, u_3=1$,
(4) $N=1, u_1=0$,
(5) $N=1, u_1=1$.

In cases (1) and (4), which were considered in Sec. III B, the boundary conditions on the two edges of each needle are the same. In cases (2), (3), and (5), on the other hand, one or both of the needles has a different boundary condition on each of its two edges. The stress tensor averages given above allow us to calculate the force between these needles.

We illustrate the approach in the particularly simple case of *collinear* semi-infinite needles generated by the mapping (3.8) with $b=1$ and $\alpha=\pi$. Needles I and II occupy the portions $-\infty<x<-|z(1)|=-4\mathcal{B}$ and $0<x<+\infty$, respectively, of the x axis, and the four intervals of the boundary of the w plane map onto the upper and lower edges of needles I and II according to

$$\text{(i)}\to\mathrm{II}_{\mathrm{lower}},\quad \text{(ii)}\to\mathrm{II}_{\mathrm{upper}},$$
$$\text{(iii)}\to\mathrm{I}_{\mathrm{upper}},\quad \text{(iv)}\to\mathrm{I}_{\mathrm{lower}}. \tag{D7}$$

Starting with + at $u=-\infty$, Eq. (D7) implies

$$\begin{pmatrix}\mathrm{I}_{\mathrm{upper}} & \mathrm{II}_{\mathrm{upper}}\\ \mathrm{I}_{\mathrm{lower}} & \mathrm{II}_{\mathrm{lower}}\end{pmatrix}=\begin{pmatrix}+&+\\+&+\end{pmatrix},\begin{pmatrix}-&-\\+&+\end{pmatrix},\begin{pmatrix}+&-\\-&+\end{pmatrix},\begin{pmatrix}-&+\\-&+\end{pmatrix},\begin{pmatrix}+&+\\-&+\end{pmatrix} \tag{D8}$$

in cases (1)–(5), respectively. The force acting on needle I follows from Eqs. (2.3) and (2.5), the collinear needle mapping $z(w)$, and the averages $\langle T(w)\rangle_{\ldots}$ in Eqs. (D1) and (D2). The component f_x is given by [50]

$$16|z(1)|f_x/(k_BT)=1,\quad 1+16\tilde t=9,$$
$$-7,1-32\tilde t=-15,\ 1-8\tilde t=-3;\quad \tilde t\equiv 1/2, \tag{D9}$$

in cases (1)–(5), respectively, and the component f_y vanishes in all the cases except (5), where $|z(1)|f_y/(k_BT)=-2\tilde t/\pi\equiv -1/\pi$.

It is remarkable that in case (2) of Eqs. (D8) and (D9), the attraction is 9 times stronger than in case (1). To help understand this result, note that for the same *nonvanishing* distance $|z(1)|$ between the needle tips, the free energy is greater in case (2) than in case (1), since in case (2) the spins change direction near the needle tips. However, when the tips touch, the free energy is the same in cases (1) and (2), since the upper and lower halves of the z plane are decoupled. Thus, the free-energy varies more rapidly with the tip separation in case (2).

3. Semi-infinite needle perpendicular to an infinite needle

Next we consider a semi-infinite needle I in the upper half z plane oriented *perpendicular* to an infinite needle II on the x axis, as described by Eq. (3.2) with $\alpha=\pi/2$. The tip of needle I is at $z=z(1)=4\mathcal{A}i$, and the preimage of the origin $z=0$ is at $w=u=-1$. Allowing for both a homogeneous boundary (+ for all x) and a boundary with a "chemical step" at the origin (i.e., a mixed boundary with + for $x<0$ and − for $x>0$), and allowing for different boundary conditions on the right and left edges of needle I, we consider the six cases

$$\begin{pmatrix}\mathrm{I}_{\mathrm{left}} & \mathrm{I}_{\mathrm{right}}\\ \mathrm{II}_{\mathrm{left}} & \mathrm{II}_{\mathrm{right}}\end{pmatrix}=\begin{pmatrix}+&+\\+&+\end{pmatrix},\begin{pmatrix}+&-\\+&-\end{pmatrix},\begin{pmatrix}-&+\\+&-\end{pmatrix},\begin{pmatrix}-&-\\+&+\end{pmatrix},\begin{pmatrix}-&+\\+&+\end{pmatrix},\begin{pmatrix}+&+\\+&-\end{pmatrix}. \tag{D10}$$

The stress tensor averages $\langle T(w)\rangle$ in the first five cases are the five defined in the first paragraph of Sec. II with $b=1$ and in the sixth case $N=2$, $u_1=-b=-1$, $u_2=0$, corresponding to

$$\text{(i)}\to\mathrm{II}_{\mathrm{left}},\quad \text{(ii)}\to\mathrm{II}_{\mathrm{right}},\quad \text{(iii)}\to\mathrm{I}_{\mathrm{right}},\quad \text{(iv)}\to\mathrm{I}_{\mathrm{left}}. \tag{D11}$$

Together with Eqs. (3.1), (2.3), and (2.5) this leads to [50]

$$32|z(1)|f_y/(k_BT)=-3,\ -3(1+16\tilde t)=-27,\ 37,$$
$$-3+128\tilde t=61,\quad 3(-1+16\tilde t)=21,$$
$$-3+32\tilde t=13;\quad \tilde t\equiv 1/2. \tag{D12}$$

The parallel force component f_x vanishes in cases (1)–(5), and in case (6), $|z(1)|f_x/(k_BT) = -2\tilde{t} \equiv -1$. The factor 9 increase in attraction on going from (1) to (2) has an explanation similar to the one below Eq. (D9).

In principle, one can calculate the force for arbitrary configurations of two semi-infinite or infinite needles with an arbitrary configuration of "chemical steps" with this approach.

As a final example, we consider the Casimir force exerted on the semi-infinite needle I by the boundary II of the upper half z plane in the presence of chemical steps at two arbitrary points,

$$x_1 \equiv X_1|z(1)| < x_2 \equiv X_2|z(1)|, \tag{D13}$$

which separate the x axis into regions with $+, -, +$ boundary conditions. Needle I has boundary condition $+$ on both of its edges and extends along the y axis from $y = |z(1)|$ to $y = +\infty$. The arrangement is reminiscent of an atomic-force microscope probing an inhomogeneous boundary. The force follows from the mapping (3.2) with $\alpha = \pi/2$ and the stress tensor in Eq. (D1) with $N = 2$ and $u_1 = -|u_1|, u_2 = -|u_2|$, where

$$|u_j| = 1 + 2X_j^2 - 2X_j\sqrt{1+X_j^2}; \quad j = 1,2, \tag{D14}$$

and the calculation yields

$$|z(1)|\frac{f_x}{k_BT} = 4\tilde{t}\left\{-\frac{2}{|u_1|-|u_2|}\left[\frac{|u_1|^{3/2}}{1+|u_1|} - \frac{|u_2|^{3/2}}{1+|u_2|}\right] + \sum_{j=1}^{2}\frac{|u_j|^{1/2}(|u_j|+3)}{2(1+|u_j|)^2}\right\},$$

$$|z(1)|\frac{f_y}{k_BT} = -\frac{3}{32} + 4\tilde{t}\left(\frac{1}{1+|u_1|} - \frac{1}{1+|u_2|}\right)^2, \tag{D15}$$

where $|u_j|$ is defined in Eq. (D14):

To get a feeling for the result, we discuss two special cases:

(A) *Boundary with a single step.* In the limit $x_2 \to +\infty$, i.e., $|u_2| \to 0$, only the single step on the boundary at x_1 remains. It separates regions with $+$ and $-$ boundary conditions to its left and right, respectively. The corresponding force on needle I is

$$|z(1)|\frac{f_x}{k_BT} = -2\tilde{t}\frac{|u_1|^{1/2}(3|u_1|+1)}{(1+|u_1|)^2},$$

$$|z(1)|\frac{f_y}{k_BT} = -\frac{3}{32} + 4\tilde{t}\frac{|u_1|^2}{(1+|u_1|)^2}, \tag{D16}$$

with $|u_1|$ given by Eq. (D14). While the parallel force component f_x is negative for all x_1, the perpendicular component f_y changes sign from positive to negative on increasing x_1 beyond a critical value of the order of $|z(1)|$. This is expected, since needle I with its $+$ edges is attracted to the $+$ region and repelled by the $-$ region of the boundary. For $x_1 \to [-\infty, 0, +\infty]$, $|z(1)|f_x/(k_BT) \to -\tilde{t}[3/|X_1|, 2, 1/X_1]$ and $|z(1)|f_y/(k_BT) \to -(3/32) + \tilde{t}[4 - (2/X_1^2), 1, 1/(4X_1^4)]$. For $x_1 = 0$ one recovers case (6) defined below Eq. (D10), and Eq. (D16) reproduces the corresponding force components given in the paragraph containing Eq. (D12). For $x_1 \to -\infty$ and $x_1 \to +\infty$, Eq. (D16) approaches the force in cases (4) and (1) of Eq. (D12)

(B) *Boundary with two steps at equal distances from the needle.* Since the configuration, with steps at $\pm x_1$ separating the x axis into regions $+,-,+$ is mirror symmetric about the y axis, the parallel component f_x of the force vanishes. The perpendicular component follows from Eqs. (D14) and (D15), which yield $|u_2| = 1/|u_1|$ and

$$|z(1)|\frac{f_y}{k_BT} = -\frac{3}{32} + 4\tilde{t}\frac{X_1^2}{1+X_1^2}. \tag{D17}$$

For $x_1 = 0$ the boundary with two steps reduces to a homogeneous $+$ boundary, and we are back to case (1) of Eqs. (D10) and (D12). For a large distance between the steps, $|x_1| \gg |z(1)|$, Eq. (D17) yields

$$|z(1)|\frac{f_y}{k_BT} \to -\frac{3}{32} + 4\tilde{t} - \frac{4\tilde{t}}{X_1^2}. \tag{D18}$$

Here the first two terms on the right-hand side represent the force exerted on the needle by a homogeneous $-$ boundary, and the third term is contributed by the $+$ boundaries beyond the two distant steps. As expected, the latter contribution is twice the corresponding contribution $-2\tilde{t}/X_1^2$ of a single distant step, given below Eq. (D16).

For switches of the boundary universality class between $+$ and O instead of $+$ and $-$, $\langle T(w)\rangle_{u_1}$ and $\langle T(w)\rangle_{u_1,u_2}$ are again given by Eq. (D1), [48], but with $\tilde{t} = \tilde{t}_{+O} = 1/16$ instead of $\tilde{t} = \tilde{t}_{+-} = 1/2$. Thus, all of the results of this Appendix which are based on the stress tensor for $N = 1$ or $N = 2$ hold, with the appropriate value of $\tilde{t}$, for $+O$ as well as $+-$ switches in the boundary conditions.

[1] C. Hertlein, L. Helden, A. Gambassi, S. Dietrich, and C. Bechinger, Nature (London) **451**, 172 (2008).

[2] A. Gambassi, A. Maciolek, C. Hertlein, U. Nellen, L. Helden, C. Bechinger, and S. Dietrich, Phys. Rev. E **80**, 061143 (2009).

[3] M. E. Fisher and P. G. de Gennes, C. R. Acad. Sci. Paris **287**, B-207 (1978).

[4] M. Krech, *The Casimir Effect in Critical Systems* (World Scientific, Singapore, 1994).

[5] I. Brankov, D. M. Danchev, and N. S. Tonchev, *Theory of Critical Phenomena in Finite-Size Systems: Scaling and Quantum Effects* (World Scientific, Singapore, 2000).

[6] A. Gambassi, J. Phys.: Conf. Ser. **161**, 012037 (2009).

[7] M. Kardar and R. Golestanian, Rev. Mod. Phys. **71**, 1233 (1999).

[8] M. Bordag, U. Mohideen, and V. M. Mostepanenko, Phys. Rep. **353**, 1 (2001).

[9] T. Emig, N. Graham, R. L. Jaffe, and M. Kardar, Phys. Rev. A **79**, 054901 (2009).

[10] H. Gies and K. Klingmuller, Phys. Rev. Lett. **97**, 220405 (2006); A. Weber and H. Gies, Phys. Rev. D **80**, 065033 (2009).

[11] R. Garcia and M. H. W. Chan, Phys. Rev. Lett. **83**, 1187 (1999).

[12] A. Ganshin, S. Scheidemantel, R. Garcia, and M. H. W. Chan, Phys. Rev. Lett. **97**, 075301 (2006).

[13] O. Vasilyev, A. Gambassi, A. Maciolek, and S. Dietrich, Europhys. Lett. **80**, 60009 (2007).

[14] R. Garcia and M. H. W. Chan, Phys. Rev. Lett. **88**, 086101 (2002).

[15] A. Maciolek, A. Gambassi, and S. Dietrich, Phys. Rev. E **76**, 031124 (2007).

[16] E. Eisenriegler, in *Soft Matter*, edited by G. Gompper and M. Schick (Wiley-VCH, Weinheim, 2006), Vol. 2, p. 87.

[17] E. Eisenriegler, J. Chem. Phys. **124**, 144912 (2006); **125**, 204903 (2006).

[18] F. Schlesener, A. Hanke, R. Klimpel, and S. Dietrich, Phys. Rev. E **63**, 041803 (2001).

[19] D. Kleshchanok, R. Tuinier, and P. Lang, J. Phys.: Condens. Matter **20**, 073101 (2008).

[20] M. F. Maghrebi, Y. Kantor, and M. Kardar, Europhys. Lett. **96**, 66002 (2011); Phys. Rev. E **86**, 061801 (2012).

[21] P. G. de Gennes, *Scaling Concepts in Polymer Physics* (Cornell University, Ithaca, NY, 1979).

[22] R. Golestanian, M. Goulian, and M. Kardar, Phys. Rev. E **54**, 6725 (1996).

[23] A.-F. Bitbol, P. G. Dommersnes, and J.-B. Fournier, Phys. Rev. E **81**, 050903 (2010); A.-F. Bitbol, K. Sin Ronia, and J.-B. Fournier, Europhys. Lett. **96**, 40013 (2011).

[24] C. Yolcu, I. Z. Rothstein, and M. Deserno, Europhys. Lett. **96**, 20003 (2011); R. C. Haussman and M. Deserno, Phys. Rev. E **89**, 062102 (2014).

[25] U. Nellen, L. Helden, and C. Bechinger, Europhys. Lett. **88**, 26001 (2009).

[26] K. Binder, in *Phase Transitions and Critical Phenomena*, edited by C. Domb and J. L. Lebowitz (Academic Press, London, 1983), Vol. 8, p. 1; H. W. Diehl, in *Phase Transitions and Critical Phenomena*, edited by C. Domb and J. L. Lebowitz (Academic Press, London, 1986), Vol. 10, p. 76; Int. J. Mod. Phys. B **11**, 3503 (1997).

[27] M. Hasenbusch, Phys. Rev. B **81**, 165412 (2010).

[28] R. Evans and J. Stecki, Phys. Rev. B **49**, 8842 (1994).

[29] T. W. Burkhardt and E. Eisenriegler, Phys. Rev. Lett. **74**, 3189 (1995); **78**, 2867 (1997); E. Eisenriegler and U. Ritschel, Phys. Rev. B **51**, 13717 (1995).

[30] S. Kondrat, L. Harnau, and S. Dietrich, J. Chem. Phys. **131**, 204902 (2009).

[31] T. Baumgart, A. T. Hammond, P. Sengupta, S. T. Hess, D. A. Holowka, B. A. Baird, and W. W. Webb, Proc. Natl. Acad. Sci. USA **104**, 3165 (2007); S. L. Veatch, O. Soubias, S. L. Keller, and K. Gawrisch, *ibid.* **104**, 17650 (2007).

[32] B. B. Machta, S. L. Veatch, and J. P. Sethna, Phys. Rev. Lett. **109**, 138101 (2012).

[33] The composition-mediated interaction in biological membranes considered in Ref. [32] should be distinguished from the shape-fluctuation-mediated interaction in membranes considered in Refs. [22–24], in which the fluctuations are Gaussian and where inclusions of needle shape have also been considered.

[34] J. L. Cardy, in *Phase Transitions and Critical Phenomena*, edited by C. Domb and J. L. Lebowitz (Academic Press, New York, 1986), Vol. 11, p. 55; Nucl. Phys. B **240**, 514 (1984).

[35] O. A. Vasilyev, E. Eisenriegler, and S. Dietrich, Phys. Rev. E **88**, 012137 (2013).

[36] G. Bimonte, T. Emig, and M. Kardar, Europhys. Lett. **104**, 21001 (2013).

[37] J. L. Cardy, Nucl. Phys. B **275**, 200 (1986).

[38] Needle-shaped particles have also been considered in the context of quantum spin chains. See J. M. Stephan, J. Stat. Mech. (2014) P05010; M. A. Rajabpour, Europhys. Lett. **112**, 66001 (2015), and references therein.

[39] Our "chemical steps" separate intervals of the half-plane boundary which prefer different components of the mixture. Colloidal particles in three spatial dimensions interacting with chemical steps in the planar boundary of the embedding half space have been studied theoretically in Ref. [40] and experimentally in Ref. [41].

[40] M. Troendle, S. Kondrat, A. Gambassi, L. Harnau, and S. Dietrich, J. Chem. Phys. **133**, 074702 (2010); F. P. Toldin, M. Troendle, and S. Dietrich, J. Phys.: Condens. Matter **27**, 214010 (2015) and references cited therein.

[41] F. Soyka, O. Zvyagolskaya, C. Hertlein, L. Helden, and C. Bechinger, Phys. Rev. Lett. **101**, 208301 (2008); M. Troendle, O. Zvyagolskaya, A. Gambassi, D. Vogt, L. Harnau, C. Bechinger, and S. Dietrich, Mol. Phys. **109**, 1169 (2011).

[42] The force between two collinear needles has been calculated in Ref. [36] for the free Gaussian model with conformal charge $c = 1$.

[43] We use the terms "distant," "small," and "short" interchangeably to describe a needle that is short compared with its distance from the rest of the system but large on a microscopic scale.

[44] K. G. Wilson and J. B. Kogut, Phys. Rep. C **12**, 75 (1974); A. Z. Patashinskii and V. L. Pokrovskii, *Fluctuation Theory of Phase Transitions*, International Series in Natural Philosophy Vol. 98 (Pergamon Press, New York, 1979); A. A. Belavin, A. M. Polyakov, and A. B. Zamolodchikov, Nucl. Phys. B **241**, 333 (1984).

[45] The free energy of interaction δF is the free energy required to move the two needles from infinite separation to the configuration of interest.

[46] For the Cartesian stress tensor T_{kl} in the first paragraph of Sec. II and in Eqs. (A2) and (B18), we use the same normalization as in field theories in arbitrary spatial dimensions; see, e.g., L. S. Brown, Ann. Phys. (NY) **126**, 135 (1970). In two dimensions this leads to $T(r_x + ir_y) = -\pi[T_{xx}(r_x,r_y) - iT_{xy}(r_x,r_y)]$ and $\bar{T}(r_x - ir_y) = -\pi[T_{xx}(r_x,r_y) + iT_{xy}(r_x,r_y)]$, where T and $\bar{T}$ are the components of the complex stress tensor of Ref. [34]. With this normalization, $\langle T(z)T(z')\rangle_{\rm bulk} = (1/4)(z-z')^{-4}$, $\langle T\bar{T}\rangle_{\rm bulk} = 0$, and $\langle \bar{T}\bar{T}\rangle_{\rm bulk}$ is the complex conjugate of $\langle TT\rangle_{\rm bulk}$. Cardy's Cartesian tensor $T_{kl}^{\rm (Cardy)} = -2\pi T_{kl}$ in two dimensions differs from ours by a factor -2π.

[47] H. Kober, *Dictionary of Conformal Representations* (Dover, Mineola, NY, 1957); see Secs. 12.1, 12.3, 13.11, and 13.12.

[48] T. W. Burkhardt and T. Xue, Nucl. Phys. B **354**, 653 (1991).

[49] The amplitudes $\tilde{t}$ and $t(h)$ of the stress tensors in Eqs. (3.4) and (4.22), respectively, depend on the surface universality classes $H_{\rm I}, H_{\rm II}$ of the two needles I, II, i.e., $\tilde{t} \equiv \tilde{t}_{H_{\rm I},H_{\rm II}}$ and $t(h) \equiv t_{H_{\rm I},H_{\rm II}}(h)$. To keep the notation simple, we suppress the subscripts $H_{\rm I}, H_{\rm II}$ in most of our formulas. Note that $\tilde{t}$ and $t(h)$ do not change on swapping the two surface universality classes. The invariance of $\langle T(w)\rangle$ in Eq. (4.22) on swapping the surface universality classes of the two boundary circles follows from its transformation under the inversion $w \to h/w$. This result and Eq. (2.1) imply that $\langle T(z)\rangle$ for a given configuration of two needles is also unaffected by an exchange of the two surface universality classes.

[50] A useful formula for evaluating the integrals in Sec. III and Appendix D is $\int_0^\infty dU U^{\mu-1}[(U+b)(U-a+i0)]^{-1} = -\pi \csc(\pi\mu)[b^{\mu-1}+i^{2\mu}a^{\mu-1}]/(a+b)$, where a and b are positive.

[51] N. I. Akhiezer, *Translations of Mathematical Monographs* (American Mathematical Society, Providence, RI, 1970), Vol. 79. We follow Akhiezer's definition of the function $\vartheta_1(v)$, which is related by $\vartheta_1(v) = \vartheta_1^{\text{alternate}}(\pi v)$ to the alternate function of Abramowitz and Stegun, Gradshteyn and Ryzhik, and *Mathematica*.

[52] For finite needles that nearly touch, h is very close to 1. This regime can be studied analytically with the help of "Jacobi's imaginary transformation," which relates ϑ_1 with parameter h to ϑ_1 with parameter $h' \equiv \exp[-\pi^2/\ln(1/h)]$, since $h' \to 0$ for $h \to 1$. For details, see Sec. 22 of Akhiezer's book [51].

[53] Since rotating a needle by 180° does not change the force and torque (see Ref. [55]), case (D) can also be represented by $z_{12} = z_{34}$, which is generated by $\varphi_4 = -\varphi_1, \varphi_3 = -\varphi_2$.

[54] Rotating configuration (D) of Sec. IV A 1 counterclockwise by an angle of $\pi - \Phi_{12}$, where $0 < \Phi_{12} < \pi$, yields a configuration (D′) with needle vectors $z_{12} = -|z_{12}|$ and $z_{34} = |z_{34}|$ antiparallel and parallel to the real axis, respectively, and with needle I located above needle II, as shown in Figs. 3(D) and 3(D′). In Sec. V and Appendix C this new orientation is more convenient. The angle Φ_{12} is related to the new x and y components by $\cot\Phi_{12} = -(r_{1,x} - r_{4,x})/W$, $W \equiv r_{1,y} - r_{4,y} = |r_{1,y} - r_{4,y}|$.

[55] Cardy's expression (4.22)–(4.24) for the stress tensor holds for an annulus in the w plane with boundary conditions which are rotationally invariant about the center. Thus, the boundary condition on circular segment ii in Fig. 2 is the same as on segment i, and the boundary condition on segment iv is the same as on segment iii. This implies that each of the corresponding needles I and II in the z plane has the same boundary condition on both edges. In this case the force and torque are unchanged if needle I or II is rotated by 180°, i.e., if z_1 and z_2 or z_3 and z_4 are swapped. This is consistent with expressions (2.3), (2.5), (2.10), and (2.11) for the force and torque, since interchanging w_1 and w_2 or w_3 and w_4 leaves $z'(w)$ in Eq. (4.2) and $S(w)$ unchanged and does not affect $\langle T(w)\rangle$.

[56] At bulk criticality the free energy of an annulus bounded by two concentric circles with radii $h\varrho$ and ϱ contains a scale-free contribution $f_{\text{annulus}}(h)$ which is independent of ϱ, depends only on h, and vanishes for $h \to 0$. Since $h(d/dh)f_{\text{annulus}}/(k_BT) = -t(h)$, this contribution is directly related to $t(h)$ in Eqs. (4.22)–(4.24). While $t(h \ll 1)$ is given in Eqs. (4.26) and (4.27) and is relevant for the small-particle expansion, $t(h \to 1) = -2\pi(1-h)^{-2}\Delta$ is determined by the interaction between the parallel boundaries of an infinitely long strip, where the Derjaguin approximation is exact [29]. Here $\Delta = \pi[-1,-1,23,2]/48$ is the amplitude [34] in the Casimir contribution Δ/W to the free energy per k_BT and per unit length of the strip with width W and boundary universality classes $OO, ++, +-, O+$ and is related [48] via $\Delta = \pi(\tilde{t} - 1/48)$ to the amplitude $\tilde{t}$ in Eq. (3.4). This is consistent with $h \to 1$ for needles much longer than their minimum separation.

[57] E. Eisenriegler, J. Chem. Phys. **121**, 3299 (2004).

[58] Only in exceptional cases does the force between two finite needles have a simple analytic form, free of special functions, for arbitrary distance to size ratios. One such case is collinear needles of equal length D in configuration (i) of Sec. IV A 1, where the force on needle I is given by $f_x/(k_BT) = \pm\{8c[(c/D)+1][(c/D)+2]\}^{-1}$ for $O+$ (upper sign) and OO (lower sign) boundaries. Here $c = z_2 - z_4 \equiv r_{2,x} - r_{4,x}$ is the distance between the closest points of the needles. This result follows from stress tensor averages $\langle T(z)\rangle$ given in Appendix B of Ref. [35] on using our Eqs. (A8) and (A11).

[59] Lateral Casimir forces on colloidal particles in three dimensions exposed to a chemically structured surface have been measured in Ref. [41].

[60] Expressions (D1)–(D4) for the stress tensor allow us to study the effect of inhomogeneous surfaces on the Casimir interaction, not only of particles embedded in a simply connected region (such as two needles of infinite length considered in Appendixes D 2 and D 3) but also, within the SPOE, of particles embedded in multiply connected regions. For example, the orientation dependence of force and torque on a short needle with ordinary boundary conditions on both edges embedded in the half plane with an inhomogeneous boundary can be analyzed with an SPOE like the one in Appendix B 2 c. Recently, J. Dubail, R. Santachiara, and T. Emig, Europhys. Lett. **112**, 66004 (2015), have studied the critical Casimir force for the simply connected case of a strip with an inhomogeneous boundary with an alternate approach utilizing conformal field theory and Majorana fermions.

[61] Certain configurations of three particles in which two of the particles touch can be interpreted in terms of two particles in a doubly connected space and can be conformally generated from an annulus. See H. Hobrecht and A. Hucht, Phys. Rev. E **92**, 042315 (2015).

[62] The treatment of the multibody interaction of small circular particles in Ref. [29] can be extended to small needles using the SPOE in Eq. (B16). For recent experimental and theoretical studies of the three-body interaction of colloidal particles in a critical system, see S. Paladugu, A. Callegari, Y. Tuna, L. Barth, S. Dietrich, A. Gambassi, and G. Volpe, Nat. Commun. **7**, 11403 (2016), and references therein.

[63] For a given particle shape, changing the boundary conditions from uniform to nonuniform generally alters the symmetry and the set of operators in the SPOE. For example, for a needle with boundary condition $+$ on one edge and $-$ on the other, the SPOE contains, due to its dipolar character, an operator $\partial_\perp\phi$ with a derivative $\partial_\perp$ perpendicular to the direction of the needle (compare, e.g., Ref. [57]). This operator is absent in the SPOE (B16) of a needle with homogeneous boundary conditions $+$.

[64] Since translating or rotating particle I relative to particle II as described in Eqs. (A3)–(A5) does not alter the nonuniversal contributions to the bulk and surface free energies and to the free energy of needle ends, $F_{\hat{G}} - F_G$ can be identified with the change in the total free energy.

[65] The $\tilde{T}$(J) term in Eq. (B16) is independent of H_J since at large distances it must reproduce the stress-tensor profile $\langle T(z)\rangle_{\text{single needle}}$ around the *single* needle J, and this single-needle profile is independent of H_J. This is because $\langle T(z)\rangle_{\text{single needle}}$ follows from a conformal mapping $z(w)$ of the stress tensor $\langle T(w)\rangle_{\text{half plane}}$ for the half plane with a uniform boundary condition, which vanishes [34], independent of H_J. Thus, $\langle T(z)\rangle_{\text{single needle}}$ is entirely determined by the purely geometrical $S(w)$ term in the transformation (2.1).

[66] Due to a possible term $\propto \partial^4\phi$ in the ellipsis of Eq. (B16), for needle classes $++$ and $+-$ we expect a term of order (needle length $/|\mathbf{r}_{\rm I} - \mathbf{r}_{\rm II}|$) raised to the power 17/4 in the ellipsis of Eq. (B25). Since this power is quite close to the power 4 coming from $\mathcal{E}$ and $\mathcal{H}$, we have not shown the explicit form of the $\mathcal{O}(B^{-4})$ term in Eqs. (B33) and (B36).

[67] The special case of *symmetric* parallel semi-infinite needles, corresponding to Eq. (C6) with $b = 1$, is considered in Sec. 12.3 of Kober's book [47].

[68] The expression for f_x for parallel semi-infinite needles derived in Appendix C also follows from the results of Sec. III B for the force between needles which form a nonvanishing angle $\alpha > 0$. Before taking the limit $\alpha \searrow 0$, one replaces the positive real constant $\mathcal{B}$ in Eqs. (3.7)–(3.11) by $|\mathcal{B}|e^{-i\alpha/2}$, so that needles I and II form angles $\alpha/2$ and $-\alpha/2$ with the x axis and from the outset f_x is an odd function of the difference of the x coordinates of the needle tips.

[69] B. M. McCoy and T. T. Wu, *The Two-Dimensional Ising Model* (Harvard University Press, Cambridge, MA, 1973).

[70] T. W. Burkhardt and I. Guim, Phys. Rev. B **47**, 14306 (1993); see, in particular, Eq. (17).